Pulsed laser deposition of nitride films

Submitted by

Cheung Hoi Yan

For The Degree of

Master of Philosophy in Physics

at

The Hong Kong Polytechnic University

in August 2002

Abstract

The present research is aimed at using Pulsed Laser Deposition (PLD) method to fabricate epitaxial cubic TiN and TaN thin films on MgO(001) and Si(001). Crystalline TiN and TaN layers have been deposited under a base pressure of ~ 10^{-6} Torr and at substrate temperatures ranging from 550°C to 750°C. Epitaxial TiN films of cube-on-cube grown on Si(001) in a 4-on-3 mode (Volmer-Weber type) at 600°C and in a 5-on-4 mode (Stranski-Krastinov type) at 600°C have been obtained. The resistivity of these epitaxial TiN film is about 44 μΩ cm at room temperature. They show a typical positive $\frac{d\rho}{dT}$ characteristics of a metal. Epitaxial TaN(001) films, on the other hand, have been successfully grown on MgO(001) single crystal and TiN(001) buffered Si(001) substrates. Very good crystalline TaN films with cube-on-cube $<001>_{TaN}||<001>_{MgO}$ heteroepitaxy are obtained. In spite of the ball-shaped particles, a very sharp TaN/MgO interface is observed. The room temperature resistivity is about 600 μΩ cm with negative $\frac{d\rho}{dT}$.

TaN films grown on TiN(001) buffered Si(001), however, show a mixture of TaN_x (with $x \leq 1$) components. Although the (001)-oriented TaN is always present prominently, the nitrogen deficient TaN_x components are often co-existed in the films and show up as a broad peak in the X-ray diffraction profile. Stoichiometric and single phase TaN(001) films can only be obtained in a narrow temperature window at around 550°C and heteroepitaxial relationship of $<001>_{TaN}||<001>_{TiN}||<001>_{Si}$ has been demonstrated. An interesting finding is that this bi-layer structure could produce a nearly flat R-T curve with $\frac{d\rho}{dT}$ close to zero.

The crystallinity and surface morphology of the epitaxial STO films with underlying TiN layer are also presented. All the STO films are cube-on-cube grown on the TiN/Si substrates over a wide temperature range (550 to 750°C). The substrate temperature dependence growth modes of the TiN can change the orientation relationship of the STO films. It changes from (001) to (101) oriented at elevated temperature. It is suggested that better crystallinity STO films can be achieved by improving the quality of the TiN buffer layer.

The fundamental mechanical properties of epitaxial nitride films have been studied. TiN films grown at optimum temperature of 650°C under 4 x 10^{-6} Torr, yields a hardness (H) value of about 25 GPa and a Young's modulus (E) of 375 GPa. The lack of crystallinity and decrease in hardness (20 GPa) for TiN films grown at 550°C appear to be related to the low processing temperature. The H value for single-layered TaN is 22 GPa and E is about 313 GPa. A remarkably increase in hardness for the TaN/TiN bi-layer films were also obtained.

Acknowledgements

I would like to acknowledge my supervisor, Dr. K. H. Wong for his close supervision and enlightening suggestions throughout these two years. I also wish to thank Dr. C. W. Ong, for his invaluable suggestions and discussions on my research work.

I would like to thank all my research companions especially Mr. K. M. Yeung for leading help in many technical problems and giving valuable advice. The interest of other fellow students is also greatly appreciated. I wish to thank Mr. M. N. Yeung for his assistance in SEM characterization. I also wish to thank S. F. Wong for his assist in nanoindentation tests. Special thanks should be given to Dr. Xu, the technician in the Department of Mechanical Engineering for his help in AFM analysis. Last, but not least, I would like to thank my parent for their mentally support.

This work was supported by a Research Grant of the Hong Kong Polytechnic University under the Code No. G-V847. I am grateful for the award of a research studentship by the Hong Kong Polytechnic University.

Table of contents

Chapter 1

Introduction

Thin films of transition metal nitrides, such as TiN, TaN, have been extensively studied in recent years [So et al., 1988; Xin et al., 1993]. These nitrides exhibit very low electrical resistivity [Toth, L. E., 1971], exceptional mechanical properties and chemical inertness. In addition, they possess extremely high melting points (2000-4000° C) and therefore are frequently referred to as "refractory nitrides". This group of nitrides are useful materials with numerous industrial applications ranging from protective coatings for cutting tools to electronic devices [Au et al., 1990, Hugh O. Pierson., 1996]. In particular, TiN and TaN have been extensively used as diffusion barriers in VLSI metallization [Nicolet, M. A., 1978; Wittmer Marc., 1984]. Recent development in the sub-0.25 μm ULSI circuits of silicon using Cu as the interconnections has renewed studies on diffusion barrier on Si [Takeo et al., 1996]. Cu is a fast diffusion species in SiO_2 and Si. It causes deep-level trapping which seriously degrades the electronic properties of the silicon devices. For this reason, a reliable and highly conductive thin film diffusion barrier should be employed to effectively prevent Cu from intermixing and reacting with Si. In this respect, TaN has been identified as the most promising diffusion barrier materials. It is known to be thermodynamically stable with Cu [Chen et al., 2000]. Furthermore, enhanced diffusion barrier performance and resistance to oxidation can be obtained in using stable NaCl-type cubic phase TaN films. Recently, pure cubic TaN films grown on single crystal MgO substrates have been demonstrated [Greene et al., 1999]. However, epitaxial TaN grown on Si substrate has not been reported. As

microelectronics devices are made with ever denser integration of circuits, the demand for unique and reliable properties of thin films has increased dramatically. Improvements on the control of microstructure and composition are of great importance.

Among the many different deposition methods such as chemical vapor deposition, plasma-assisted chemical vapor deposition, electron beam evaporation, magnetron sputtering, etc., pulsed laser deposition (PLD) is a promising and versatile technique for the growth of thin films [Chrisey, D. B., and Hubler, C. K., 1994]. It has been extensively employed in preparation of high quality thin films of nitrides, ceramic oxides and diamond-like carbon. The present research is aimed at using Pulsed Laser Deposition (PLD) method to fabricate epitaxial cubic TiN and TaN thin films on MgO(001) and Si(001). High quality epitaxial TiN/Si, TaN/MgO and TaN/TiN/Si heterostructures have been successfully grown at relatively low temperature. Their structural, electrical and mechanical properties are studied. There are in general 4 main areas to be addressed. The first is the preparation of epitaxial thin films. The second is the fabrication of the heterostructures. The third is thin films characterization (both structure and composition), and the fourth is thin films properties.

In chapter 2 a brief description on the history and fundamental mechanism of PLD will be presented. Besides, the advantages as well as disadvantages of using PLD for thin film deposition will also be discussed.

The experimental techniques and set-up will be illustrated in chapter 3. We will

focus on the detail discussion of thin film-deposition technique, the practical considerations of laser selection, vacuum chamber, and the films formation. Working principles for some major characterization equipment such as X-ray diffractometer (XRD), atomic force microscope (AFM) and four-point probe will also be described.

The fabrication and characterization of Titanium nitride (TiN) films will be presented in chapter 4. The theme of this chapter is to summarize the results on studying the unique structural properties of TiN grown on Si. The temperature dependent growth mode of TiN and the lattice relaxation in thick TiN films are described.

In chapter 5 we will report the current results of Tantalum nitride (TaN) films grown on single crystal MgO and TiN buffered Si substrates. Emphasis is placed on the correlation between the film quality and the deposition conditions. An interesting result of $\frac{d\rho}{dT} \approx 0$ for TaN/TiN bi-layer film is also reported.

In chapter 6 we will present the fabrication and characterization of Strontium titanate ($SrTiO_3$) STO/TiN on Si substrates. Mechanical properties of the nitride films will be described in chapter 7. In particular, the enhancements of hardness and Young's modulus in TaN/TiN bi-layer films is described. A conclusion and the future development will be given in chapter 8.

Chapter 2

Pulsed laser deposition (PLD)

2.1 History and background

Remarkable advances have been made in recent years in the science and technology of thin films deposition processes. Among various techniques known to date, pulsed laser deposition (PLD), also called laser ablation, is proving to be the most simple and efficient technique for fabrication of high quality multi-component thin films. It has been shown to be an excellent film growth technique not only offering superior electrical and optical properties but also allowing fabrication of integrated multilayer heterostructures by *in-situ* single chamber processing. In the past, PLD has been extensively employed for the growth of metal-oxide films including T_c superconductors, ferroelectrics, piezo-electrics, and magnetoresistive materials [Chrisey, D. B., and Hubler, C. K., 1994]. More recently, PLD has been extended to fabricate films of other materials such as nitrides, carbides, fluorides and borides [Adams et al., 2000; Shengwen Yu et al., 2000].

The first laser was demonstrated by Maimanin, T. H. in 1960 at the Hughes Research Laboratories. Like many other technical discoveries, the various laser applications were not initially defined but were the consequences of natural evolution fueled by theoretical studies. After the demonstration of the first laser, some of the early studies were predominantly theoretical investigations on the laser-target interaction. The first experiment demonstrating PLD of thin films was performed by [Smith, H. M., and Turner, A. F., 1965] using ruby laser. Historically,

the main interest in the studies of the fundamentals of PLD has been concentrated on the behaviour of the laser generated plasma plume [Saenger, K. L., 1989]. The technique gained its prominence and established itself as a major film growth method in the late eighties, during which an explosion of studies on high-temperature superconductor had occurred. PLD has been demonstrated to be the most successful technique in producing high quality superconducting oxide films.

Experimentally, PLD is a relative simple technique to deposit thin films. It is often described as a 3-step process consisting of vaporization of a target material, transport of the vapor plume, and film growth on a substrate. Film growth can be carried out in a reactive environment containing any kind a gas with or without plasma excitation. It can also be operated in conjunction with other types of evaporation sources in a hybrid approach. All these desirable features have made PLD a powerful deposition technique.

The mechanism that leads to material ablation depends on laser characteristics, as well as the optical, topological, and thermodynamical properties of the target. Regardless of the detailed mechanisms, many important applications depend on laser ablation. These include industrial processes such as laser welding or hole drilling, materials processing to produce thin films or microstructures.

Great research effort focused on PLD in the past decade has resulted in a better understanding of the process, with new phenomena detected and new materials synthesized. One of the latest trends in PLD development is the heteroepitaxial

growth of oxides and nitrides on semiconductors such as MgO/Si [X. Y. Chen., and K. H. Wong., 2001], YSZ/Si [Fork et al., 1990], MgO/GaAs [Chang et al., 1992; Fork et al., 1992; Prusseit et al., 1992]. The growth of ferroelectric perovskite oxide films is also an area showing good potential promises [Ramesh et al., 1990; Horwitz et al., 1991]. Recently, PLD has been used to grow nitride films with good crystalline quality and superior optical properties [Chowdhury et al., 1996; Lee et al., 1994]. More emphasis is now placed on the synthesis of poly-component thin films and multi-layer film structures with highly advanced electrical, optical and mechanical properties.

2.2 Advantages of pulsed laser deposition

Pulsed laser deposition (PLD) is an advanced technique for thin film fabrication. It shows many unique advantages compared with other techniques including thermal evaporation (TE) [Bunshah, R. F., 1982], electron beam or ion beam evaporation, chemical vapor deposition (CVD), reactive molecular beam epitaxy (MBE) [Parker, E. H. C., 1986] and magnetron sputtering. Some shortcomings of these latter methods have been identified in depositing multi-component materials. Nonstoichiometry, high substrate temperature and poor crystallinity are the few noted ones. For this reason, the applications of PLD have been successfully utilized to fabricate many multi-component ceramics films.

PLD is a reliable, economical, and relatively simple technique for fabricating high quality thin films. Additionally, the approach benefits from all the advantages, particularly the flexibility and the possibility to work with targets of relatively small size. The chamber-pressure, the target distance, the target orientation with respect to the laser beam are significantly decoupled enabling a great degree of freedom in the deposition system design. PLD leads itself to low temperature processing because the average energy of particles in the laser evaporated species is considerably higher than those achieved by thermal evaporation. In addition, the plasma plumes of laser-ablated materials contain highly excited species. The high energy of such excited species facilitate their migration on the surface and relaxation into stable lattice sites to grow highly crystalline films at a relatively low temperature. PLD also allows congruent evaporation and the deposited films tend to have the same stoichiometry of the target. Therefore PLD can be used to grow thin films of any

kind of materials. Ablation and excitation in PLD involve optical process. The light source is located outside the deposition chamber. Therefore the film growth parameters, such as the substrate temperature and growth environments, can be controlled independently. The combination of the highly activated particles and a good control on the growth parameters help to improve the film-to-film reproducibility, accurate stoichiometry, single-phase purity or crystal orientation.

When the laser radiation is absorbed by a solid surface, electromagnetic energy is converted first into electronic excitation and plasma formation. Evaporants form a "plume" consisting of a mixture of energetic species including atoms, molecules, electrons, ions, clusters and micron-sized solid particulates. The collisional mean free path inside the dense plume is very short. This process attributes to many advantages as well as disadvantages. One of the disadvantages of PLD is the fact that large particles tend to be generated from the target material and become embedded in the films. These particles range in size from < 0.1 to several microns in diameter. This problem is more severe in the multi-layer systems because these will greatly affect the growth and the interface quality, hence producing film layers with very rough surfaces. One simple way to prevent these undesirably large particles from reaching the surface of the substrate is by insertion of an opaque mask between the target and the substrate. This forms a shadow mask to block the large particulates emitted from the target. The technique is often referred to as the "eclipse method" and has been first suggested by Iwabuchi et al [Iwabuchi et al., 1994]. Therefore, the growth of thin films with smooth surface and particulate free can be obtained.

In fact, the PLD is simply based on physical process, arising from the impact of high power pulsed laser radiation on the targets and leading the removal of partially ionized plasma from the impact zone. Theoretical and experimental investigations of the PLD process have shown that it is possible to establish a direct relation between experimental conditions and some film properties. Further quantitative experiments are needed in order to find optimum conditions for depositing thin films of advanced properties.

2.3 Mechanisms of pulsed laser deposition

The laser-induced treatment is a physical way for changing material properties. Variously termed vaporization, sputtering, laser ablation or etching processes are extremely complex. Analysis of the laser interaction processes allow formulation of requirements on laser parameters and optical set-ups in order to ensure high accuracy, reproducibility and cleanliness of the technological process. In this section, the fundamental of films growth mechanisms on the PLD will be described.

2.3.1 Four stages for the PLD process

Generally speaking, the laser-plasma deposition process consists of 4 stages and each of them influences the properties of the obtained films. These stages are:

(1) Laser radiation interaction with the solid target.

Interaction of laser with the substrate's surface plays an important role in the thin

films deposition. The radiation incident on the target is partially reflected and partially absorbed by the surface layer. Absorption of light energy leads to local heating and rapid congruent evaporation of the target material. The ejected materials consists of atomic and molecular species as well as clusters and particulates of the target materials. In order to obtain a stoichiometric film, the dissociation energy of molecules of the target material should be higher than the thermal energy of the evaporated particles. In general, photo-ablation by UV laser tends to produce significant amount of highly excited or ionic species, which help to crystallize the deposited films but also induce various type of damage and droplets.

(2) Expansion of the ablated products (plasma).

The laser ablation process produces a highly excited and luminous plasma plume. The non-thermal equilibrium nature and the flow dynamic of this plume has led to a highly forward-directed gas jet of materials moving with speed of ~ 10^5 cm/s. On reaching the substrate surface, the plasma flux condenses to form thin films. The thermal and kinetic energy of the plasma particles can significantly influence the properties and qualities of the thin films.

(3) Interaction of the ablated products with the substrate.

The interaction between the incident flow and the ejected atoms results in the formation of a collision region characterized by increased temperature and particle density which hinders the motion of the incident flow upon the surface.

Condensation and defect formation take place until the energy of the incident particles drops below the defect-formation threshold. Condensation simply means the transformation of gas into liquid or solid. The most frequently encountered defects in evaporated films are dislocations. Since the substrate and the film usually have different lattice parameters, there will be a displacement misfit between islands. Dislocations can result from this misfit when islands grow and coalesced.

(4) Nucleation and growth of thin film on the substrate surface.

Many factors such as density, energy, ionization degree, and type of the condensing particles that may influence strongly the quality of thin films. There are two main thermodynamic parameters to determine growth mechanism: 1) the substrate temperature and 2) the supersaturation Δm.

$$\Delta m = kT \ln (R/R_e)$$

Where k is the Boltzmann constant, R is the deposition rate, and R_e is the equilibrium value at temperature T. The plasma fluxes are characterized by a high degree of supersaturation and ionization. When a thermalized region forms close to the substrate's surface, film growth occurs via condensation of particles, it corresponds to near-equilibrium conditions.

Each of these processes plays a decisive role in the deposition of high quality films. The adjustable experimental parameters are the laser fluence; target-substrate

distance; target composition; reactive background gas and pressure; substrate and substrate temperature. The low temperature processing of PLD is highly desirable. This is achieved by the impingements of the high energy of the excited species which facilitates the translational migration of the deposited species on the substrate surface and relaxation into stable lattice sites. Thus, high quality crystalline films can be obtained. Understanding how the experimental conditions affect the nucleation and growth of laser-deposited films is also an area of intense research activity.

2.3.2 Three modes of the film growth

In considering film nucleation and growth processes, it is convenient to group them into 3 major modes. They are Volmer-Weber (3-dimensional island growth), Frank-Van der Merwe (2-dimensional growth), and Stranski-Krastinov modes [Lewis and Anderson., 1978; Venables et al., 1984]. Fig. 2.3.2a is the schematic diagram of 3 different growth modes.

These growth modes can be described in terms of surface energies, γ. If we deposit material A on B, we get layer growth if $\gamma_A < \gamma_B + \gamma^*$, wher γ^* is the interface energy, and vice-versa for island growth. The Volmer-Weber is the island growth mode provided that the cohesive energy of the film atoms is much greater than the cohesive binding between the film and substrate atoms. For the high nucleation density tends to promote complete monolayer with a smooth epitaxial film. PLD is known to have very high deposition rate. The process therefore favour Frank-Van der Merwe mode growth, at least in the initial growth stage.

The most obvious feature that could cause Stranski-Krastinov growth mode to occur is an increase of stress when increasing the layer thickness. Strong chemical bonding between the substrate and the film is also involved, altering the surface energy of the initial layers owing to the mismatched lattice spacing. Initially the growth of films is in the Frank-Van der Merwe mode. After the substrate surface being covered by a monolayer of the deposited materials, successive layer deposition is overridden by factors such as surface energy and strain energy owing to lattice mismatch and defects. Film atom migration tends to favour island formation. Generally for high quality films and epitaxial single crystal films, Frank-Van der Merwe growth mode is required. By contrast, the Volmer-Weber is less desirable. However, all these growth modes are perhaps only important for ultra-thin films (~ nm) and not a matter of concern for films over 100 nm thick.

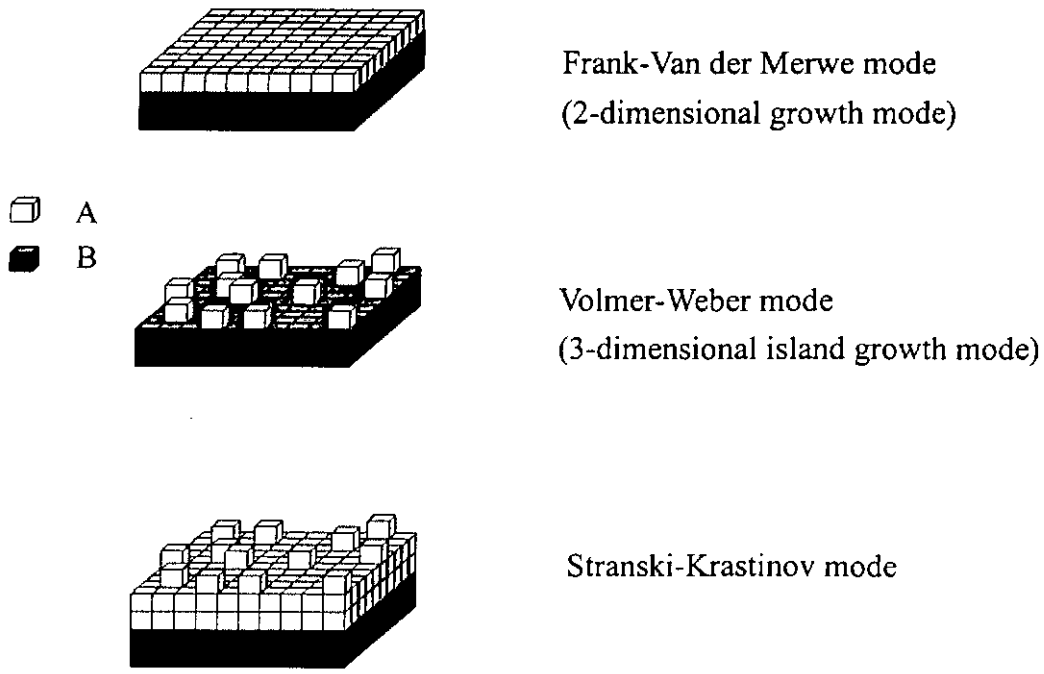

Fig. 2.3.2a The schematic diagram of 3 different growth modes.

Chapter 3

Experimental set-up

3.1 Introduction

In a simple pulsed laser deposition (PLD) system, it consists of a laser, high vacuum chamber, a rotating multi-target holder and a temperature controlled substrate holder. As mentioned in the previous chapter, PLD is an extremely versatile technique for preparing high quality thin films and multi-layer structures. The laser is situated outside of and is independent from the deposition system. Therefore, the complex ceramic and multi-layer films are produced straightforwardly either by moving various targets into and out of the laser beam's focal spot or by using mirrors to change the beam path.

In the present programme, the crystal structures of the deposited films were characterized by 3-axis X-ray diffractometer (XRD) using CuK_{α} radiation. All diffraction profiles were taken at room temperature. Surface morphology of films was examined by scanning electron microscopy (SEM) and atomic force microscopy (AFM). Electrical measurements were achieved by four-point probe technique. The properties of the laser-deposited films strongly depend on the deposition parameters. These parameters can also be controllably changed over a wide range by varying the experimental conditions. In this way, the correlation of the structural, electrical and mechanical properties with the deposition conditions were studied.

In this chapter, the basic PLD equipment of our research and some thin film

characterization techniques are introduced. Some fundamentals of lasers, vacuum chamber and their operating characteristics are also discussed.

3.2 Apparatus

3.2.1 Excimer laser

For non-thermal ablation, the useful range of laser wavelengths for thin film growth by PLD lies between 200 nm and 400 nm. Excimer Laser is a type of pulsed gas discharge laser which can emit high flux of UV photons. All the samples in the present study were prepared by a standard pulsed laser deposition technique using a Krypton Flouride (KrF) excimer laser systems with a wavelength of 248 nm (Lambda Physik COMPex 205). Due to its high UV output energy, high efficiently and stable operation KrF laser is indeed a most popular choice among lasers being used in the PLD community. The gas mixtures for these excimer lasers are comprised of three components: rare gas (Kr), halogen (F_2) and Ne as a buffer with partial pressure of 130 mbar, 4 mbar and 3210 mbar, respectively. The ionic and electronically excited species are created by the avalanche electric discharge excitation (about 40 KV). At the same time, laser transition take place during the dissociation of the excimer molecules as the ground state is repulsive and they rapidly dissociate. The light output from an excimer laser is derived from a molecular gain medium in which the laser action takes place between a bound upper electronic state and a repulsive or weakly bound ground electronic state. Because the ground state is repulsive, the excimer molecule can dissociate rapidly as it emits a photon during transition from upper state to ground state. In our KrF laser, high outputs delivering in excess of 0.5 J/pulse are available. Typically laser pulse

repetition rates of several hertz with energies near 300 mJ/pulse for a pulse duration of 25 ns were used.

3.2.2 Optics

The beam delivery system is formed by a set of lens and mirror. The mirror direct laser beam to the rotating target surface. The function of the lens is to collect radiation and focus it to a spot on the target. The spot size can be varied by controlling the position of the lens focal plane with respect to the target surface. It is fixed to a value that gives the desired energy density (fluence). In PLD technique, one of the most important deposition parameters that control the film stoichiometry and crystallographic quality is the laser energy density (expressed in joules/squares centimeter) incident on the target. In most cases, it is noted that the laser energy density has to be above a minimum threshold value in order to obtain films with the same stoichiometry as the target.

All the optics in our system, such as lens, mirrors and windows were carefully kept absolutely. For example, materials deposited on the window will interact with the laser beam. Fingerprints and dust not only interfere with the beam path, but also couple energy into the optical element and causing permanent damage. In our case, the laser intensity after passing through the window and lens was about 60% of the original laser output. The viewing window at the side of the chamber allows us to observe the situation inside the vacuum chamber during the deposition as well as for *in-situ* alignment. Spherical lens with the focal length of 50 cm is used in our PLD set-up. It is located at between the mirror and the chamber. This kind of arrangement

is suggested because there is an energy density damage threshold for the mirror. To avoid damaging the mirror with a focused beam, extreme care should be taken in handling the laser in the deposition process. The reflected stray laser has to be block-off. Also, the laser window of the vacuum chamber should be made of laser-quality optical material such as fused silica for 248 nm. They need to be polished to a very high degree of flatness and to be free of defects or else they will absorb the laser and deteriorate the beam quality.

3.2.3 Vacuum chamber

The deposition chamber is the central components in a PLD system. A good designed chamber can fabricate the PLD process enormously. Targets should be accessed easily within the chamber. Their mounting and demounting should be as simple as possible. In terms of target erosion and consumption, the most common practice is to rotate the target during the deposition process. Since the evaporants are ejected as a high forward-directed plume of material along the target normal, the substrate must be held directly opposite the target.

Once the laser beam has passed through the optics, it enters the vacuum chamber via a fused silica window. Fig. 3.2.3a shows an overall schematic diagram of the PLD system in our laboratory. The vacuum chamber has several ports and they were used for heater, pressure gauge, gas inlet, target holder, laser window and viewing. The nitride thin films are deposited under high vacuum in order to obtain a high quality film and to reduce the oxidation process. During the ablation of the films, the deposition chamber was evacuated by a mechanical rotary (ULVAC

D-330K) and a cryopump (CTI-CRYOGENICS CRYO-TORR 8) to an ultimate base pressure of 5 x 10^{-7} Torr. The ambient gas pressure was measured by a Baratron pressure gauge (MKS Type 122A) which was mounted on one of the chamber port. A digital meter (MKS Type PDR-D-1 Power Supply Digital Readout) was connected to the pressure gauge to display values. The measured pressure can be ranged from 1mTorr to –12 Torr with an accuracy of ± 0.01% of F.S.

The heater was made of stainless steel and was heat-shielded by a thin plates of stainless steel wrapped around the sides of the heater. We used Kanthal wire (25% chromium, 5% aluminium, 3% cobalt and 67% iron) as the ohmic filament inside the heater for heating purpose. The diameter of the Kanthal wire is 0.559 mm and its resistance per unit length is 5.1 Ωcm^{-1}. A total resistance of this wire used was 12 Ω. A K-type (Nickel-Chromium, Nickel-Aluminium) thermocouple was inserted into the heating block for measuring the relative substrate temperature. The temperature was controlled by a temperature controller (PAC15-0321E). Substrates were pasted onto the face plate of the substrate heater with high temperature silver paste (G3691). In a well-designed chamber, the heat will be distributed uniformly over the surface.

The target-to-substrate distance can be varied from 40 to 80 mm. It must be noted that the deposition rates are higher at shorter target-to-substrate distances, but at shorter distances undesired plasma plume-growing film interference can develop and micron-size droplets may be deposited on the films. Therefore, the distance of 45 mm is chosen for our deposition process. One of the great advantages of PLD techniques is the ease of forming *in-situ* multi-layer structures. A rotating multi-target arrangement for such *in-situ* multi-layer deposition is depicted in

Fig.3.2.3b. Once the ablated species reach the heated substrate surface, condensation and thin film growth begin.

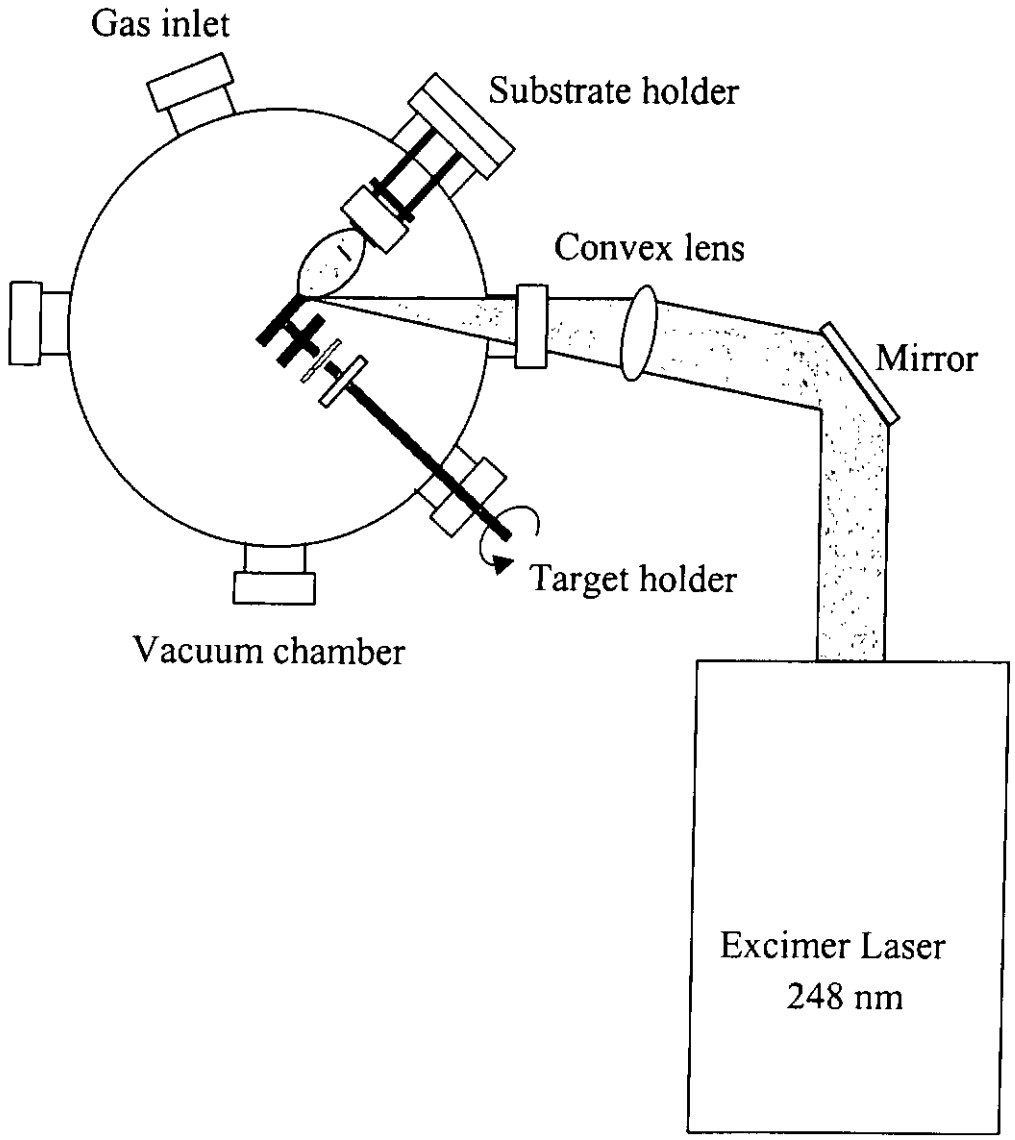

Fig. 3.2.3a The schematic diagram of the pulsed laser deposition system.

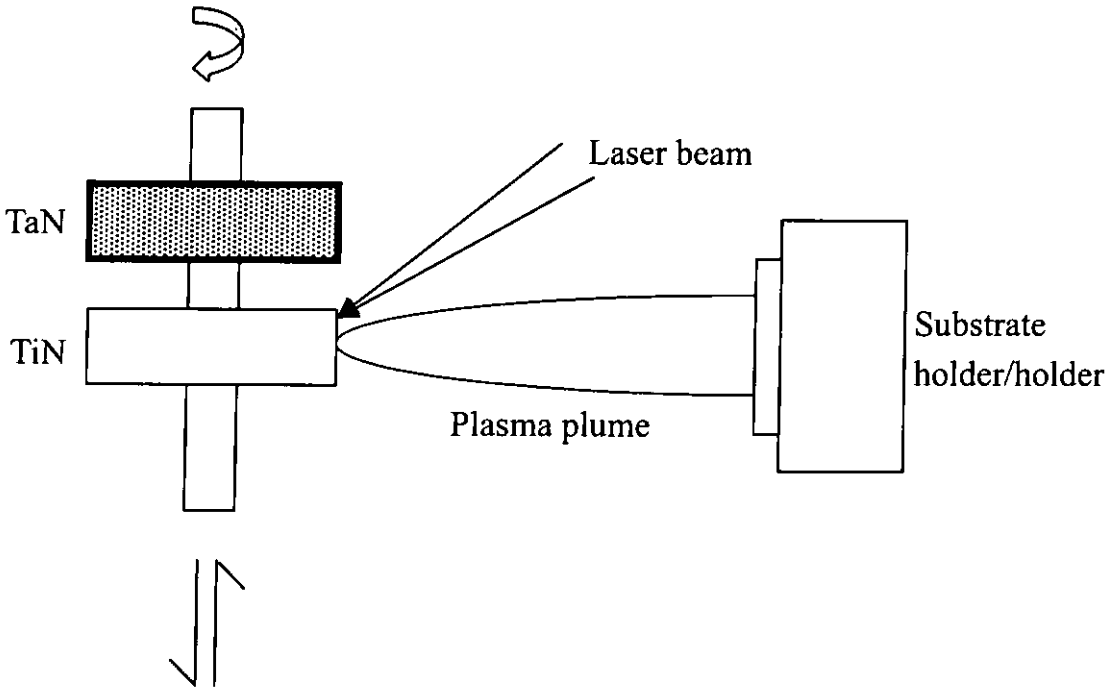

Fig. 3.2.3b The diagram of the multi-targets holder.

3.3 Experimental procedures

3.3.1 Substrate preparation

The silicon wafers (001) oriented, p-type with resistivity of 5-10 Ω cm and MgO(001) single crystal were used as substrates for the growth of nitride films. The size of the substrate was 5 mm x 10 mm. The Si(001) substrates were first ultrasonically degreased with acetone and then dipped into 10% HF solution for 5 minutes in order to remove the native oxide layers. MgO substrates were similarly cleaned but without the dipping into HF solution. They were rinsed thoroughly with deionized water and acetone. Afterward they were immediate adhered well to the face plate of the substrate heater with high temperature silver paste.

3.3.2 Thin films deposition process

A KrF excimer laser (λ = 248 nm) with a repetition rate of 10 Hz was used in our PLD experiments. A rotating multi-target holder incorporate into the chamber was used for the thin films deposition. Before deposition the chamber was evacuated by a cryopump to a typical base pressure of 5 x 10^{-7} Torr. The laser beam was focused through a UV grade optical window into the laser ablation chamber. The laser energy density for the ablation of material can be varied from 5-10 J/cm^2. The ablated plume was ejected at normal to the target surface and deposited on to the substrates that were mounted 45 mm away and parallel to the targets. The laser beam was focused by a UV grade plano-convex lens with a 50 cm focal length. The beam energy density or fluence was varied by changing the laser spot size on the target by altering the lenses to target distance.

The substrates were pasted to the face plate of the substrate heater. A thermal couple was embedded in the face plate directly underneath the substrate for accurate monitoring the deposition temperature of the films. Deposition temperature was typically in the range of 500°C to 700°C.

For the deposition of nitride films, they all need to be grown under high vacuum. After the cryopump has evacuated for sometime, we can gradually heat up the substrate. When it reached the desired temperature, the laser was switched on and films were deposited at a pulse repetition rate of 10 Hz. The thickness of the films was estimated about 200 nm. Actually, the growth rate achieved by PLD can be varied through adjusting the repetition rate of the laser, which is useful for thickness control down to atomic level and growth rate manipulation.

In order to achieve good crystalline film, *in-situ* annealing process is necessary after the film growth. It is done by keeping the deposition temperature for about 20 minutes under high vacuum. It permits greater atomic migration such that more atoms on the crystal edges can migrate into the faces of neighbouring layers and improve the crystalline quality of those films.

3.4 Structural analysis and electrical property characterization of thin films

The structure of the thin films was characterized by X-ray diffractometry (XRD). For the characterization of the epitaxy of the deposited films, θ-2θ scan, ω scan (rocking curve) and 360°-Φ scan were carried out.

For the epitaxial growth of thin films, only one set of planes of the family (00*l*) are detected and no trace of other reflection shall be seen. But if we observe just a single family of peaks in θ-2θ scan, there is no guarantee that the films are epitaxially grown on the substrates. There is the possibilities for the poor plane-to-plane alignment such as twisting between planes or poor in-plane mosaicity. All we can conclude is that the films are highly oriented in the out-of-plane direction.

The degree of orientation can be characterized by the ω-rocking curve. The smaller the FWHM of the rocking curve profile, the higher the degree of orientation of the films. Typically a FWHM with less than 1° is considered to be highly oriented films. Both single crystal substrates such as MgO and Si show a FWHM of 0.2°, the instrumentation resolution limit of our XRD.

To confirm the epitaxy of the deposited films 360°-Φ scans of the substrate and of the films are required. Since all our substrates and films are of cubic structures it is useful to determine whether the films are lattice matched and "cube-on-cube" grown on the substrates. A Φ scan is done by fixing θ and 2θ angles corresponding to

the (202) diffraction of substrates and films whereas angle φ is tilted by 45°. For a simple cubic structure, four characteristic peaks separated by 90° are observed in the 360°-Φ scan. If the four peaks of the film are on the same φ angles as those of the substrates, we can say that the film was epitaxially grown on the substrates.

3.4.1 X-ray diffractometer (XRD)

The crystal structures of our obtained thin films were characterized by using an X-ray diffractometer (Philips X'pert system) operated in a four-circle mode. In our XRD measurements, parallel optics for thin film geometry was employed. The K_α radiation of Cu (λ = 1.54 Å) was used throughout and the K_β line was filtered by Ni filter. Fig. 3.4.1a shows the X-ray diffraction of a crystal. When X-rays fall on atoms in a crystal, each atom scatters a small fraction of the incident beam. Thus, the reflected beams from all atoms in the crystal planes involved may interfere. The resultant reflected beams is only strong if the path difference between successive planes is a whole number of wavelength of the incident X-ray radiation. Thus, reinforcement only occurs for planes p and q when AB + BC = nλ where n is a positive integer and λ is the wavelength of the X-rays. If d is the distance between planes of atoms and θ is the angle between the X-rays beam and the crystal plane, then AB + BC = 2d sinθ. The reflected beam has a maximum intensity when

$$2d \sin\theta = n \quad \text{(Bragg's Law)} \ldots\ldots\ldots\ldots\ldots\ldots (3.4.1i)$$

and the d value for a simple cubic lattice can be calculated as

$$d = \frac{a}{\sqrt{h^2 + k^2 + l^2}} \ldots\ldots\ldots\ldots\ldots\ldots (3.4.1ii)$$

where a is the lattice constant of the crystal structure and h, k, and l are the reciprocal lattice indices for a-axis, b-axis and c-axis respectively.

For example, to calculate the 2θ angle of Si(004)

As a = 5.43 Å for Si(001), λ = 1.54 Å for K_α radiation of Cu in X-ray,

From equation (3.4.1ii),

Then $d = 5.43 / (0+0+4^2)^{1/2}$ Å = 1.3575 Å

Hence

$$2\theta = 69.11^\circ$$

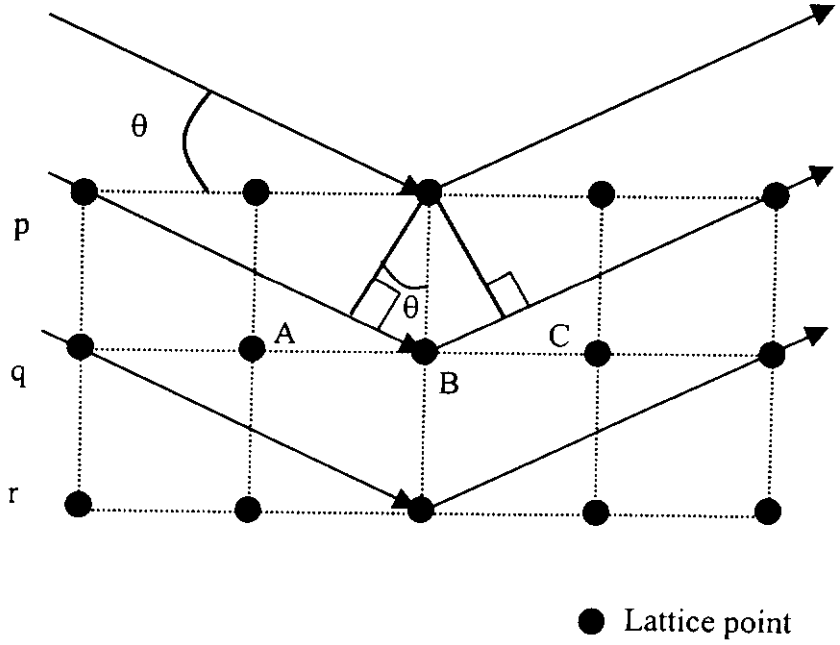

Fig. 3.4.1a The schematic diagram of X-ray diffraction of a crystal. The X-rays striking the crystal interact with a number of lattice planes.

We perform several modes of angle scanning of the X-ray diffraction for characterization of the crystal structure of our thin films. They include θ-2θ scan, ω scan and 360°-Φ scan. Fig. 3.4.1b shows the three axes rotation of the sample, i.e. θ axis, φ axis and Φ axis. For the normal θ-2θ scanning, it is commonly used to determine the crystal phase formed with the orientation normal to the substrate surface. The degree of orientation of a certain peak or phase is reflected by the Full Width Half Maximum (FWHM) of the rocking curve in performing the ω scan. The smaller the value of FWHM of the rocking curve, the better are the crystallinity and orientation of the films. The Φ scan is used to characterize the in-plane epitaxy of the films. To confirm the epitaxy of the deposited films, a 360°-Φ scan should be additionally made. For cubic structures it is done by fixing θ and 2θ angles corresponding to the (202) substrates and setting φ to 45°. For good epitaxial cubic structured films, four characteristics peaks separated by 90° are observed. They are corresponding to (022), (202), $(02\bar{2})$ and $(20\bar{2})$ reflection planes and should coincide with those of the substrates.

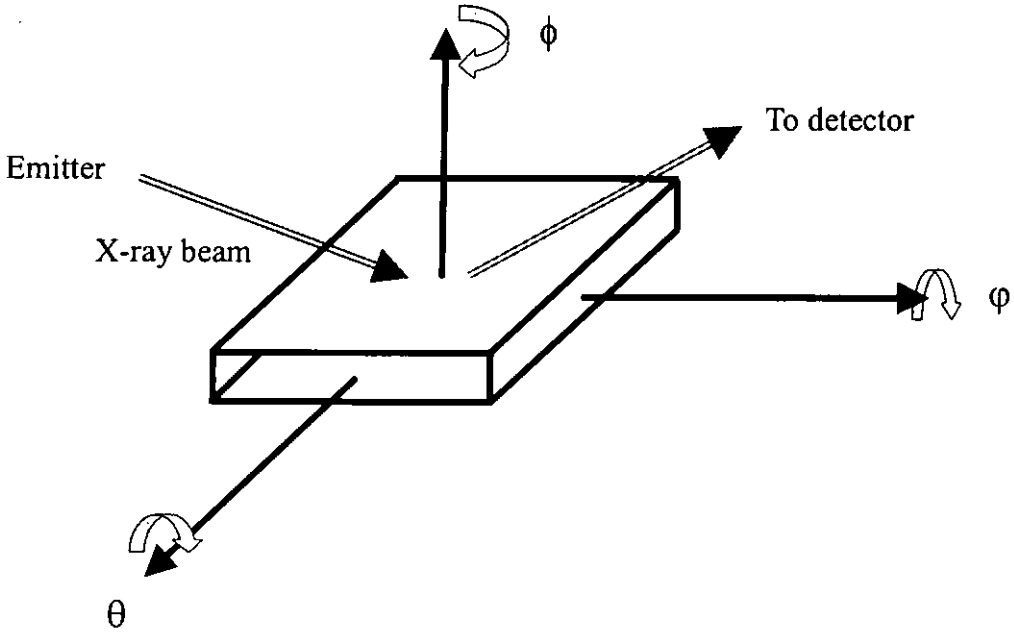

Fig. 3.4.1b The rotation axes of the sample relative to the X-ray emitter and detector.

3.4.2 Scanning electron microscopy (SEM)

Scanning electron microscopy (SEM) is a powerful and versatile technique for providing unique, yet often complementary, images and information of thin films. The SEM model we are using is a Leica Stereoscan 440. It gives a maximum amplification of 300,000. In contrast to optical microscopy, SEM combines very high resolution with great depth of field and has the ability to distinguish fine details. It is presently used in a variety of applications including the structure determination of composite materials, thin films; fracture analysis; and confirmation of chemical, and metallurgical composition of the samples.

Since the electron microscopy use electrons instead of light to carry the information generated during image information, all images are black and white. The first stage in the process of creating images is the production of the beam of electrons. The electrons are generated in the electron gun. The lanthanum hexaboride guns, are commonly used and are called lab-six guns. A voltage applied between the two terminals of the wire causes heating of the lanthanum hexaboride crystal. The hot crystal then emits electrons. After the beam of electrons has been formed, they pass through the anode aperture. They are then focused and deflected by a set of sophisticated electron optics. When the beam of electrons strikes the sample, a complex series of interactions occurs, resulting in the production of secondary electrons from the sample, which are collected by the detector. Then they are converted to a voltage and being amplified. The absorption and escape of secondary electrons are the major factors that contribute to their ability to produce a predominately topographical image in the SEM. An elastic interaction constitutes the

backscattered electrons, i.e., beam of electrons that have been scattered backward. Backscattered electrons are not strongly absorbed by the sample because of their high energies. The production of backscattered electrons is mainly dependent on the atomic number of the sample. The higher the atomic number, the more backscattered electrons are emitted.

In the SEM, nearly all samples require some type of preparation before mounting on the metal holders. They must be firmly mounted and electrically conductive. For samples that are non-conductive, may cause severe problems during the imaging and photographic process may arise. A negative charge builds up gradually from bombardment by the beam of electrons. Abnormal contrast and splitting of the image result from the uneven distribution of the negative charge on the sample. In order to prevent the formation of undesirable negative charges, the most common practice is to apply a thin layer of gold coating on the sample's surface. This uniform coating can minimize such effect and produces a high quality SEM image.

3.4.3 Atomic force microscopy (AFM)

Atomic force microscopy (AFM) is another ultra-high resolution microscopic technique. Instead of using a beam of electrons to image the sample, it uses a fine mechanical probe to scan the surface of the sample. In AFM, a very fine tip is mounted on a triangular piece of metal foil called the cantilever. The AFM probes the surface of a sample with this sharp tip, which is only a couple of microns long and often less than 100 Å in diameter. A laser beam is also directed at an angle toward the surface of the foil. The deflected beam of the laser is detected by a photodiode. Forces between the tip and the sample surface cause the cantilever to bend, or deflect. A detector measures the cantilever deflection as the tip is scanned over the sample. In addition, the sample is mounted on the piezoelectric device. The measured cantilever deflections allow a computer to generator a map of the surface topography. AFMs can be used to study insulators and semiconductors as well as electrical conductors. A better resolution image can be produced in the same manner as that of an SEM.

The force associated with AFM is an interatomic Van Der Waals force. The dependence of the force upon the distance between the tip and the sample is shown in Fig. 3.4.3a. Two distance regimes are labeled. One is the contact regime and the other is the non-contact regime. In the contact regime, the cantilever is held less than few angstroms from the sample surface, and the interatomic force between the cantilever and the sample is repulsive. In the non-contact regime, the cantilever is held on the order of tens to hundreds of angstroms from the sample surface, and the interatomic force between the cantilever and the sample is attractive.

For cases where a sample of low moduli may be damaged by dragging the tip across its surface, intermittent-contact mode (so called tapping mode) of AFM operation is preferred and applied in our experiments. In this mode, the cantilever tip is vibrated to tap the sample. The cantilever's oscillation amplitude changes in response to tip-to-sample spacing. An image representing surface topography is obtained by monitoring this changes.

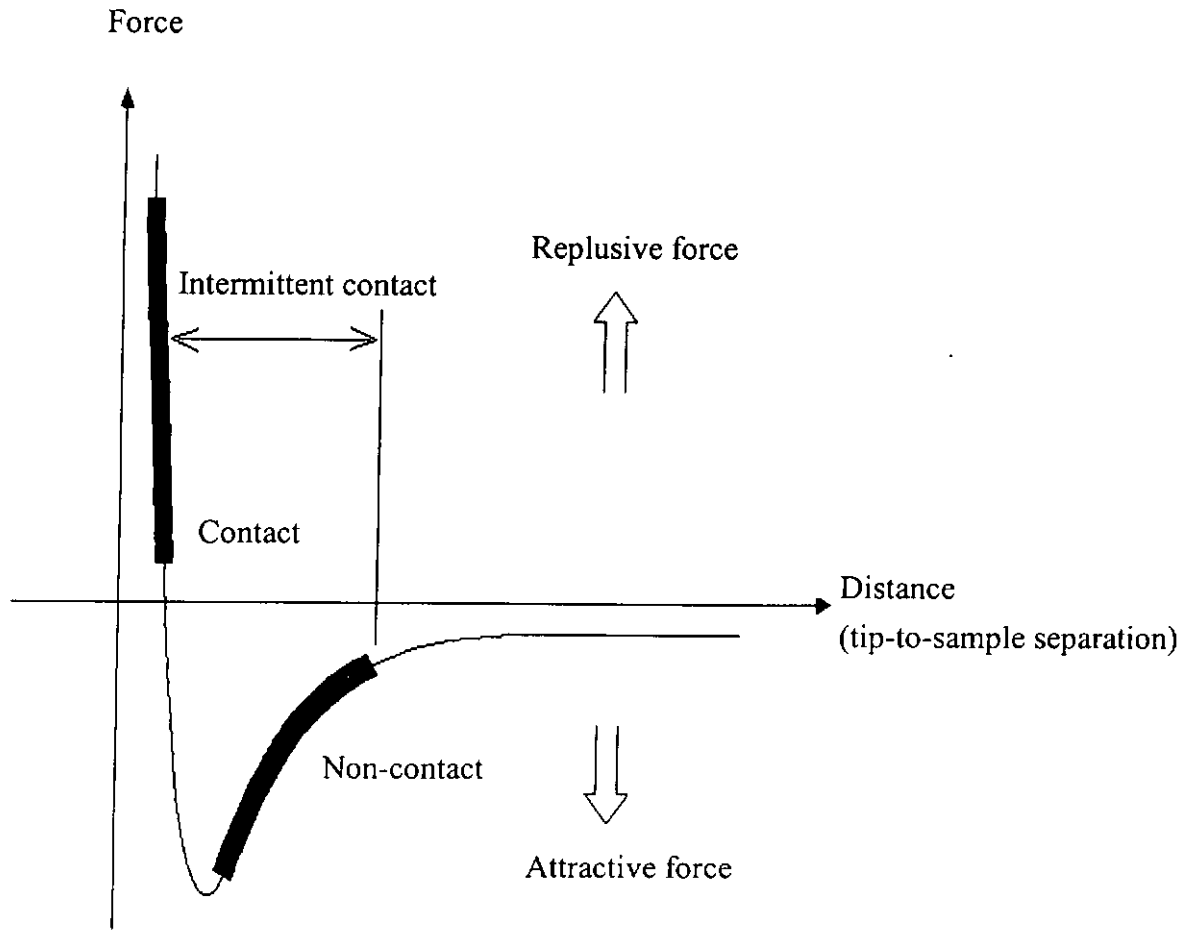

Fig. 3.4.3a The schematic curve of interatomic force versus distance.

In the most common scheme, as shown in Fig. 3.4.3b, a laser beam bounces off the back of the cantilever onto a position-sensitive photodetector (PSPD). As the cantilever bends, the position of the laser beam on the detector shifts. The PSPD itself can measure displacements of light as small as 10 Å. As a result, the system can detect sub-angstrom vertical movement of the cantilever tip.

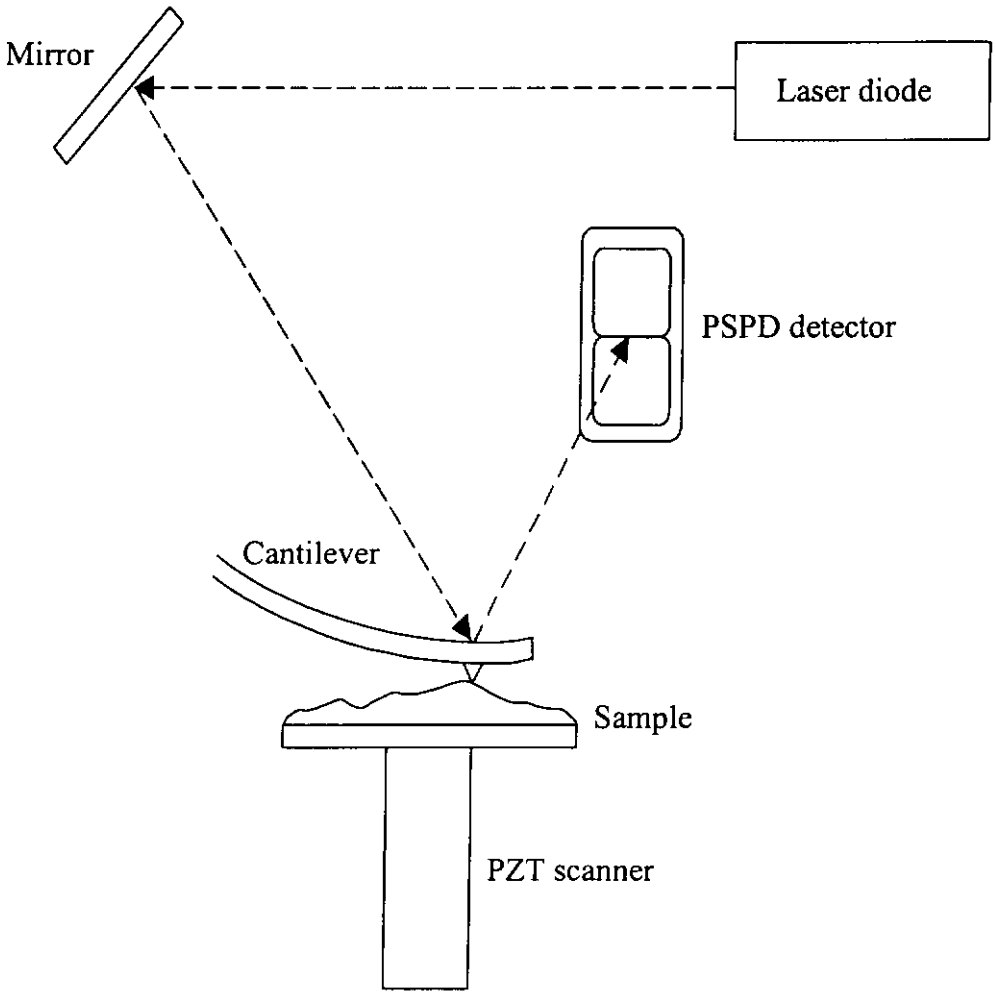

Fig. 3.4.3b The schematic diagram of beam-bounce detection.

3.4.4 Electrical properties measurements

In the present study, a four-point probe technique was used to characterize the electrical properties of the deposited films. It is a precise method as it can eliminate the contact resistance between the sample and the probes. A platinum wire, in which the potential difference between the wire terminals at constant current is proportional to the temperature, was used as the temperature sensor. A temperature control from room temperature to the liquid nitrogen temperature was achieved by a cryostat.

A constant current I, was allowed to flow through the two outer electrodes. A voltage V, developed between the two inner electrodes was measured and output to the y-axis of a plotter. The x-axis of the plot was the voltage measured from the platinum thermometer under different temperatures. As a constant current is supplied to the four-point probe, the change in the voltage is directly proportional to the change in the resistivity of the films.

A standard 747 Operational Amplifier in a negative feedback inverting amplifier mode was used to maintain a constant current. By adjusting the supply voltage, a constant current can be obtained. In the present set-up, the current was kept at 1 mA. Due to the Operational Amplifier is limited to 14 V swing, different value of constant current should be used for samples with different resistivity, in order to get a measurable signal. Therefore the resistance R is simply obtained by applying the Ohm's law, $V = I R$.

The electrical resistivity ρ (in unit of Ω cm) of the samples was calculated by the equation:

$$\rho = R \times t \times C.F.$$

Where R is the measured resistance, t is the thickness of the film, C.F. is the correction factor. The correction factors for a circular and rectangular samples are shown in Table 3.4.4a. (where s is the probe spacing)

		Square	Rectangle		
d/s	Circle	a/d = 1	a/d = 2	a/d= 3	a/d 4
1				0.9988	0.9994
1.25				1.2467	1.2248
1.5			1.4796	1.4893	1.4893
1.75			1.7196	1.7238	1.7238
2			1.9475	1.9475	1.9475
2.5			**2.3532**	2.3541	2.3541
3	2.2662	2.4575	2.7	2.7005	2.7005
4	2.9289	3.1127	3.2246	3.2248	3.2248
5	3.3625	3.5098	3.5749	3.575	3.575
7.5	3.9273	4.0095	4.0361	4.0362	4.0362
10	4.1716	4.2209	4.2357	4.2357	4.2357
15	4.3646	4.3882	4.3947	4.3947	4.3947
20	4.4364	4.4516	4.4553	4.4553	4.4553
40	4.5076	4.512	4.5129	4.5129	4.5129

Table 3.4.4a Correction factor (C.F.) for the sheet resistances measurement with the four-point probe.

Different geometry can have different values of the correction factor. It depends mainly on the ratio of the sample width and apacing between two neighbouring probes. The d/s and a/d ratios for our deposited films are about 2.5 and 2, respectively. That is, C.F. = 2.3532. The resistivity of the samples become

$$\rho = R \times t \times 2.3532$$

Therefore, the R-T profile can be easily obtained by using this automation system.

Chapter 4

Fabrication and characterization of TiN/Si

4.1 Introduction

During the past few years, the interest in transition-metal nitrides has increased substantially. These refractory nitrides are useful materials with numerous industrial applications and a promising future. For example, their refractive nature makes them an ideal material for protective and wear resisting coating in cutting tools. Their excellent electrical conductivity has also helped to make them useful in electronics as good ohmic contacts and superconductors. Commonly used conducting nitrides include Titanium Nitride (TiN), Tantalum Nitride (TaN), Niobium Nitride (NbN), Tunsten Nitride (WN) and Zirconium Nitride (ZrN).

A typical face-centered cubic close-packed structure (fcc) of TiN is shown in Fig. 4.1. TiN film is electrically conducting. It has a relatively low resistivity (20-40 μΩ cm at room temperature) and showed a metallic behaviour in the resistivity-temperature measurements [Narayan et al., 1992]. In fact, TiN has been extensively used in semiconductor industries for providing good ohmic contacts and diffusion barriers to Si substrates. It has been reported that the TiN films can be fabricated on Si substrates by various film growth techniques such as laser physical vapor deposition [Narayan et al., 1992], reactive magnetron sputtering [Choi et al., 1991], etc. Crystalline TiN can be grown in high vacuum or nitrogen ambient with parallel epitaxy under a wide deposition temperature range (400-800°C) [Timm et al., 1997]. The resistivity of polycrystalline TiN is quite high and is not suitable for

contact metallurgy of microelectronic devices. To overcome this problem, the formation of good quality single crystal TiN films grown on Si(001) substrate is highly desirable. Despite its lattice constant of 4.24 Å, which is substantially smaller than that of Si (5.43 Å), epitaxial growth of TiN/Si is achieved by the mechanism of domain matching [Tsvetanka et al., 1994] with lattice misfit ~ 4%. It provides a mechanism of epitaxial growth which eliminates grain boundaries and fast dopant diffusion along grain boundaries. It was, however, noted that below 600°C, TiN(001) grows epitaxially on Si(001) in a Volmer-Weber type 4-on-3 cube-on-cube mode, giving rise to in-plane compressive biaxial stress. At higher temperatures, the growth mode changes to a Stranski-Krastinov 5-on-4 cube-on-cube type with dilation of the strained interface layer [Willmott et al., 1998].

In this chapter, we present the results for growing pure cubic TiN thin films on Si(001) substrates by PLD method. The effect of some of the laser deposition parameters on the quality of the TiN films is investigated systematically. The characteristics of the deposited films in terms of the substrate temperature and the films thickness are also presented in this section.

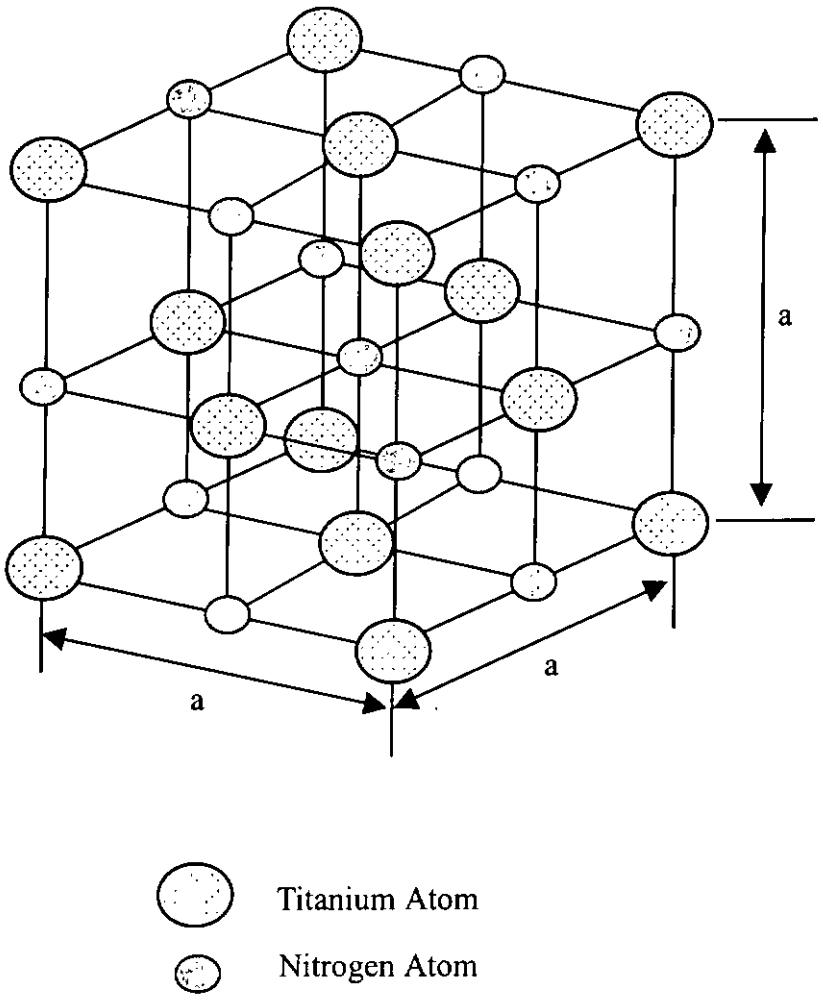

Fig. 4.1 Schematics representation of the TiN (fcc) structure.

4.2 Target analysis

Commercial hot-pressed TiN target of 99.5% purity which was bought from Electronic Space Products International (ESPI) company (grade 2N5) is used in the present studies. Apart from the deposition rate and resistivity measurement, X-ray diffraction analysis is also important for identifying crystalline quality and grain orientation of the films. The θ-2θ scan of the target is shown in Fig. 4.2.

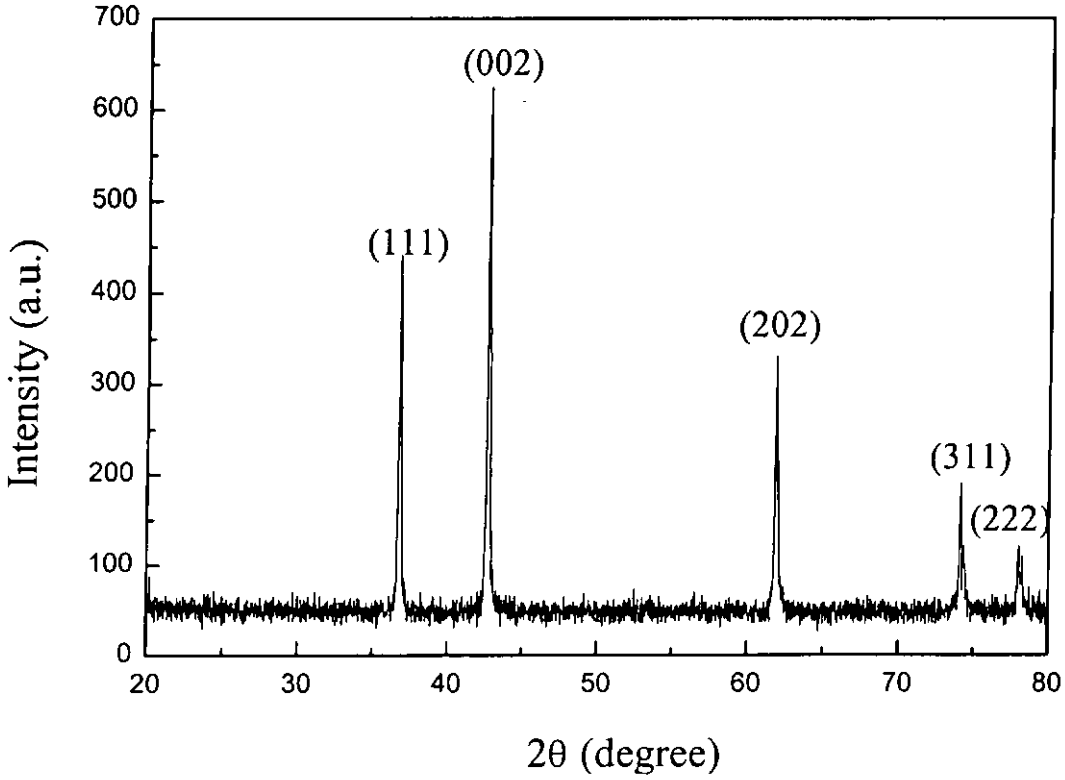

Fig. 4.2 The XRD pattern of the hot-pressed TiN target.

For the titanium nitride (TiN) target, the relative sharp peaks were identified and were labeled for reference. It was found that the (002) reflection obtained at a 2θ value of 42.4° is much stronger compared with others. For the TiN/Si single-layered structure, the prominent presence of this strong and high order reflection peak as evidenced in our experimemtal results that will be discussed in later sections.

From the X-ray diffraction pattern shown above, it suggests that the TiN target was well-crystallized and suitable for preparing thin films by PLD method.

4.3 Structural analysis of the films

TiN belongs to the family of refractory transition metal nitrides whose chemical bonds are both covalent and ionic in nature. It exhibits characteristics of a covalent compound such as high melting point, high thermodynamics stability and extremely hardness. It also possesses metallic features of good thermal and electrical conductivity. It is being extensively used as a chemical diffusion barrier for contact metallurgy in advanced microelectronic devices.

In our current experiments, all the TiN thin films were prepared by PLD at laser fluence of 4 J/cm^2 with repetition rate of 10 Hz for around 20 minutes. In order to improve the crystallinity of the deposited films, a subsequent annealing treatment is generally performed, usually for 20 minutes at the same deposition temperature. The typical thickness of the TiN films, as measured by the profiler and cross-section SEM imaging was about 200 nm. In the present study, epitaxial TiN films grown on Si(001) substrate can be obtained at a temperature ranging from 500°C to 700°C. The

stainless steel deposition chamber, evacuated by a rotary and a cryo pump, is capable of attaining a base vacuum pressure of ~10^{-6} Torr. Under visual inspection, all deposited samples show a uniform golden colour and have a low electrical resistivity (20-40 μΩ cm) comparable to pure metal. Since titanium can be easily oxidized to form titanium oxide or titanium oxynitride, it is necessary to keep the deposition chamber free of oxygen in order to avoid film oxidation.

The crystalline quality and compositional variations of TiN films on Si(001) substrates were identified by θ-2θ X-ray diffraction (XRD) analysis using CuKα radiation with a Ni filter. Fig. 4.3a shows the θ-2θ scan of TiN(001) layer grown on Si(001) substrate prepared at 650°C in high vacuum (4 x 10^{-6} Torr). The diffraction pattern reveals that the TiN films are oriented with TiN(001) parallel to the Si(001) substrate. Under these deposition conditions epitaxial TiN films are obtained, and no diffraction peaks corresponding to other titanium compounds are found. For films deposited at substrate temperature of 500°C to 750°C, the diffraction patterns are almost identical. The ω-scan rocking curve FWHM of the TiN(002) film was about 1.3° for sample prepared at 650°C. This suggests that well-oriented TiN films were formed on Si with good in-plane crystalline mosaicity as depicted in Fig. 4.3b.

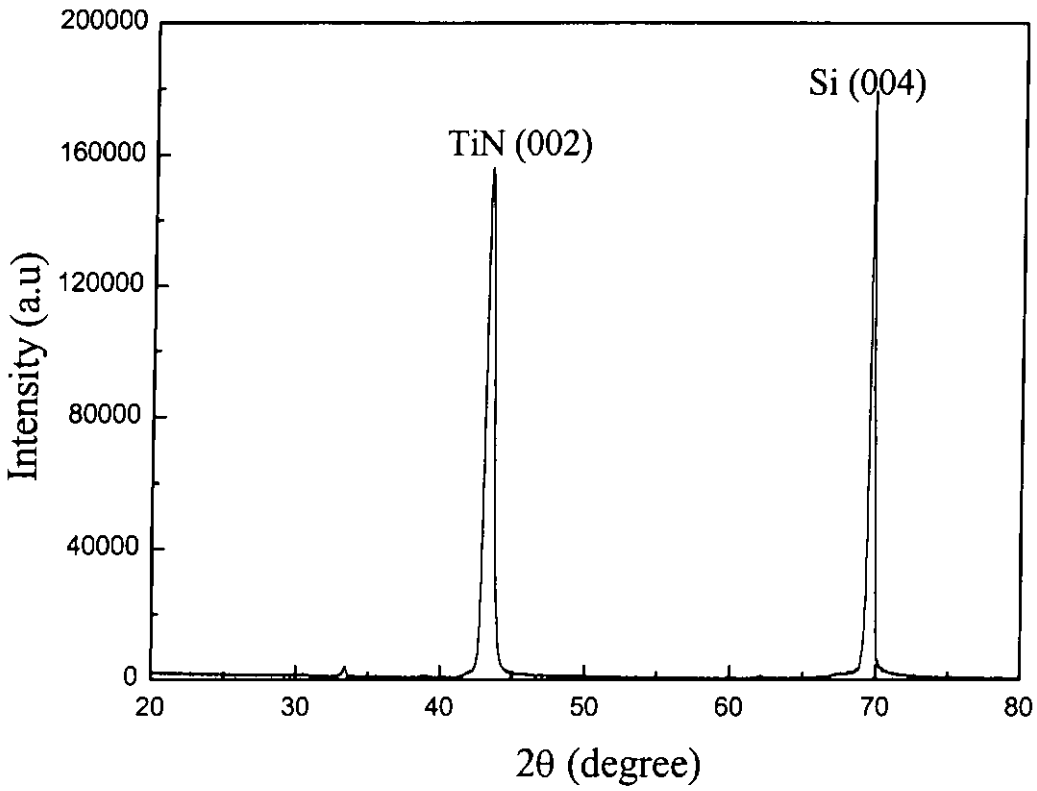

Fig. 4.3a X-ray diffraction pattern of a 200 nm thick TiN layer deposited on Si(001) substrate at 650°C under a pressure of 4×10^{-6} Torr.

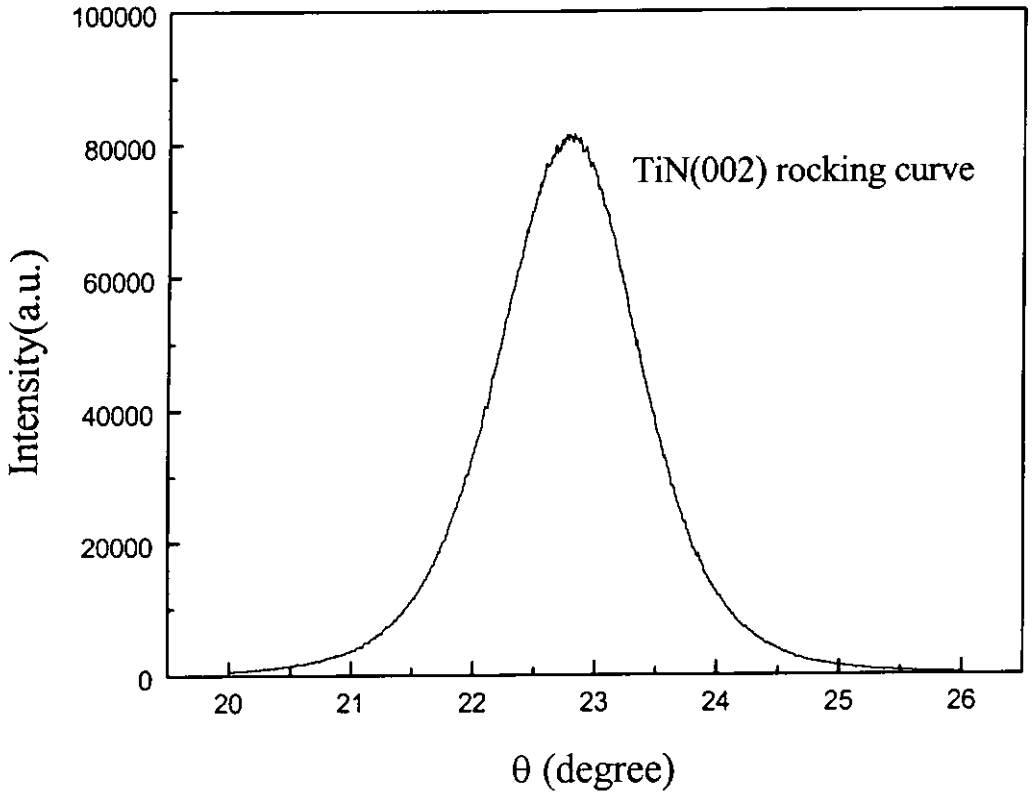

Fig. 4.3b X-ray rocking curve of TiN(002) diffraction peak exhibiting a FWHM of roughly 1.3°.

In order to determine whether the TiN films were epitaxially grown on the Si substrates, 360°-Φ scans of the TiN(202) and Si(202) reflections were performed. The presence of TiN in the cubic NaCl structure is evident, and the films show good crystallinity. Fig. 4.3c shows a clean characteristic 4-fold symmetry reflections corresponding to the (202) reflections of TiN and Si. Four sharp peaks of a cubic structure are observed. The positions of the peaks from the film are good matched with those of the Si(202) reflections. This strongly suggests that the TiN films were epitaxially cube-on-cube grown on top of the Si(001) substrates.

Based on the results shown above, it may be concluded that all the deposited films are highly oriented and a cube-on-cube parallel epitaxy is achievable even with large lattice mismatch. As we can see in our deposited films, epitaxial growth depends critically upon the nature of the interface, purity and the structure of the deposited layer. Structural characterization by XRD reveals an epitaxial relationship of $<001>_{TiN}||<001>_{Si}$.

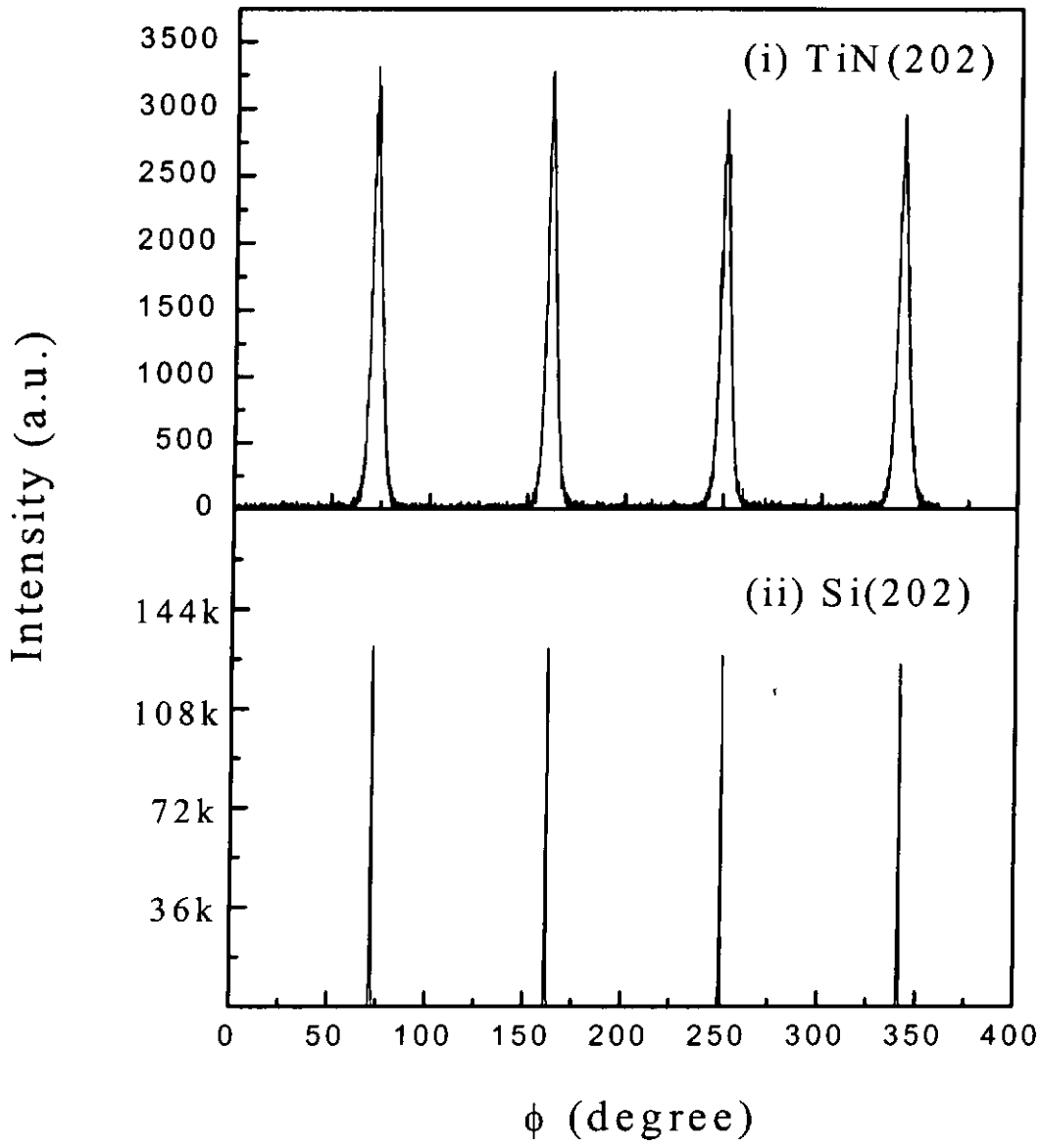

Fig. 4.3c X-ray diffraction Φ scan from heteroepitaxial TiN/Si structure, showing (i) TiN(202) and (ii) Si(202) family reflections with the rotation axis normal to the plane of the substrate.

4.4 Substrate temperature dependence

The microstructures of the TiN films were found to be strongly dependent on the substrate temperature. In the present work, the (002) peak intensity associated with TiN was found to increase with the substrate temperature. The variation of TiN(002) peak intensity and full-width at half-maximum (FWHM) with substrate temperature are depicted in Fig. 4.4a and Fig. 4.4b. The FWHM for Si substrates is about 0.15°. The FWHM of the TiN(002) reflection rocking curves were 2.2°, 1.9°, 1.34° and 1.17° for films prepared at 550°C, 600°C, 650°C and 720°C, respectively. Apparently, the FWHM value was decreased continuously, though slightly, by increasing the substrate temperature. Thus, these trends strongly imply that the orientation and crystalline quality of the TiN films improve with increasing substrate temperature.

Fig. 4.4c shows a series of X-ray θ-2θ diffraction patterns for TiN/Si deposited at different temperature of (i) 550°C (ii) 600°C (iii) 650°C (iv) 720°C under high vacuum of the same thickness of about 200nm. According to the 360°-Φ scan as mentioned in section 4.3, TiN can be grown directly on Si(001) through the mechanism of domain matching. At high temperatures, the growth mode of TiN changes from a 4-on-3 mode (Volmer-Weber type) to a 5-on-4 cube-on-cube type (Stranski-Krastinov) with dilation in the strained interface layer. Accompanying this change of growth mode, a reduction in the out-of-plane lattice constant was observed (From 4.23 Å to 4.12 Å).

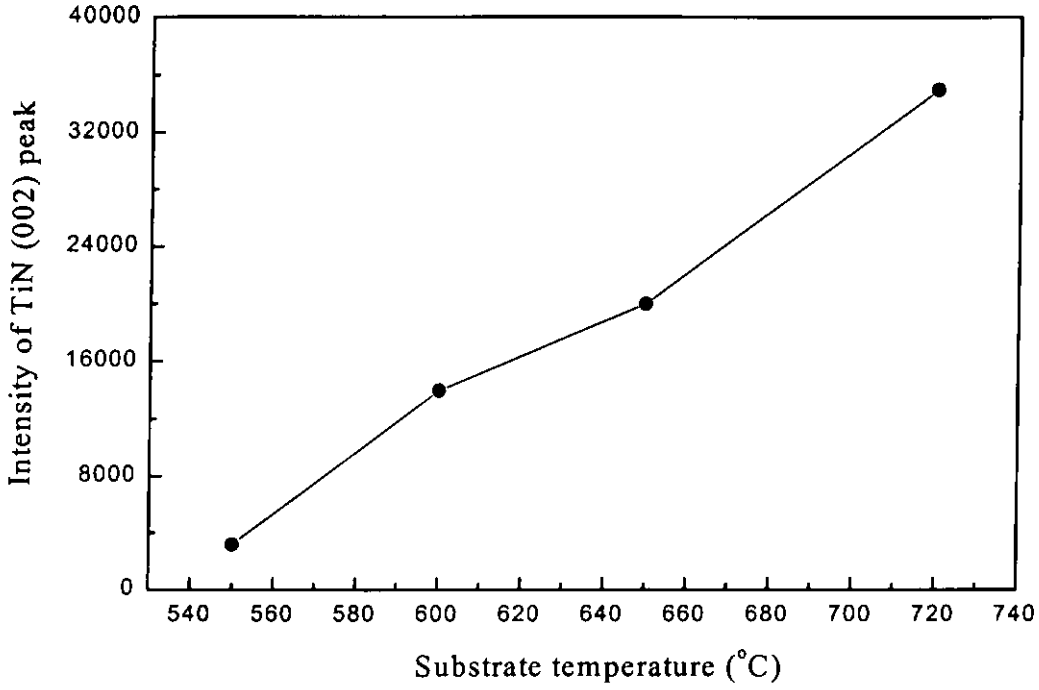

Fig. 4.4a Plot of variation of TiN(002) peak intensity with substrate temperature.

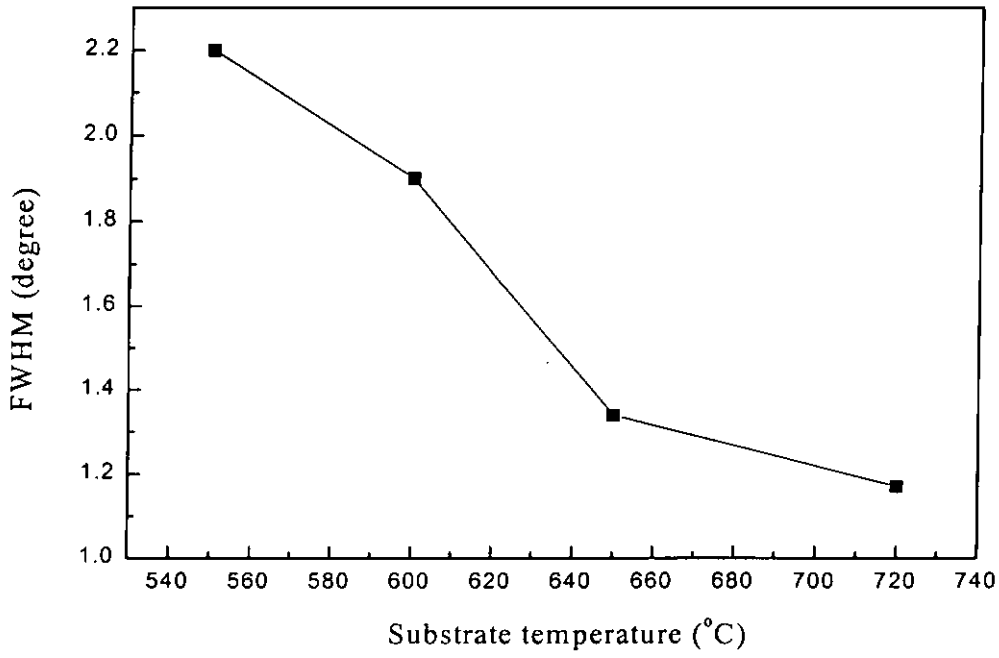

Fig. 4.4b Variation of full-width at half-maximum values with substrate temperature.

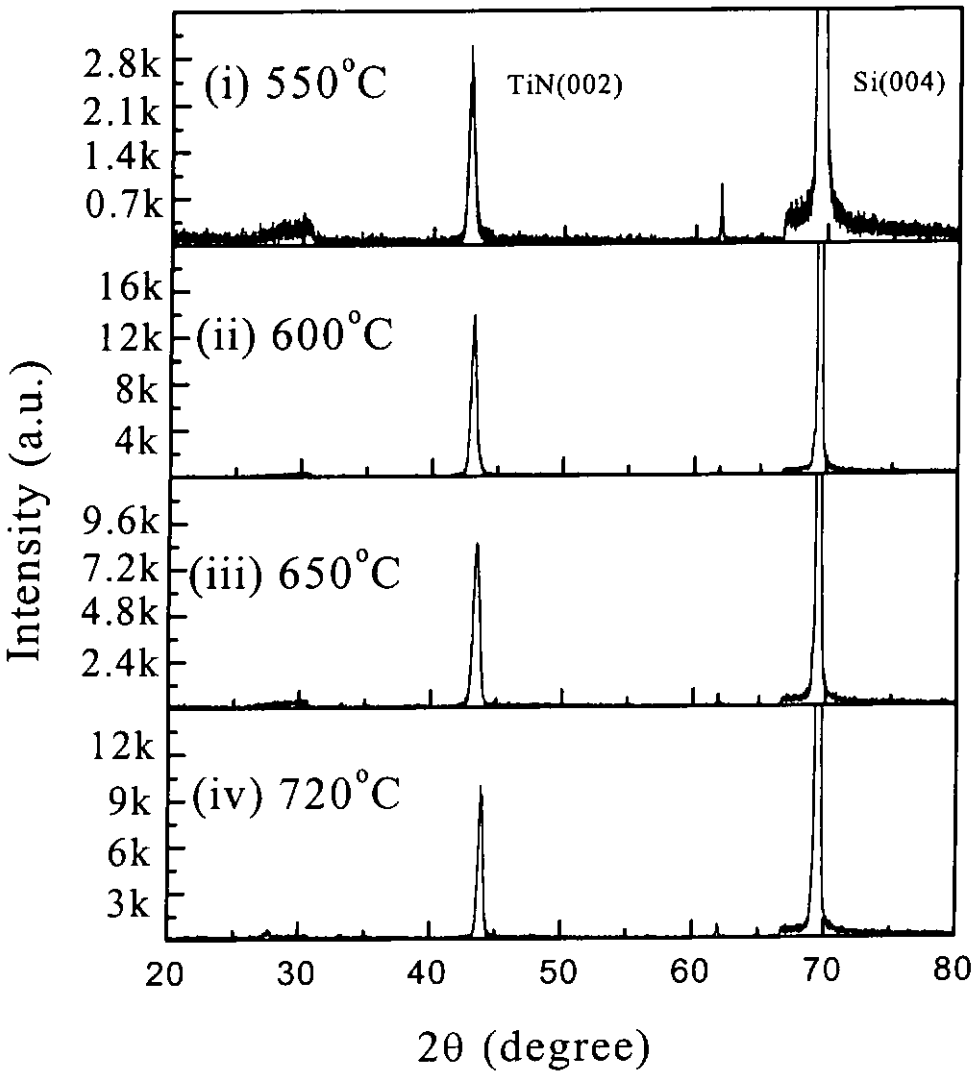

Fig. 4.4c X-ray θ-2θ diffraction pattern for TiN/Si deposited at different temperature of (i) 550°C (ii) 600°C (iii) 650°C (iv) 720°C under high vacuum with the same thickness of about 200 nm.

4.5 Films thickness dependence

We have made a detail examination of the TiN structural variation as a function of film thickness. Throughout the studies, apart from varying the laser ablation duration and substrate temperature, all other deposition conditions were remained the same. The variation in the latttice constant causes the diffraction peak to shift in its 2θ position. Such shifts were investigated for different TiN thin film thicknesses. Fig. 4.5a shows the XRD patterns obtained for the TiN film grown for 10, 20, 40 and 70 minutes, at a deposition temperature of 550°C and under a working pressure of 6 x 10^{-6} Torr. The corresponding film thicknesses are 100, 200, 350 and 740 nm respectively. The out-of-plane lattice constant is seen to decrease with film thickness. Whereas at higher film growth temperature (650°C), a remarkable result is obtained. The out-of-plane lattice constant of TiN layer increases gradually with film thickness. This is in marked contrast to film grow at 550°C. Fig. 4.5b depicts the XRD patterns of the TiN films prepared over deposition durations of 10, 20, 25, 30, 35 and 40 minutes. The deposition temperature was 650°C and the working pressure was also kept at 6 x 10^{-6} Torr. The film thicknesses varied from 81 to 648nm. Only the TiN(002) peak was observed from the X-ray diffraction patterns. The FWHM of the TiN(002) reflection was about 1.8°. As the layer gets thicker, stress relaxes at the growth temperature by generation of misfit dislocations. The stress is caused by both the lattice and thermal mismatch. The effects of lattice relaxation on the transformation must also be considered.

When increasing the deposition time at growth temperature of 550°C, the thicker films show relaxation from the strained interface layer. The TiN(002) peak

shifts to a higher 2θ position. The out-of-plane lattice constant is decreased from 4.21 Å to 4.15 Å as shown in Fig. 4.5c. On the other hand, when increasing the deposition time at the growth temperature of 650°C, the out-of-plane lattice constant is increased from 4.13 Å to 4.19 Å as evidenced in Fig. 4.5d. These lattice constants are all deviated from the normal relaxed value of 4.24 Å. For TiN films grown in high vacuum they are likely to be nitrogen deficient. The reduced lattice constant might due to non-stoichiometry of the TiN films. Deviations from stoichiometry always lead to a reduction in the lattice constant [Willmott et al., 1998]. Fig. 4.5e shows the XRD (002) reflections of the films with various thicknesses. For thinner film the reflection shifts to lower Bragg angles. This strongly suggested that an increased out-of-plane lattice constant is obtained when the films grow thicker.

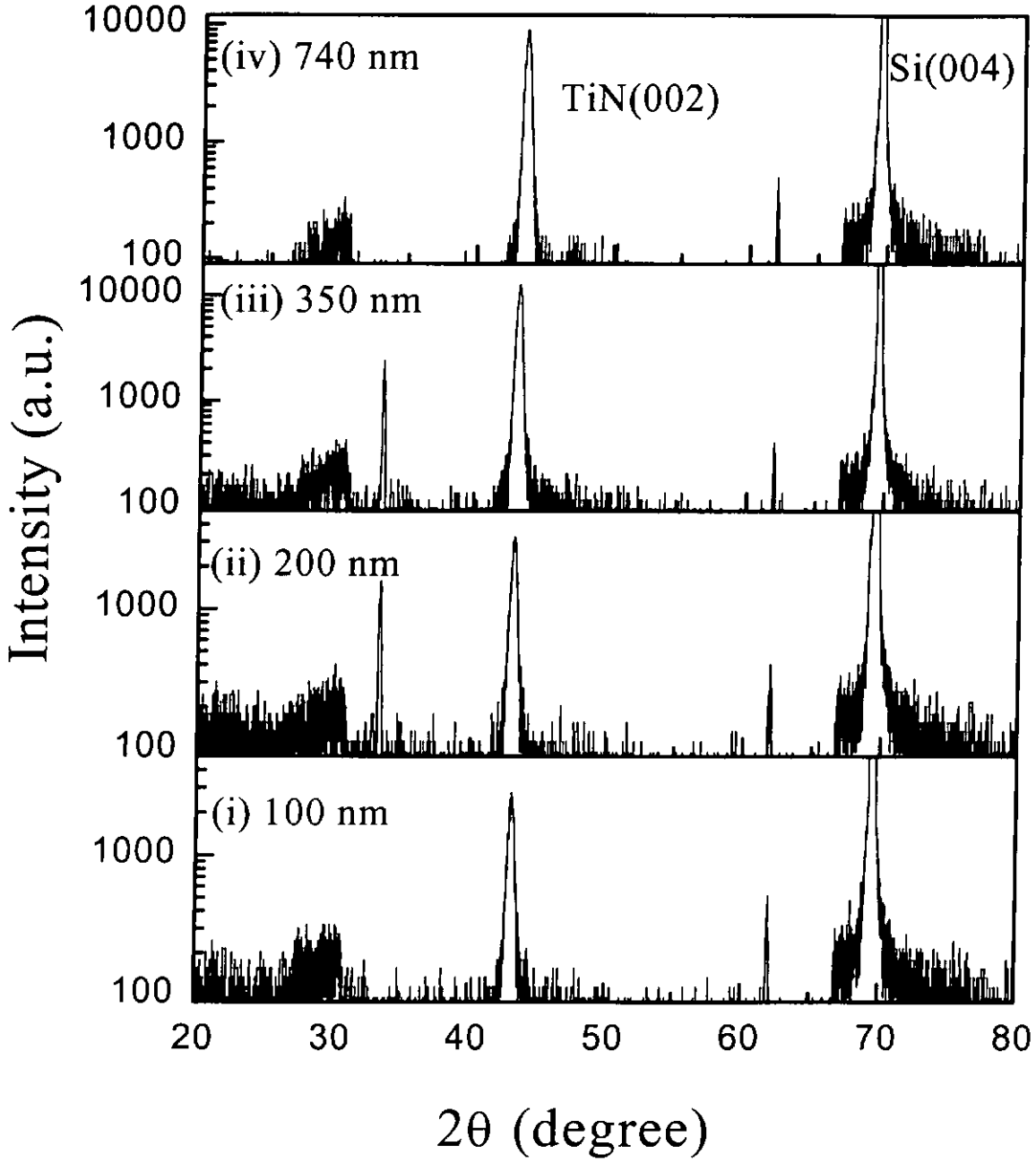

Fig. 4.5a XRD logscale patterns of the TiN films prepared for the deposition times of (i) 10, (ii) 20, (iii) 40 and (iv) 70 minutes at 550 °C.

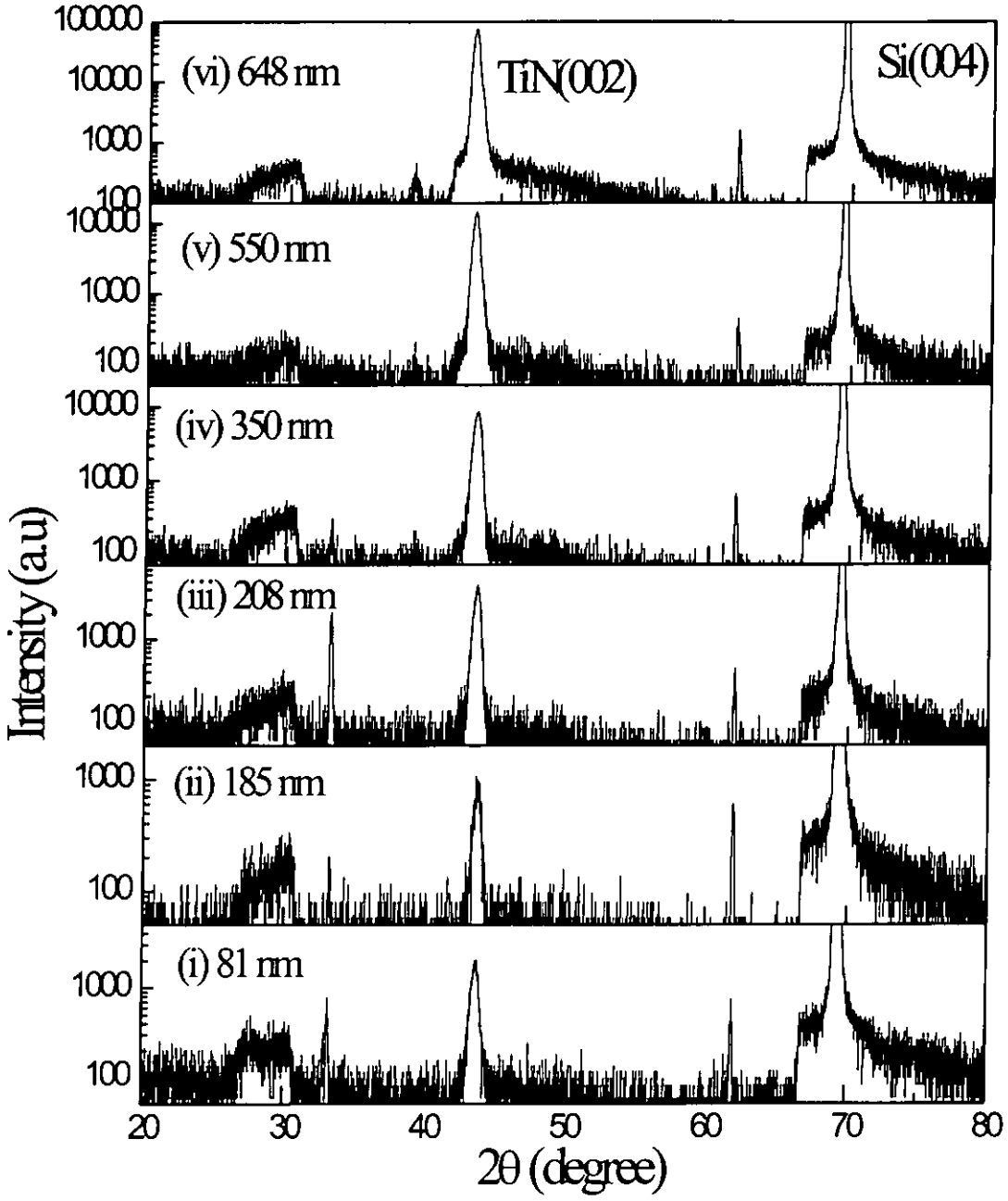

Fig. 4.5b XRD logscale profiles of the TiN films prepared for the deposition times of (i) 10, (ii) 20, (iii) 25, (iv) 30, (v) 35 and (vi) 40 minutes at 650 °C.

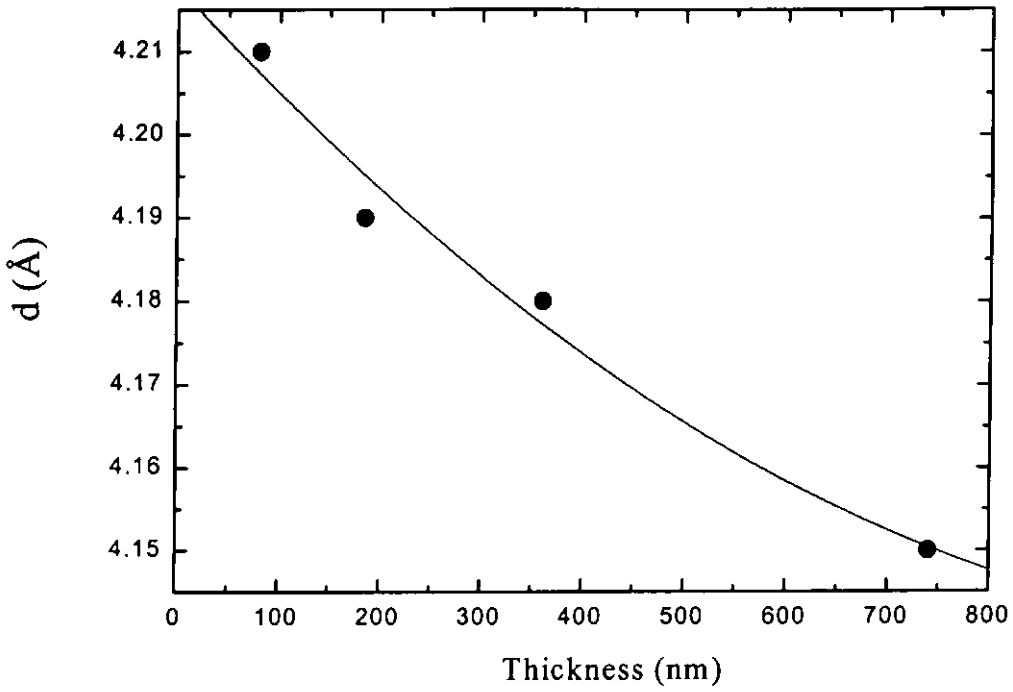

Fig. 4.5c The relationships between the out-of-plane lattice constant, d and thickness of the TiN films prepared at 550 °C.

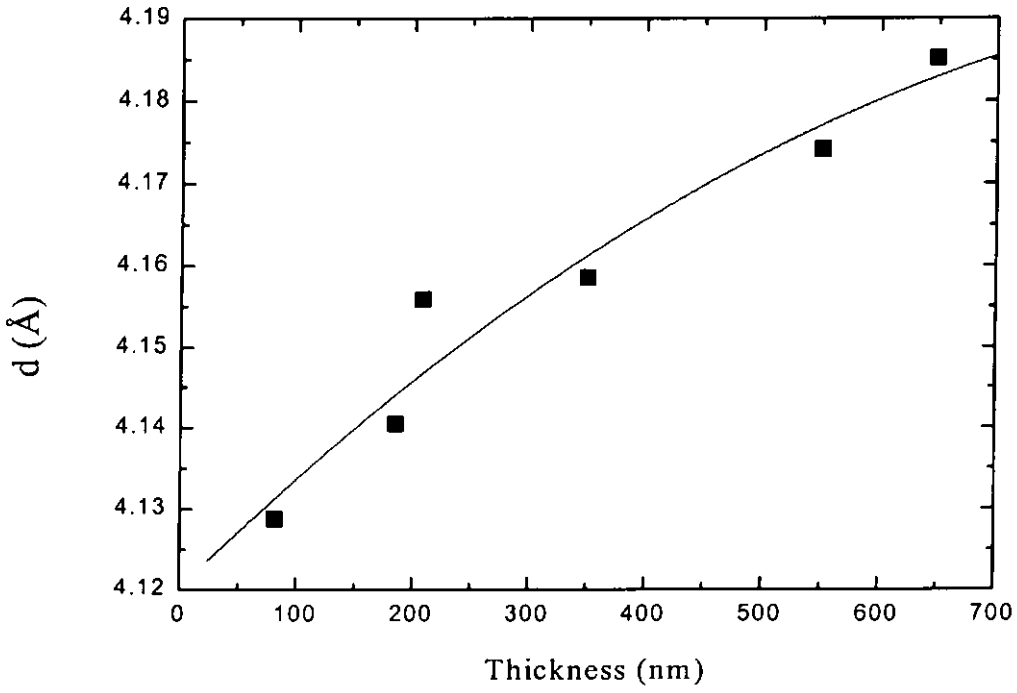

Fig. 4.5d The relationships between the out-of-plane lattice constant, d and thickness of the TiN films prepared at 650 °C.

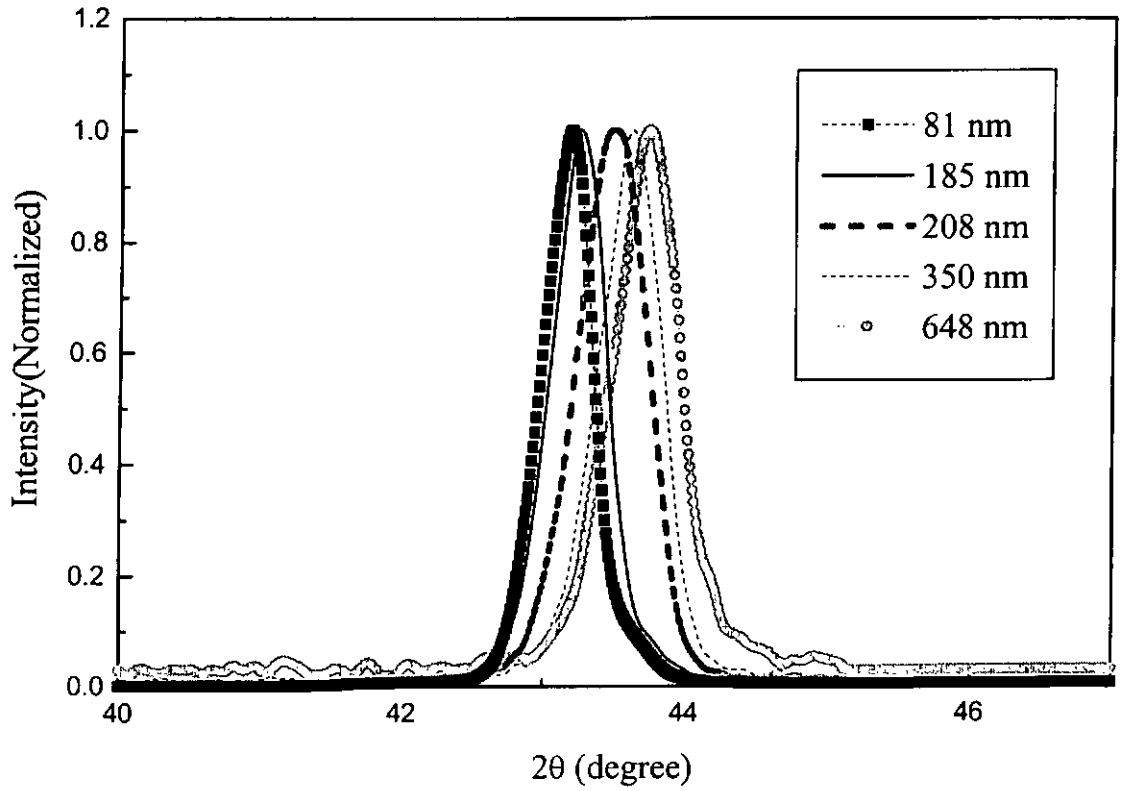

Fig. 4.5e XRD patterns of the TiN films of different thickness prepared at deposition time at 650 °C.

4.6 Electrical properties of TiN films

The electrical properties of TiN thin films with good crystallinity were measured by a standard four-point-probe technique.

Fig. 4.6 shows the R-T profile of the epitaxial TiN film deposited on Si. The substrate temperature was held at 650°C during deposition. It is seen from the figure that the electrical resistivity of the epitaxial TiN layer with 200 nm thick was as low as 44 μΩ cm at room temperature. The R-T characteristics exhibit a typically linear resistivities of metallic behavior over a wide temperature interval. It was also found that for films grown at temperature range from 500°C to 700°C, all of them showed good metallic profiles indicating that TiN is indeed an excellent electrical contact material for semiconductor devices. As the temperature decreases further, the resistivity of the film decreases gradually. For films deposited between 500 to 700°C, similar results are obtained.

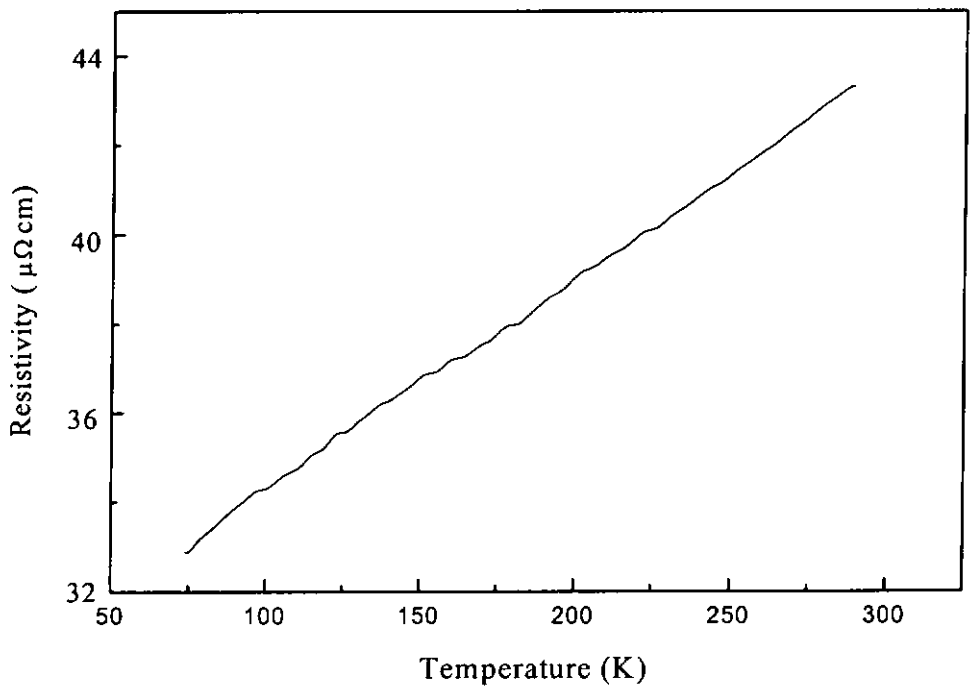

Fig. 4.6 Plots of the resistivity versus temperature (R-T) for TiN film grown at 650°C, showing a linear metallic behavior over a wide temperature range.

4.7 Surface morphology and cross-section

An excellent structural quality and sharp interface boundary of TiN/Si are revealed by plan-view and cross-sectional electron microscopy analysis. The surface roughness in films is typically attributed to the release of particles from the target. It is generally known that smoother films can be deposited by reducing substrate temperature. The TiN layer was grown at 650°C under a working pressure of 4×10^{-6} Torr. The relative thickness was about 200 nm. From the surface morphology profile of the film, an extremely smooth and crack-free surface can be obtained. The smoothness of the TiN surface can be observed from Fig. 4.7a. More detail is shown in tapping mode AFM image given in Fig. 4.7b. A remarkable surface roughness of 0.6 nm can be observed over the 1 μm x 1 μm area. The physical mechanism underlying the smooth growth is surface migration of atoms to sites of large binding energy at edges, producing a smooth crystal surface.

Fig. 4.7c shows the SEM image of fractured cross-section of TiN film. According to this figure, a sharp interface boundary is clearly shown with wide columnar grains. The thickness of the TiN film is about 200 nm. In summary, it was demonstrated that TiN films grown under optimized deposition condition (650°C), good crystal structure, a smooth surface morphology and sharp interface boundary could be obtained by PLD method.

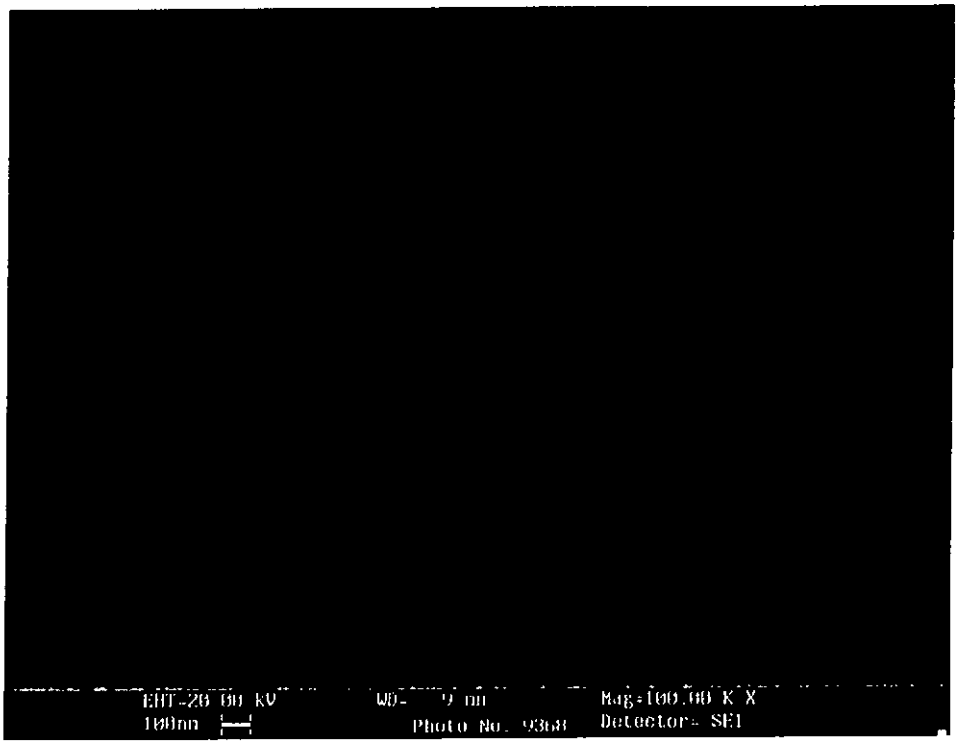

Fig. 4.7a SEM image of surface morphology of TiN thin film showing a crack free surface.

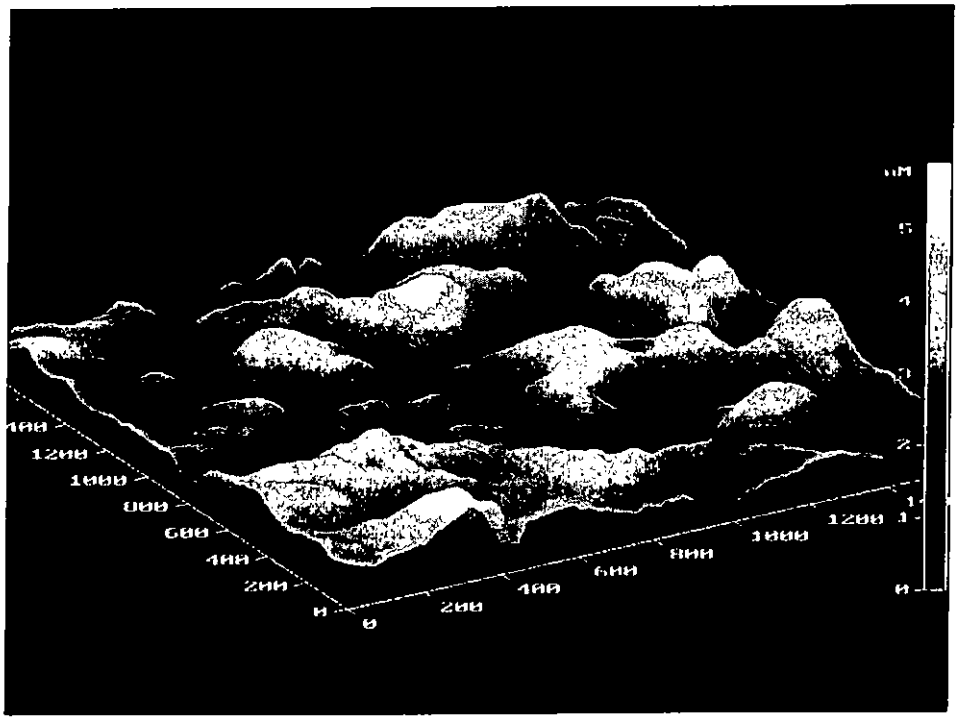

Fig. 4.7b AFM image of TiN film indicating an extremely smooth crystal surface.

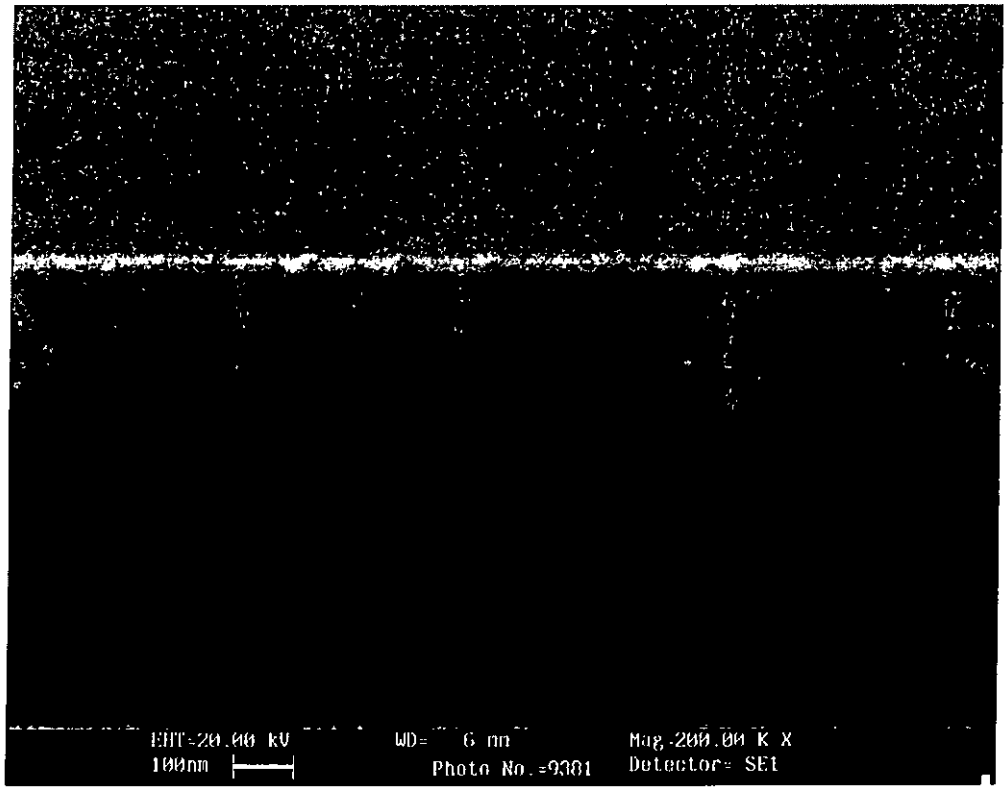

Fig. 4.7c The SEM cross-sectional micrograph showing 200 nm thick TiN film deposited on Si(001) substrate.

For TiN thin films deposited under different temperatures, the microstructures and surface roughness are not identical. The effect of substrate temperature on the growth of TiN has been studied in details by AFM. This can be seen from Fig. 4.7d and Fig. 4.7e. All the images were taken at nearly the same area of 1.6 μm x 1.6 μm. For most thin film technologies, it is essential to minimize the induced surface or interface roughness. Otherwise, it will seriously degrade the properties of the electronic devices. Often the parameter for quantitative evaluation of the surface roughness is based on root-mean-square (rms) roughness. Typically, smooth surfaces are characterized by rms values of ~1 nm or less. In Fig. 4.7e, the rms roughness of TiN films deposited at 550°C, 650°C and 720°C are 0.574 nm, 1.015 nm, and 11.68 nm respectively. AFM images have indicated that the microstructures and roughness of the films are dramatically changed when the deposition temperature increases.

The crystallinity of the as-deposited TiN films is greatly affected by the growth temperature. In general better crystallinity and larger grain size are obtained for films grown at elevated temperature. However, it is noted that film growth at too high temperature (> 720°C) should be avoided. Apart from producing a rougher surface, high temperature inevitably causes severe atomic diffusion into the Si substrate. From the experimental results, we can conclude that the surface morphology of the films is strongly affected by the substrate temperature and is best at 600-650°C.

(i)

(ii)

(iii)

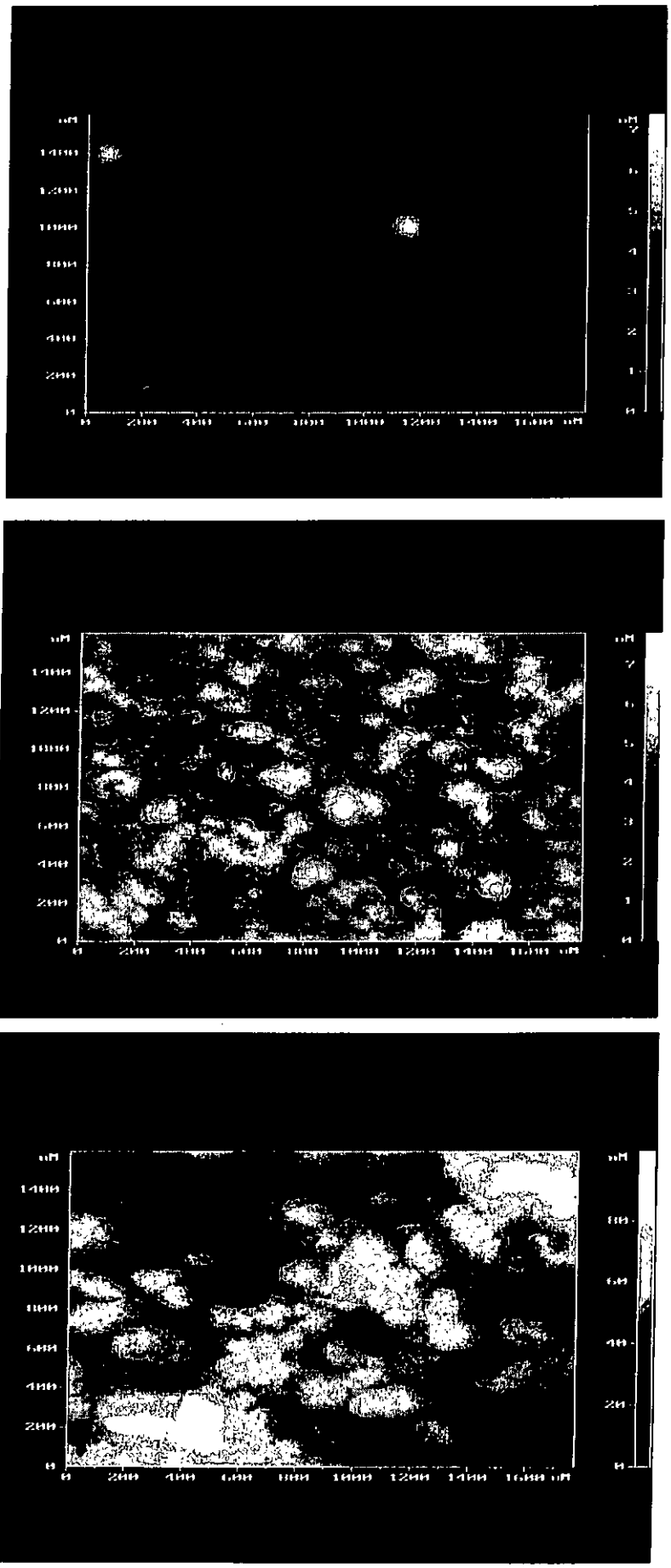

Fig. 4.7d The variation of the microstructures for films grown at (i) 550°C (ii) 650°C (iii) 720°C.

(i)

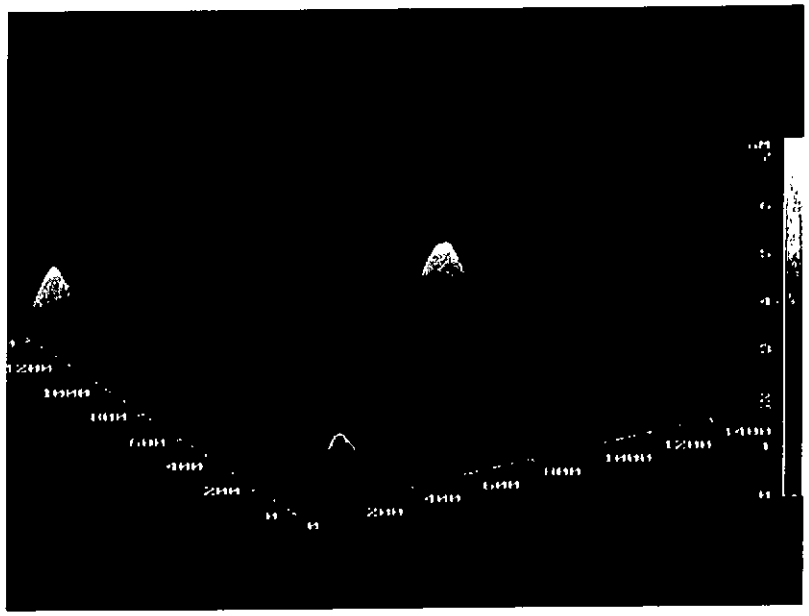

(ii)

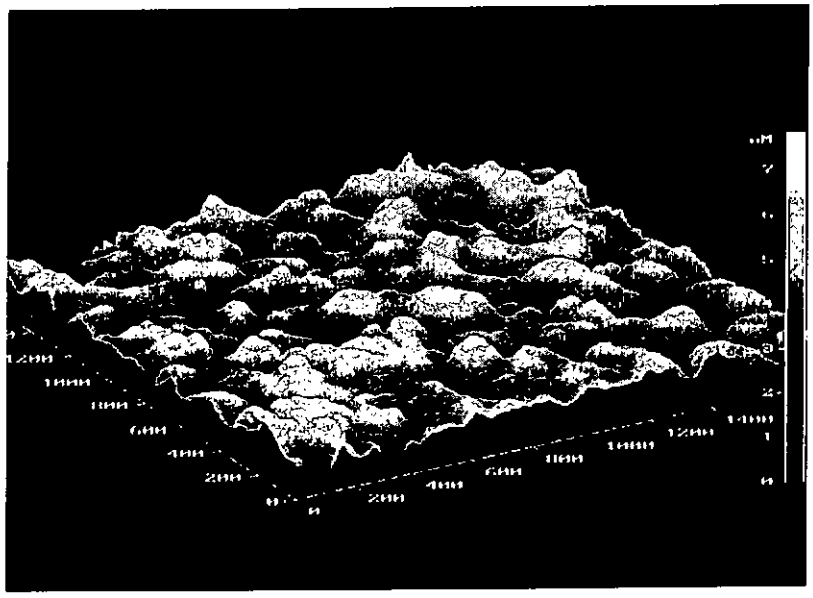

(iii)

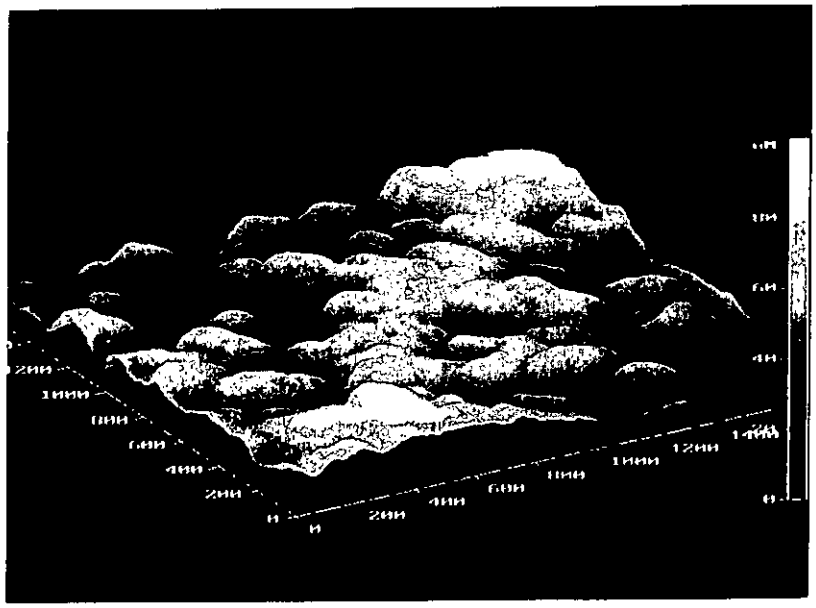

Fig. 4.7e The variation of the surface roughness for films grown at (i) 550°C (ii) 650°C (iii) 720°C.

Chapter 5

Fabrication and characterization of TaN/Si, TaN/MgO and TaN/TiN buffered Si substrates

5.1 Introduction

Owing to their high stability and excellent conductivity, refractory metal nitrides are widely recongnized as an attractive class of materials that can be used as diffusion barriers in metal-semiconductor contacts [Nicolet, M. A., 1978] and has a potential application as a hard coating material [Ezugwu et al., 1987]. Among those refractory metal nitrides, tantalum nitride (TaN) films are of particular interest as they are used extensively in microelectronics and as a thin film diffusion barrier between silicon and metal overlayers of Ni [Kanamori, S., 1986], Al [Wittmer Marc., 1982] and most recently Cu [Oku et al., 1996; Norya et al., 1993]. Several methods have been reported for the preparation of TaN films, such as reactive sputtering [Abdin, S., 1979], magnetron sputtering [Mehrotra et al., 1987], triode sputtering [Zhang et al., 1994], and ion beam assisted deposition (IBAD) [Ensinger et al., 1995]. Recently, pulsed laser deposition (PLD) has shown to be one of the most attractive methods to prepare high quality multi-component thin films.

The structure of tantalum nitrides can be described as close-packed arrangements of Ta atoms with N atoms inserted in interstitial sites. All epitaxially grown structures with sharp and clear interface will have superior electrical characteristics and excellent mechanical properties. However, tantalum nitride films

are difficult to grow on single crystal Si substrates due to large lattice mismatch. Pure cubic TaN films epitaxially grown on single oxide crystals such as MgO has been reported only recently [Greene et al., 1999]. However, epitaxial TaN grown on Si substrate has not been reported. In this chapter, we present evidence for the growth of epitaxial cubic TaN thin films on MgO and TiN buffered Si substrates. Their structural, electrical and mechanical properties are studied.

5.2 Target analysis

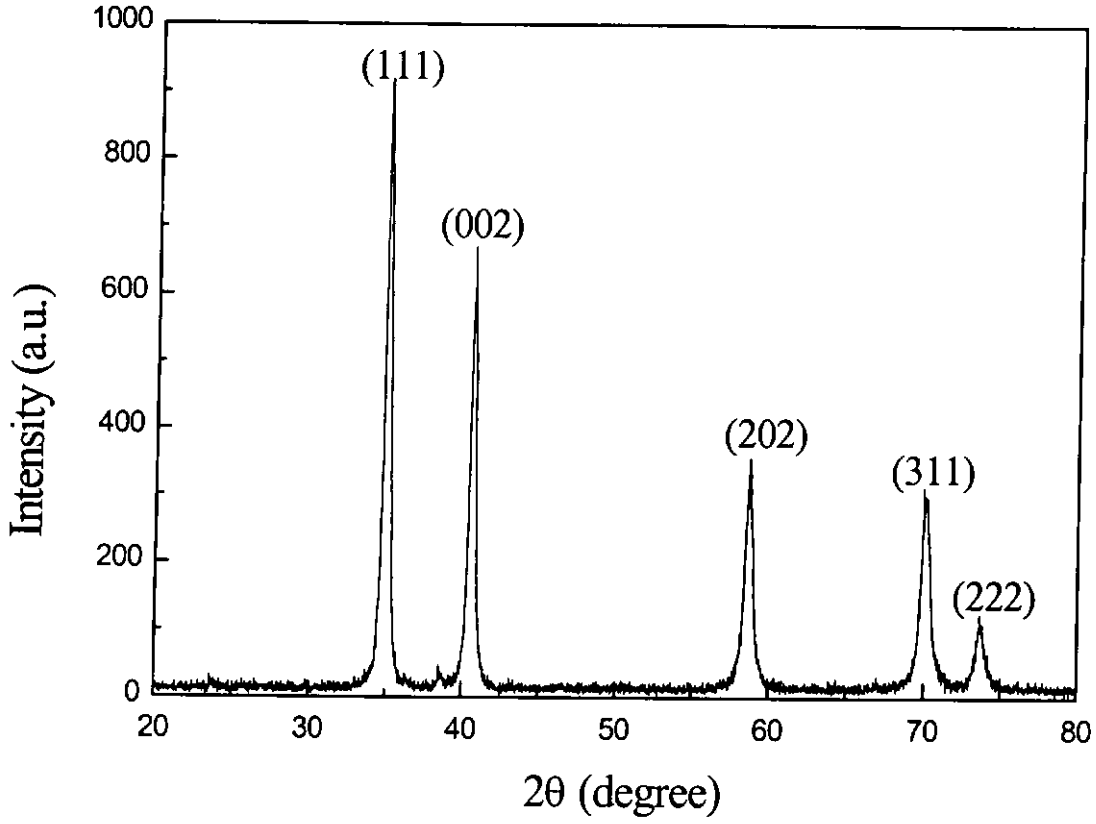

Fig. 5.2a The XRD pattern of the hot-pressed TaN target.

For the tantalum nitride (TaN) target, there are five distinct XRD diffraction peaks in the θ-2θ scan from 20° to 80°. The intensity of the first two peaks are much stronger than other peaks as shown in Fig. 5.2a. Crystal orientation indices could be found via calculation from the peak positions using a modified version of the Bragg equation as mentioned in 3.1.4. The reflection peak assignments are (111), (002), (202), (311) and (222) at 34.81°, 40.62°, 58.37°, 69.98° and 73.74° respectively.

5.3 Structural analysis of TaN films

5.3.1 TaN/Si

Among those refractory nitrides, TaN has been attractive due to its extremely high thermal stability, excellent mechanical robustness, high hardness at high temperature, stable electric resistivity, enhanced chemical inertness and good resistance to wear, oxidation and corrosion [Kirby, P. L., 1978]. All these features can be attributed to its strong electronic-bonds.

The TaN films are grown at substrate temperature of 550°C-720°C with 100 nm thick. Transition metal nitrides have been studied to establish thermal stable and adhesive metallization schemes with low resistivity [Wittmer Marc., 1980; So et al., 1988]. Like the carbides, the bonding is mostly metallic with some covalent and ionic bond components.

Although both the TaN and Si have cubic structure, their lattice mismatch is large (a = 4.336 Å for TaN and a = 5.43 Å for Si). It is difficult to fabricate epitaxial TaN films directly onto Si substrates. Structural properties of TaN/Si using X-ray diffraction indicated that there exists no preferred oriented grains, suggesting an amorphous layer at the interface is formed in the initial stage of film growth. Fig. 5.3.1a shows the XRD θ-2θ scan pattern of TaN/Si. The TaN film was deposited at 650°C under a working pressure of 2 x 10^{-5} Torr. The results show that the crystallinity of the film is poor and perhaps mainly amorphous.

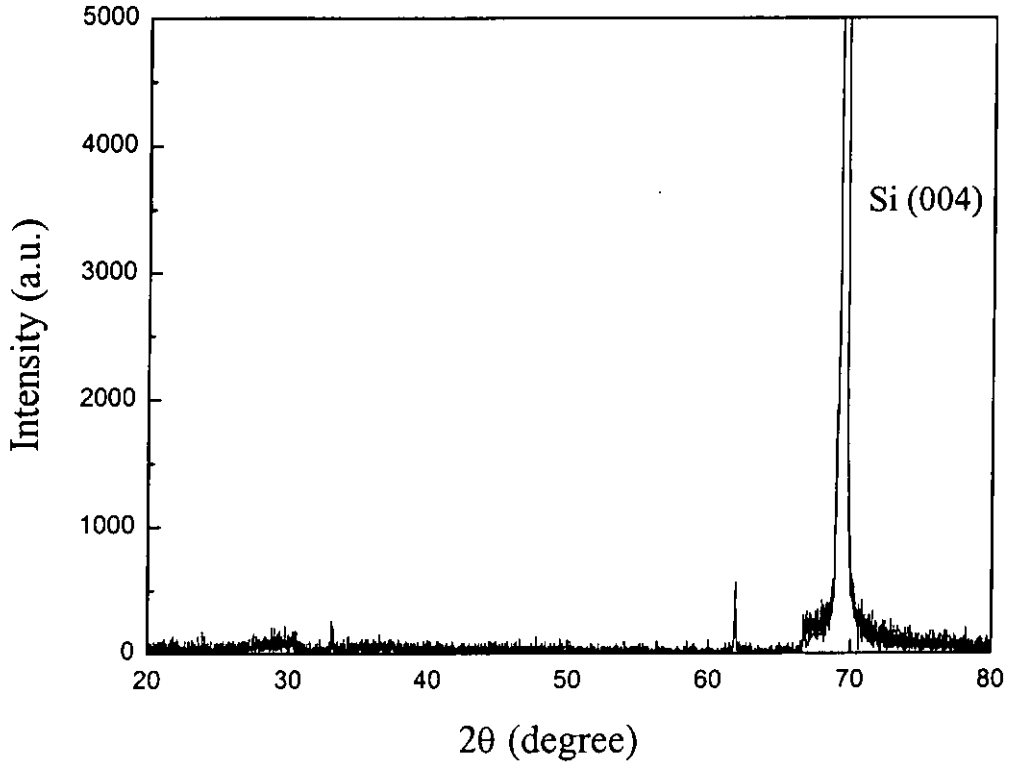

Fig. 5.3.1a The XRD profile of TaN film deposited directly onto Si substrate at 650°C under 2 x 10^{-5} Torr.

5.3.2 TaN/MgO

In this section, we present evidence for the growth of epitaxial single phase TaN thin films on MgO(001). The interfacial structure was investigated by XRD. Fig. 5.3.2a shows the linear X-ray diffraction pattern of θ-2θ of the cubic TaN film deposited at 550°C under high vacuum of 5 x 10^{-6} Torr. A single sharp peak of TaN(002) is observed. The peak, centered at 41°, indexed as NaCl structure of TaN. No hexagonal peaks were found. In Fig. 5.3.2b the logscale profile reveals that TaN is definitely single phase. Fig. 5.3.2c is the ω-scan rocking curve that reflects the in-plane crystalline mosaic in the film. The full width at half maximum (FWHM) of the X-ray rocking curve for the TaN(002) reflection was as small as 0.3°. It indicates that the deposited film is highly oriented and thus of very good crystalline quality. Moreover, this is better than the best profile obtained for epitaxy TaN film reported so far [Greene et al., 1999]. Good in-plane epitaxy of the film showing cube-on-cube growth as depicted in Fig.5.3.2d. In the 360°-Φ scans, four characteristics peaks of a cubic structure are observed. The same positions of the peaks are located from the films with those of the MgO(202) reflections. This strongly suggests that the TaN film was epitaxially cube-on-cube grown on top of the MgO single crystal substrate.

For higher deposition temperature (700°C) similar results are obtained. From the structural properties of these deposited films, it can be concluded that epitaxial TaN films were grown on MgO(001) substrates at deposition temperature range of 550 to 700°C under a base pressure 5 x 10^{-6} Torr. Apart from the (00*l*) reflections from the TaN film and the MgO substrate, no trace of other reflections is observed. Good crystalline TaN/MgO heterostructure has been successfully prepared in our

present work. Structural characterization reveals an orientation relationship of $(001)_{TaN}||(001)_{MgO}$.

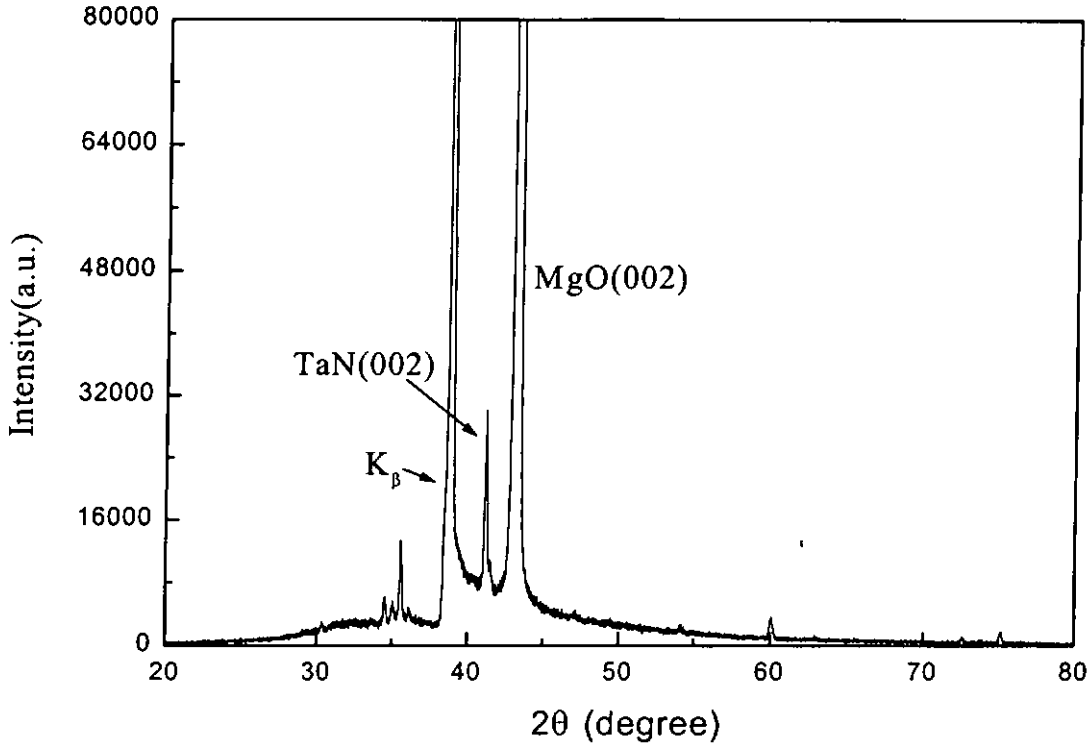

Fig. 5.3.2a The linear X-ray diffraction pattern of θ-2θ of the cubic TaN film deposited on MgO(001) at 550°C under high vacuum of 5×10^{-6} Torr.

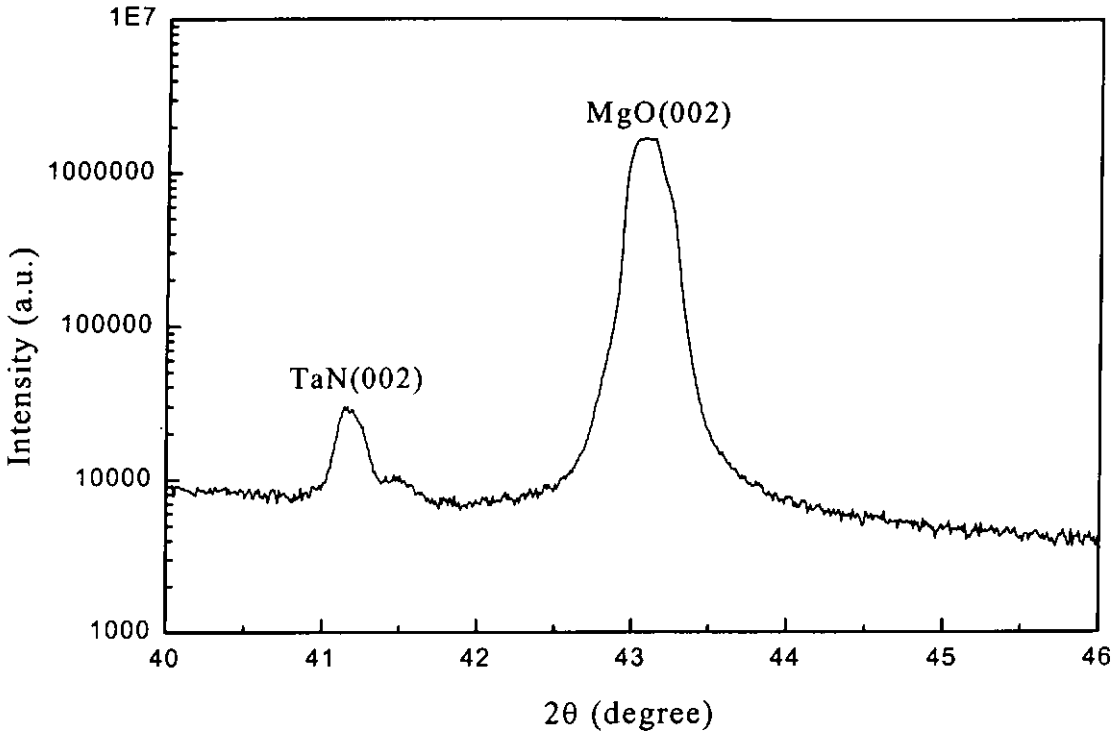

Fig. 5.3.2b XRD scan from a cubic TaN layer grown on MgO substrate deposited at 550°C.

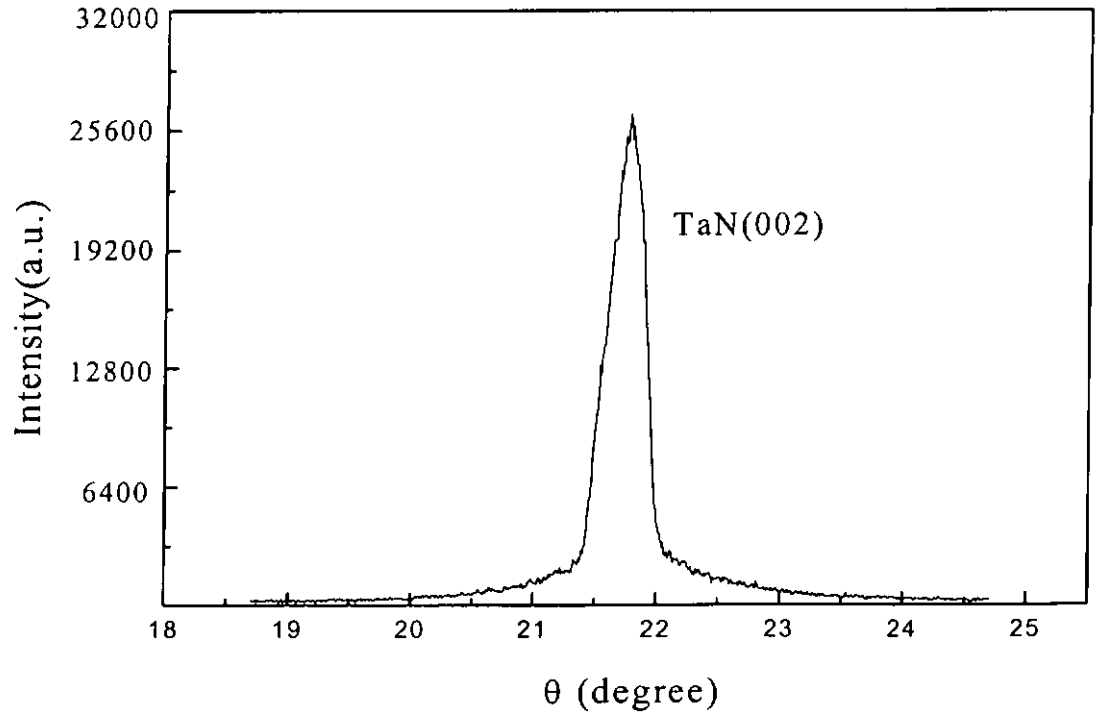

Fig. 5.3.2c X-ray rocking curve of TaN(002) diffraction peak exhibiting a FWHM of 0.3°.

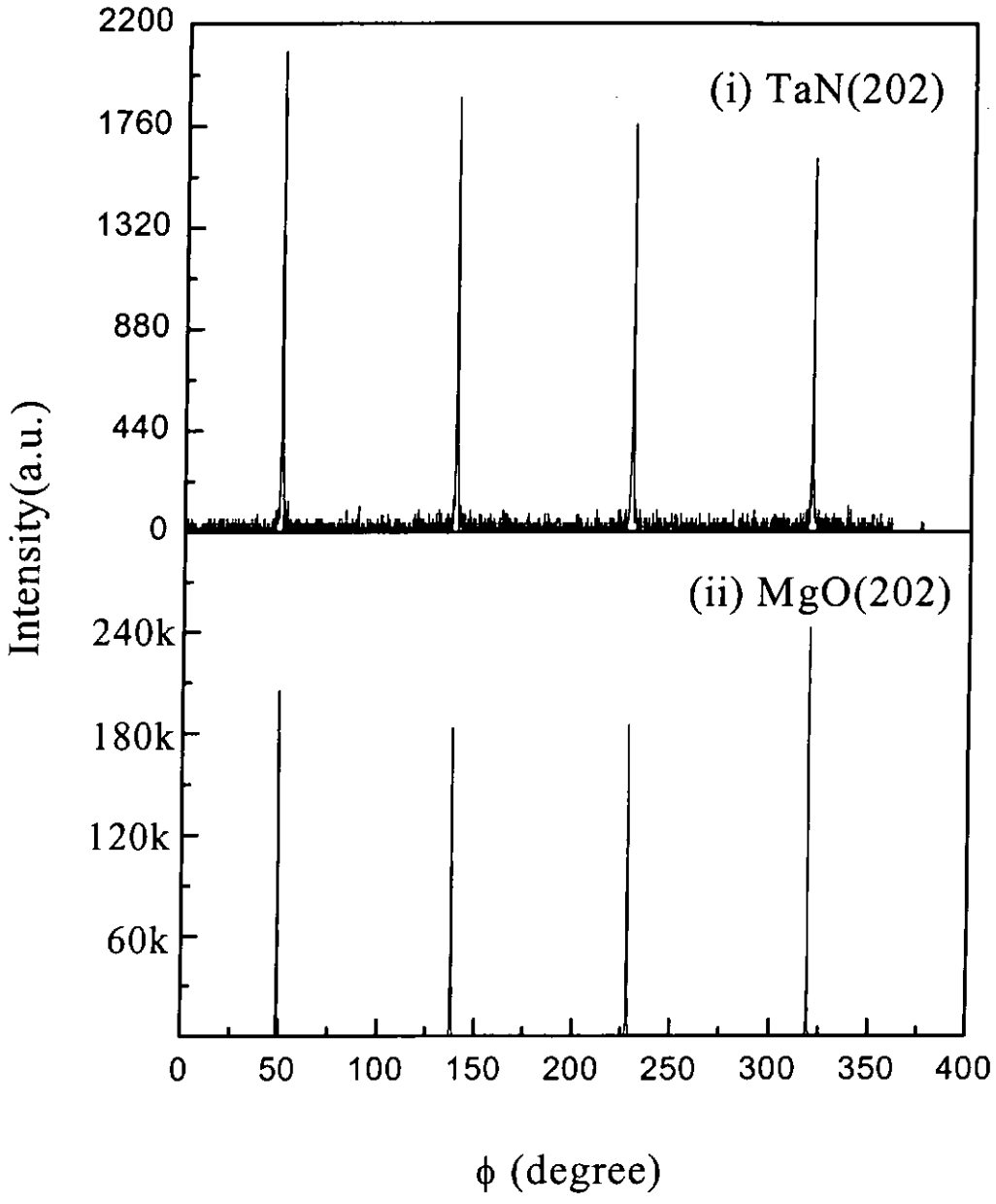

Fig. 5.3.2d X-ray diffraction Φ-scan from heteroepitaxial TaN/MgO structure, showing (i) TaN(202) and (ii) MgO(202) family reflections.

5.3.3 TaN/TiN/Si

It is well known that tantalum nitride is widely applied in microelectronics. The growth of cubic TaN can be used in hybrid integrated circuit technology and as a diffusion barrier/adhesion promoter in complementary metal oxide semiconductor devices [Mehrotra et al., 1987]. As mentioned before, the problems of large difference in the lattice constant of TaN and Si substrate during the preparation of the TaN films. This can be circumvented by depositing a buffer layer such as TiN. It has a lattice constant of 4.24 Å and can provide a near perfect lattice matching for the TaN film growth. We have shown that excellent TaN films can be grown on MgO single crystal substrates. However, it is much more useful if the TaN films can be directly grown on Si substrates. With the use of commercial hot pressed TiN and TaN targets, both the TiN and TaN layers were deposited on Si(001) substrate in succession. High quality stoichiometric and single phase TaN(001) films were prepared at 550°C under a working pressure of 5×10^{-6} Torr.

Fig. 5.3.3a shows the specular θ-2θ scan. The reflections of TaN(002), TiN(002) are identified, and no trace of other reflections are present. A small peak due to residue CuK_β radiation is present at 33°. In Fig. 5.3.3b, the FWHM of the rocking curves on the (002) reflection of TiN and TaN films are around 2.3° and 2.4° respectively. Moreover, peak occurring at every 90° in the Φ-scan indicates that a good in-plane alignment of the TaN film has been achieved. The collected intensity is distributed in four identical sets of peaks positioned at 55°, 145°, 235°, and 325°. This correspond to the 4-fold symmetry of TaN(202), TiN(202) and Si(202) reflection peaks, implying a cube-on-cube epitaxy as depicted in Fig. 5.3.3c.

Up to now, epitaxial growth of TaN on Si substrates has not been reported. As mentioned above, we have shown that good TaN epitaxy can be obtained not only in the case of MgO single crystal substrates, but also in the case of on TiN buffered Si. All deposited films appear in silvery-grey color under visual observation. Our results are clear indications that a lattice matched template layer and an appropriate buffered Si substrate are required for the growth of high quality nitride films on Si.

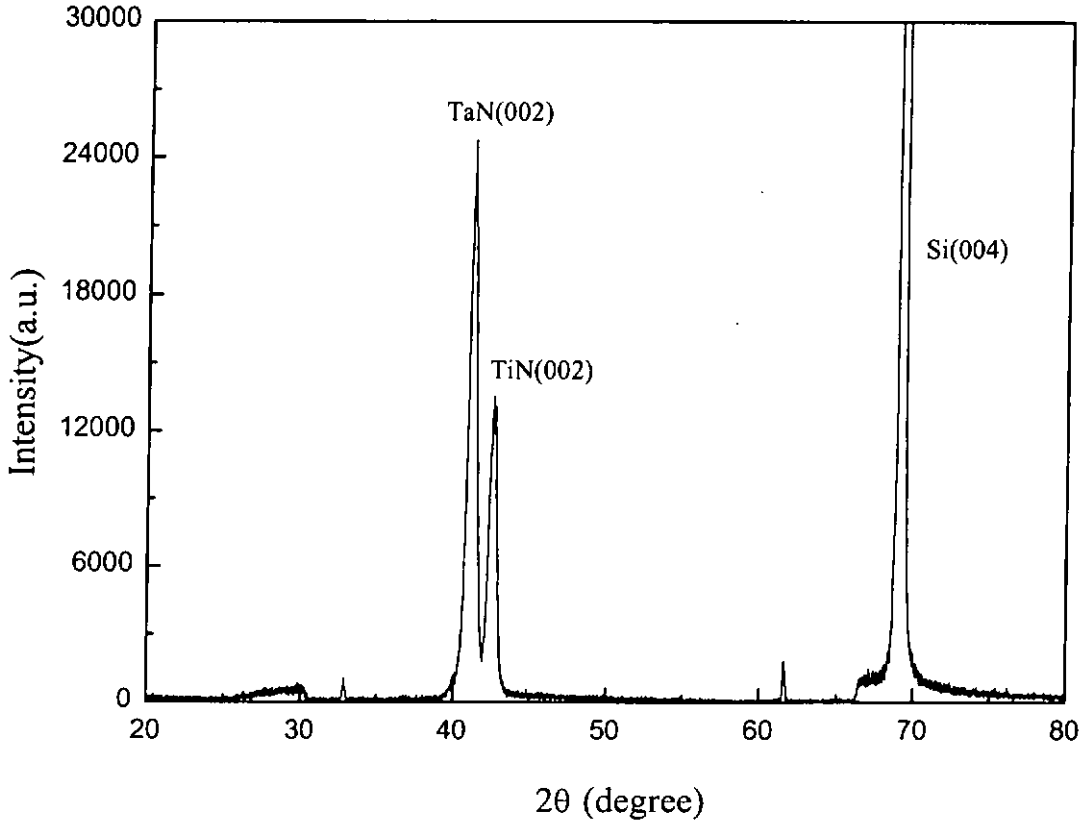

Fig. 5.3.3a The XRD linear scan of a TaN/TiN/Si heterostructure where TaN and TiN were deposited at 550°C under 5 x 10^{-6} Torr.

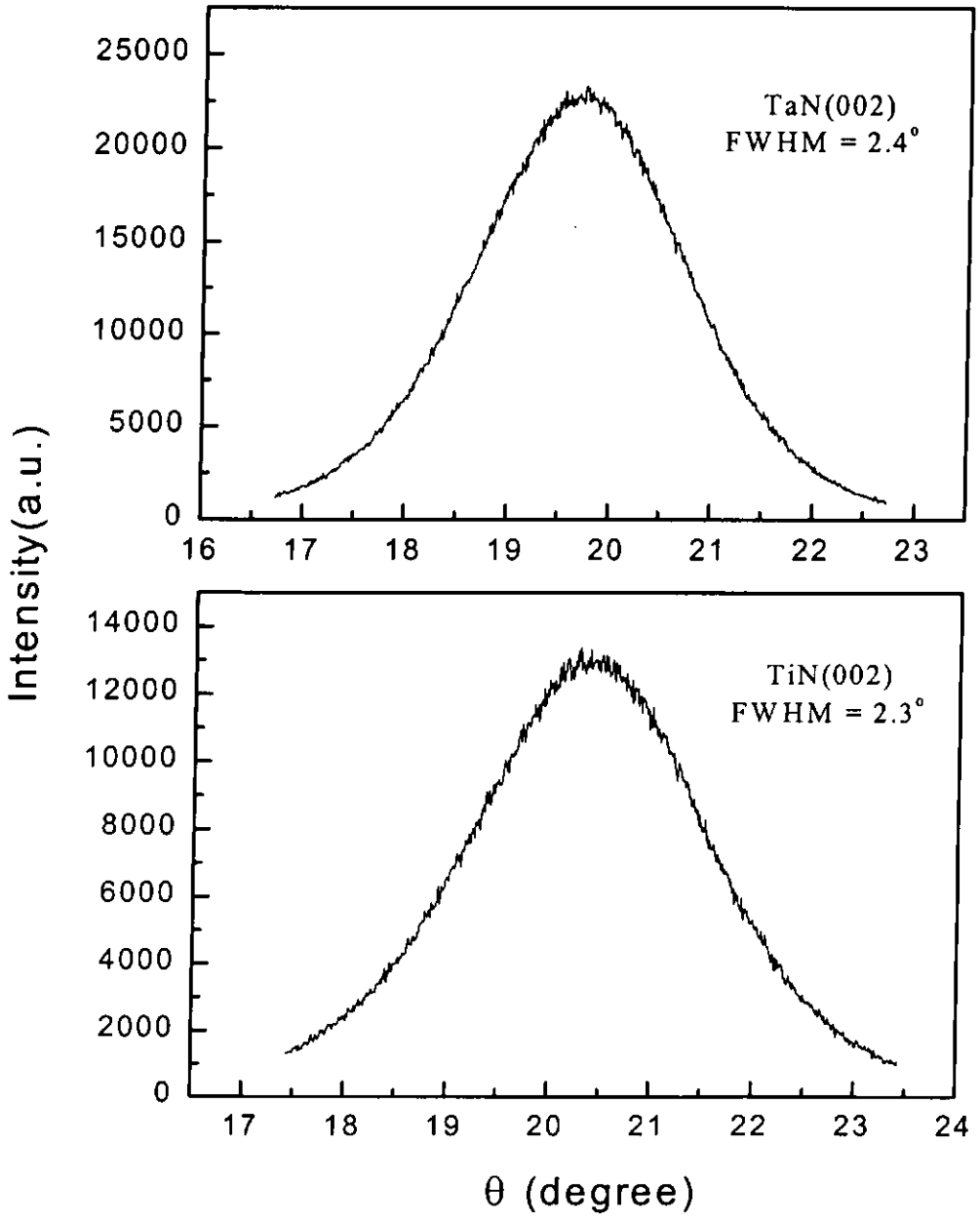

Fig. 5.3.3b The rocking curves of TaN(002) and TiN(002) reflection peaks.

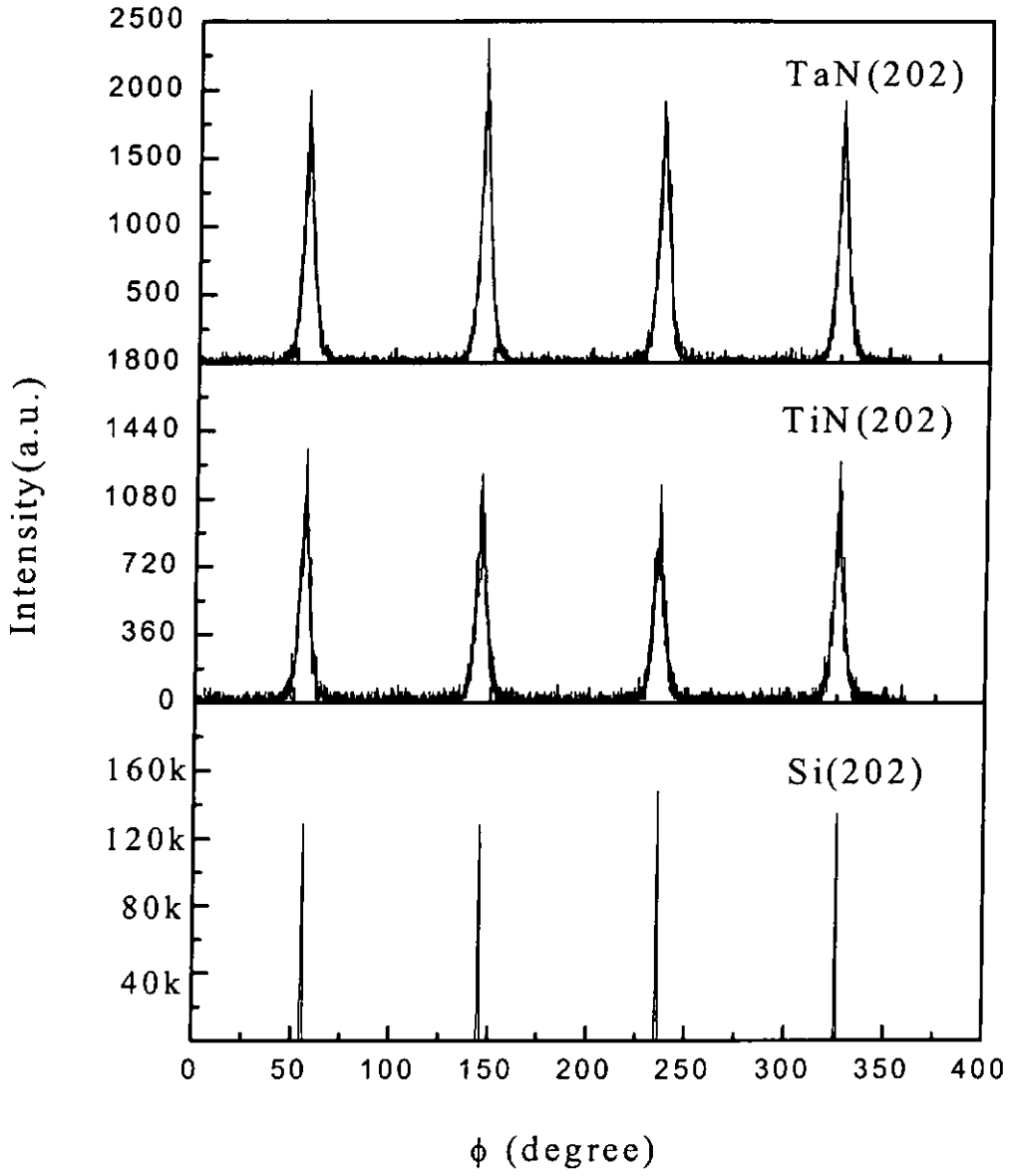

Fig. 5.3.3c The 360°-Φ scan on the TaN(202), TiN(202) and Si(202) reflections.

Most of the early attempts have indicated that TaN is an excellent metallurgical diffusion barrier between copper and Si [Olowolafe at al., 1992; Holloway et al., 1992]. However, TaN has a defective structure [Toth, L. E., 1971] and deviations from stoichiometry are common. Indeed, nitrogen-contained tantalum films often consist of a variety of Ta-N phases including the NaCl-type TaN and hexagonal Ta_2N. TaN has a higher melting point, T_m, at 3087°C and formation enthalpy, ΔH = -120 KJ/mol as compared with those of Ta_2N (T_m = 2050°C, ΔH = -98 KJ/mol). Pure TaN phase is therefore expected to be thermally more stable than Ta_2N at elevated temperature. It is highly desirable to fabricate stoichiometric cubic TaN for enhanced diffusion barrier performance and resistance to oxidation.

For TaN films deposited on TiN buffered Si substrates at temperatures 600°C, a mixture of TaN_x (with $x \leq 1$) components are present. Although the (001)-oriented TaN is always present promintly, the nitrogen deficient TaN_x components are often co-exist in the films and show up as a very broad peak in the X-ray diffraction profile as shown in Fig. 5.3.3c.

Our results showed that the structural quality of the TaN layers deteriorated during the TiN deposition as depicted in Fig. 5.3.3d. This may be attributed to the oxidation of the underlying TiN films under high temperature. The TiN layer was *in-situ* deposited at 550°C and 720°C whereas the TaN film was prepared at 720°C. For the TiN films grown at higher temperature, a larger FWHM value of the TaN reflection peak is obtained compared with one grown at lower temperature. This implies that a good oriented and crystalline film can be achieved at a relatively low processing temperature which is compatible to our PLD method.

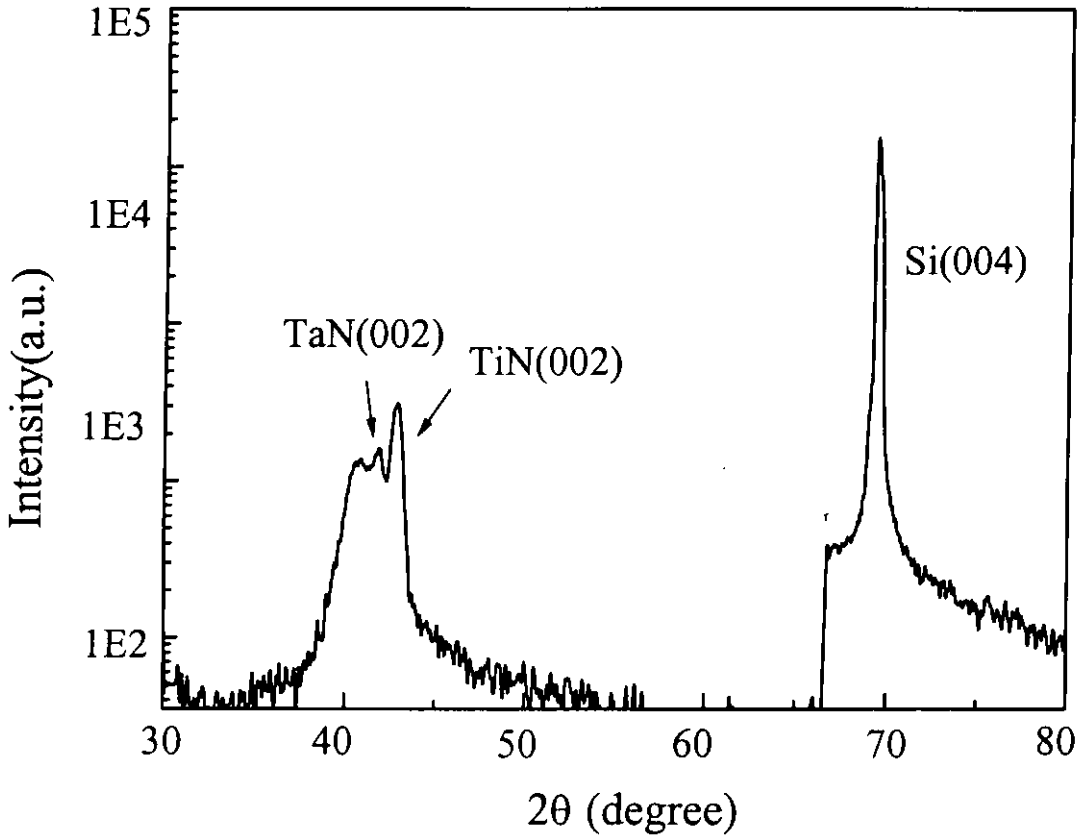

Fig. 5.3.3c A broad peak in the X-ray profile plotted in logscale.

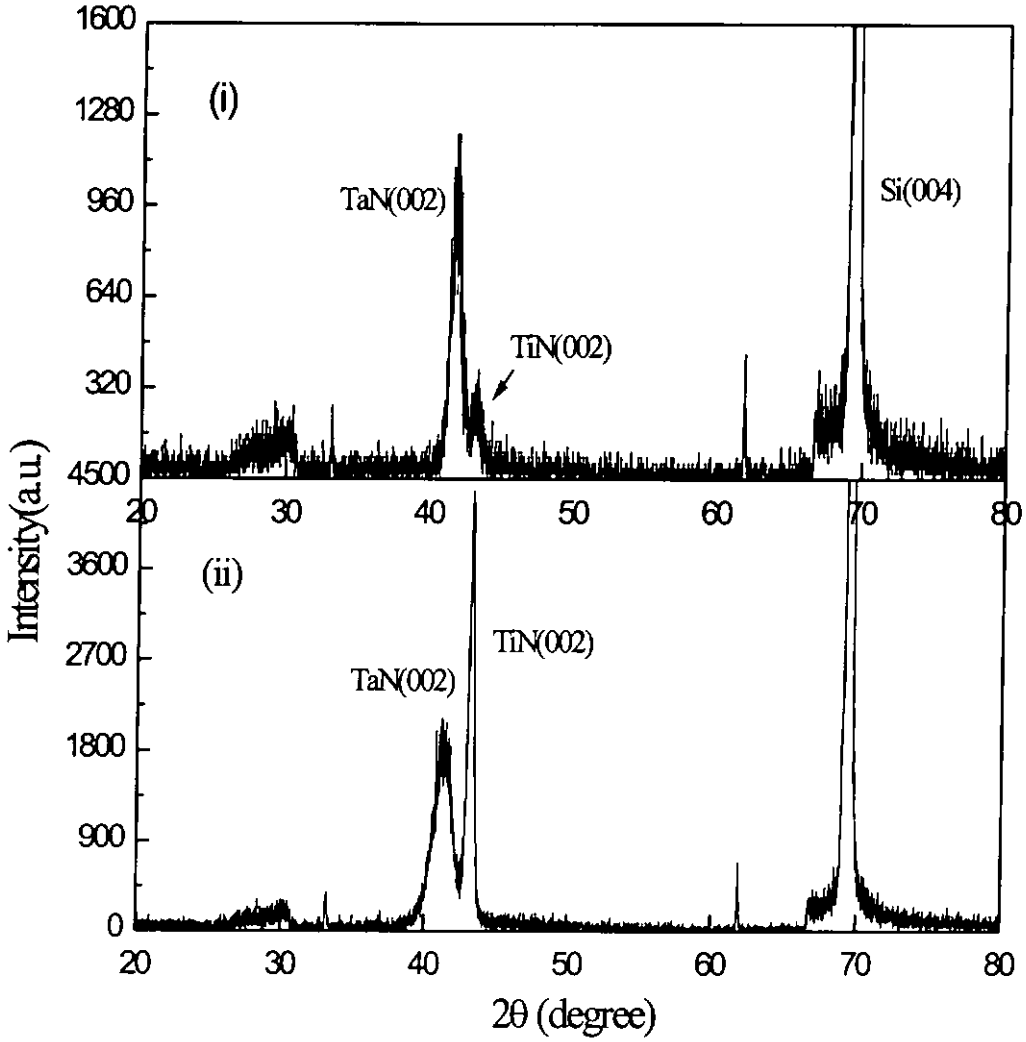

Fig. 5.3.3d The θ-2θ scans for TaN/TiN/Si(001) heterostructures with the TiN layer deposited at (i) 550°C and (ii) 720°C whereas the TaN film was fixed at 720°C.

Extensive work has been done on changing the deposition temperature of the TaN films. Stoichiometric and good crystalline epitaxy TaN thin films can only be obtained at relatively low processing temperature as mentioned before. In Fig. 5.3.3e, we investigated that when TaN grown at high temperature with the underlying TiN films, prominent structural changes occur. Single sharp peak is converted into double peaks consisting nitrogen-deficient TaN_x components. Clearly exhibiting no tendency to epitaxy. This may be due to the preferential loss of nitrogen at elevated temperature. Such that TaN thin films with different amount of controlled reactive nitrogen can exist over a range of components deviated from the stoichiometry.

Based on the above discussion, we can conclude that this compound vary from the stoichiometric composition to significantly lower nitrogen concentrations under various deposition conditions especially at high temperature. We have shown that high quality single phase TaN(001) films do can epitaxially grown on TiN buffered Si substrates. It is likely that the effective diffusion barriers obtainable with stoichiometric cubic TaN thin films can out perform the polycrystalline or amorphous films [Xin et al., 1993].

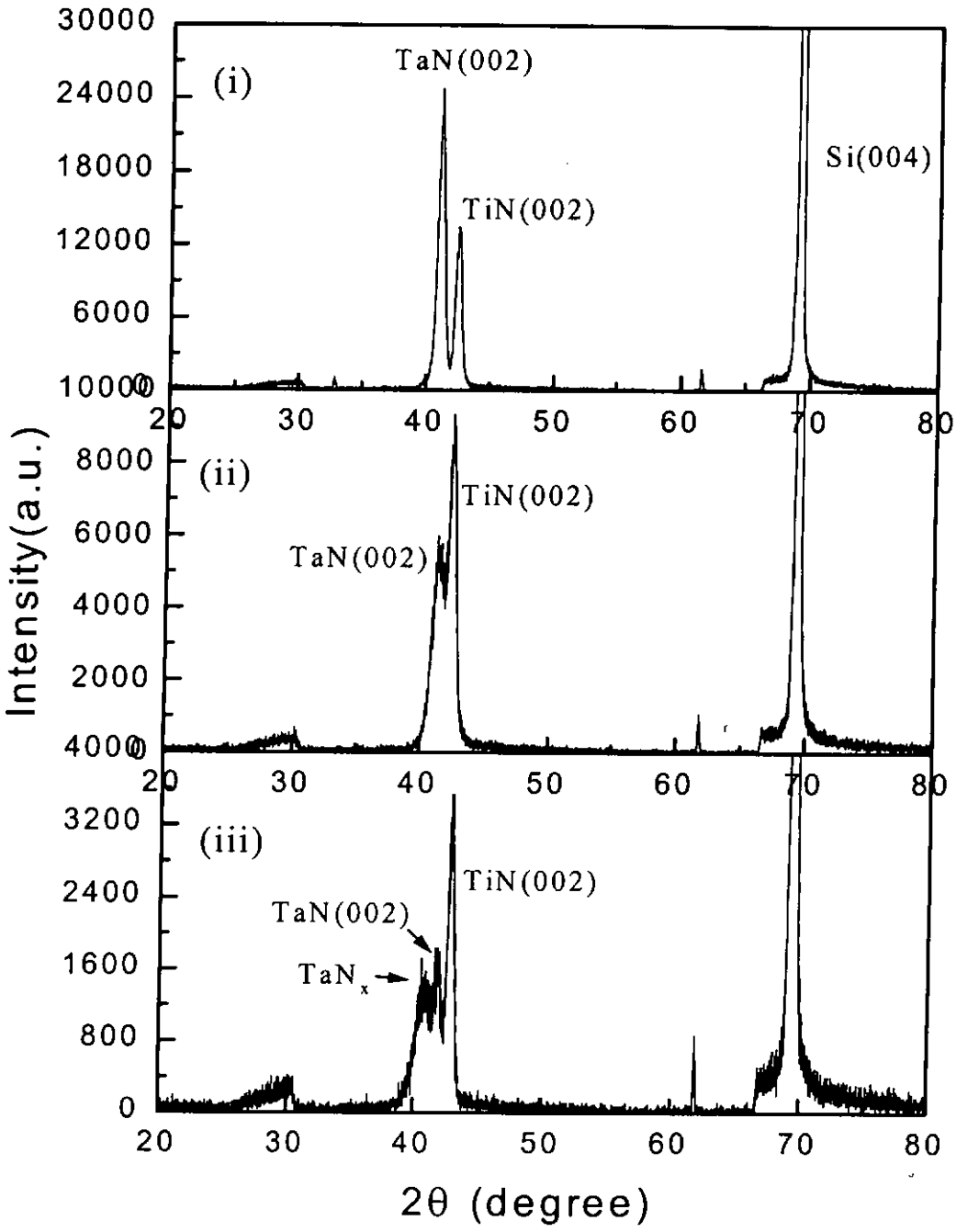

Fig. 5.3.3e The θ-2θ scans for TaN/TiN/Si(001) heterostructures with the TaN layer deposited at (i) 550°C (ii) 650°C and (iii) 720°C whereas the TiN film was fixed at 550°C.

5.4 Surface morphology and cross-section

5.4.1 TaN/MgO

Films exhibiting perfect flat surface are seldomly observed. A certain surface roughness is expected because of the randomness of the deposition and film growth processes. In the present studies the deposition temperature was kept at 550°C and under a base pressure of 5 x 10^{-6} Torr. The TaN layer was grown under these deposition conditions with different laser energy density. Fig. 5.4.1a shows the SEM micrographs of TaN film deposited on MgO single crystal substrates with the laser energy density of 3 J/cm^2. A lens with focal length of 50 cm was used in preparing this sample. On the other hand, particulate emission is increased at a higher laser energy density of 8 J/cm^2 by using a 30 cm focal length as evidenced in Fig. 5.4.1b. The deposition rate is also increased. More details were seen from AFM images as depicted in Fig. 5.4.1c and Fig. 5.4.1d. Few particulates and crack-free surface are obtained for TaN films grown at low laser energy density. In contrast, many ball-shaped and large particles were found on the surface of the films grown at high laser energy density. It was noted that the laser energy density needs to be kept low in order to minimize the particulate emission. The high absorptivity of KrF laser photons by the target was responsible for producing the uniform and particular=free films.

The laser produced particulates are generally induced either directly from the target ablation or from supersaturated condensation at the substrate surface. To some extent these particulates can be eliminated by placing a shadow mask between the

target and substrate [Venkatesan et al., 1997]. The relative roughness for both TaN films are depicted in Fig. 5.4.1e and Fig. 5.4.1f. For the TaN films grown at high laser energy density, they showed significantly more roughness but remained oriented with respect to the substrates. In spite of the ball-shaped particles, a very sharp TaN/MgO interface is observed in Fig. 5.4.1g.

Fig. 5.4.1a The SEM micrograph of TaN layer deposited on MgO with the laser energy density of 3 J/cm^2.

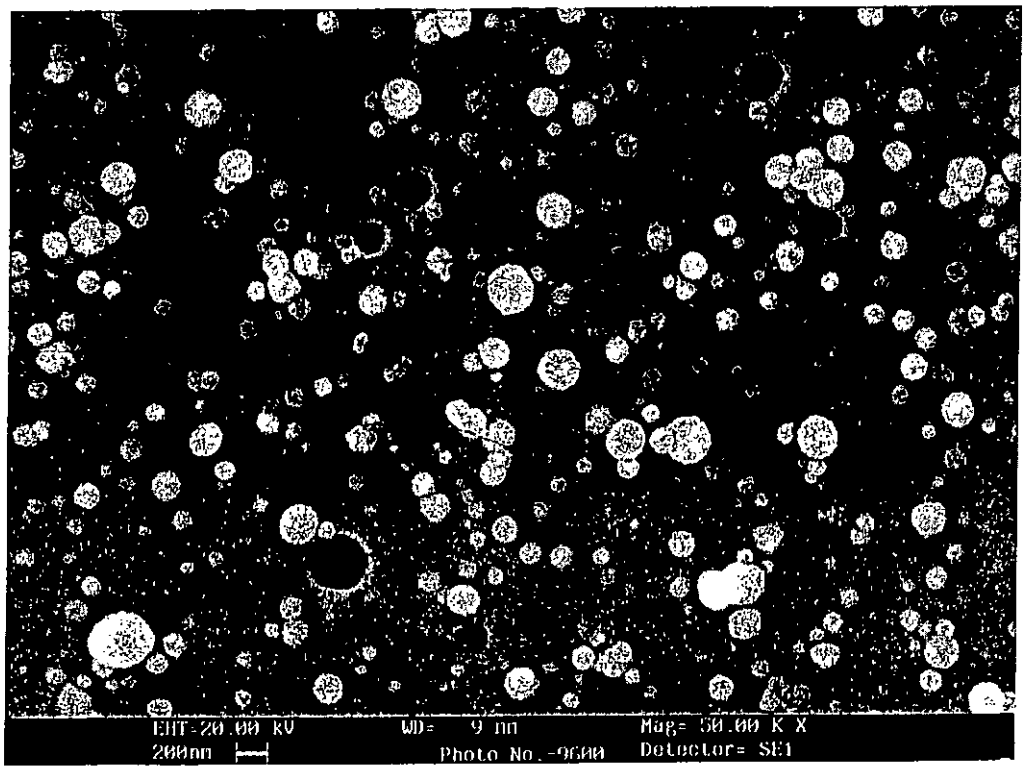

Fig. 5.4.1b The SEM micrograph of the TaN layer grown at high laser energy density of 8 J/cm^2, showing many undesirable particulates.

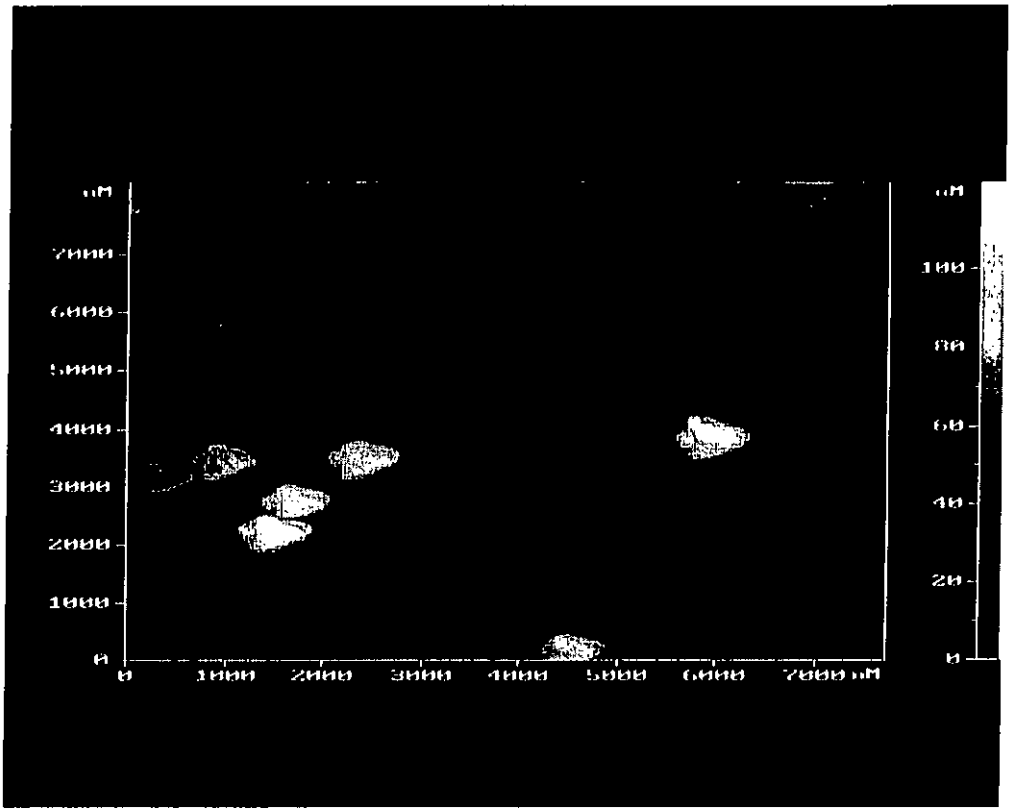

Fig. 5.4.1c The AFM image of TaN layer deposited on MgO grown at low laser energy density.

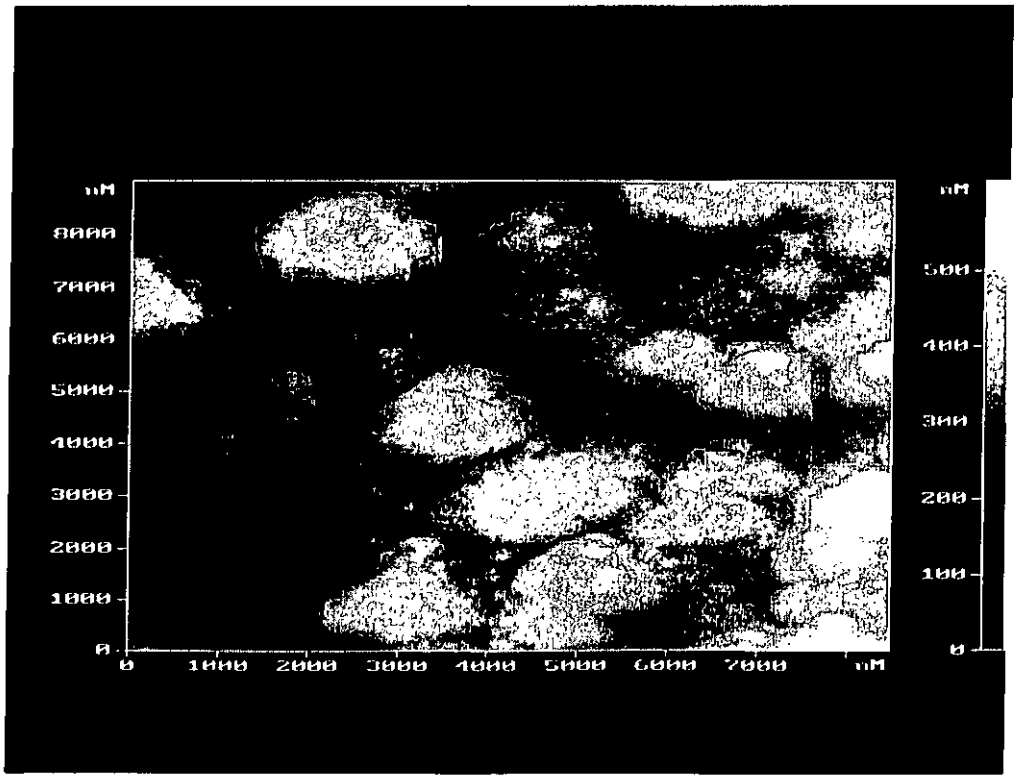

Fig. 5.4.1d The AFM image of the TaN film grown at high laser energy density.

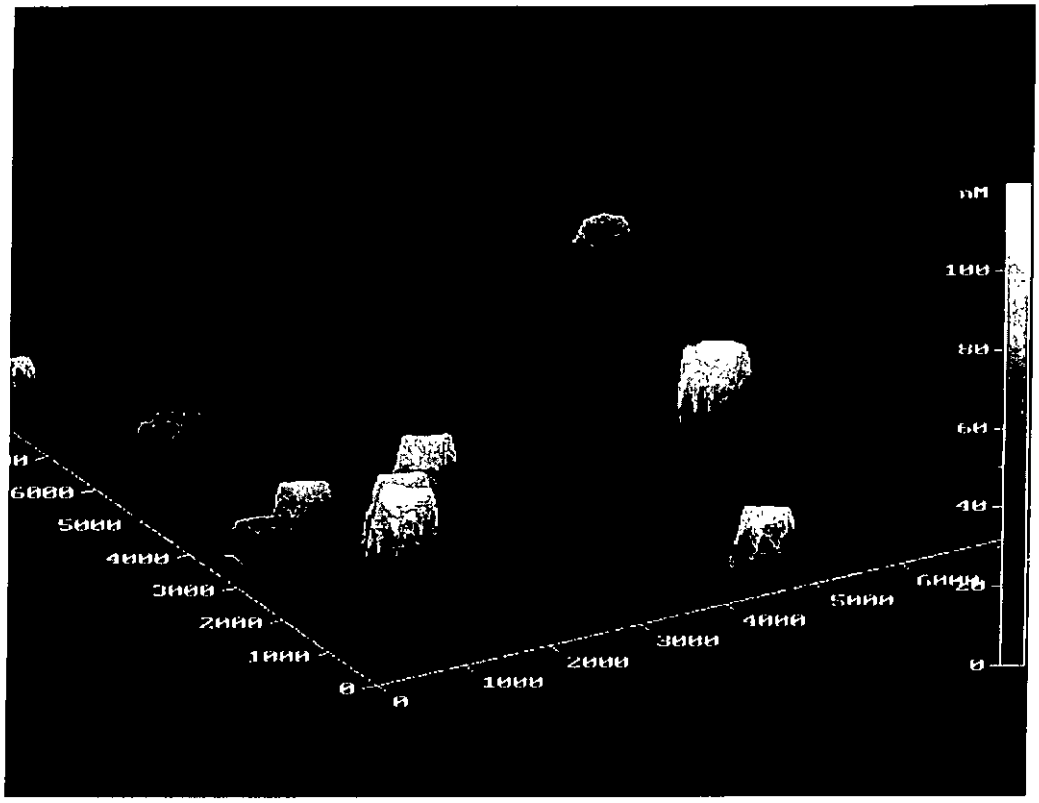

Fig. 5.4.1e The AFM image of the TaN film grown at low laser fluence showing smooth surface.

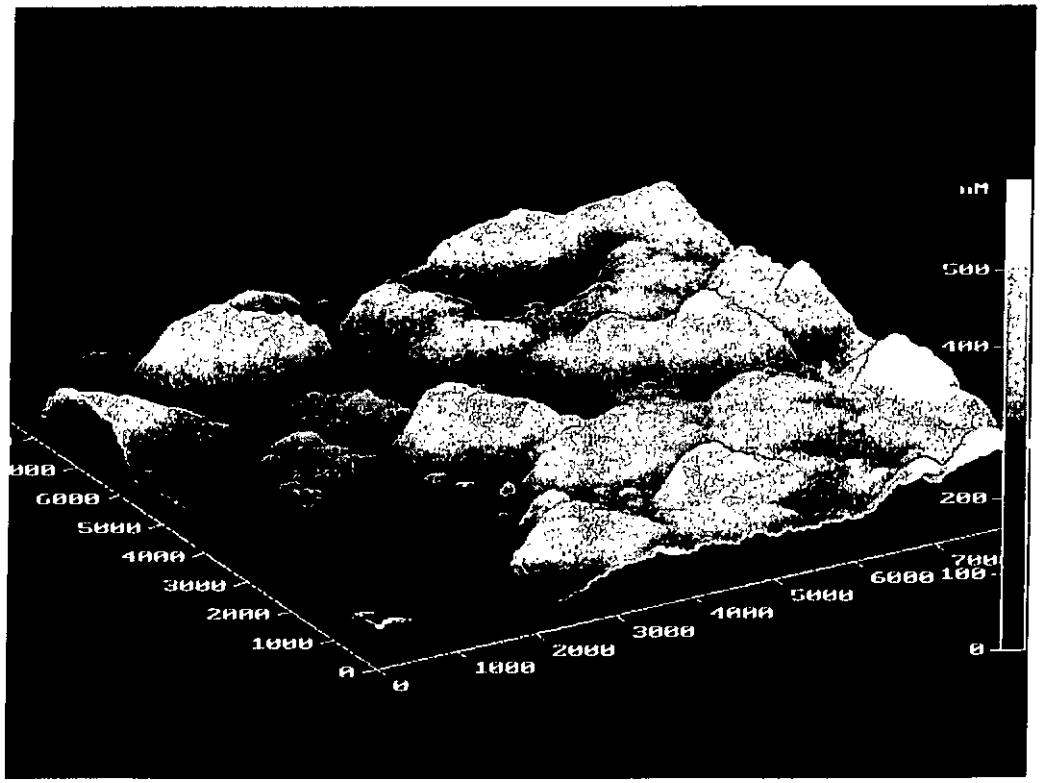

Fig. 5.4.1f The AFM image of the TaN film grown at high laser fluence showing rough surface.

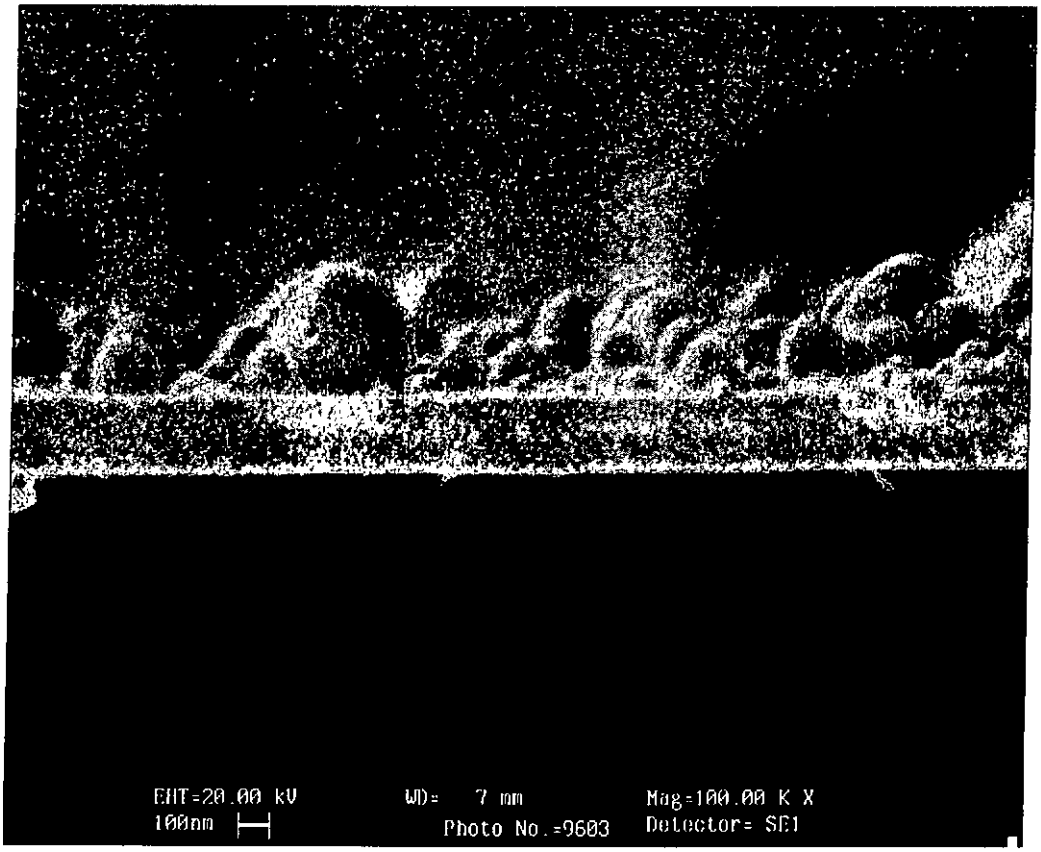

Fig. 5.4.1g The SEM cross-section profile of the 200 nm thick TaN film.

5.4.2 TaN/TiN/Si

The surface morphology of the TaN film grown on TiN buffered Si under high vacuum is depicted in Fig. 5.4.2a. In this figure, TiN and TaN layers were deposited on Si(001) substrates in succession. The top surface is very smooth and appears in silvery-grey color under visual observation. Due to the lower growth temperature, no cracks are created in this as-grown film. Apart from some undesirable particulates, there are some cone shape outgrowths. As seen in Fig. 5.4.2b, the surface is very flat and the rms roughness is about 1.387 nm. Fig. 5.4.1c shows the scanning electron microscopy images of fractured cross-section of TaN/TiN/Si heterostructure film deposited at 550°C. We can see that there are two distinct layers. Crystalline TiN and TaN layers of about 100nm thick were obtained in the present work. The structure of the film consisted of fine, nanometer-sized crystallites forming near the interface followed by 20-40 nm wide columnar grains. The columnar grains formed with a preferential (001) crystal orientation parallel to the substrate. Larger grain sizes are naturally expected for increasing substrate or annealing temperature because of an increase in surface mobility.

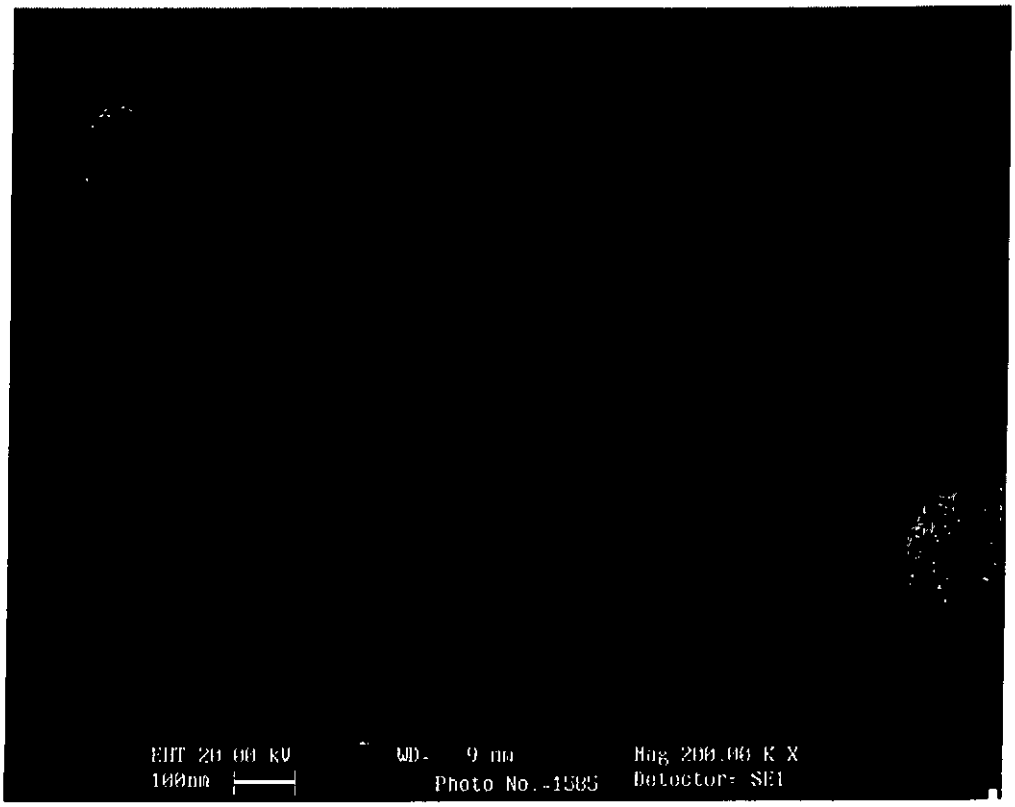

Fig. 5.4.2a SEM micrograph of the surface morphology of TaN thin films.

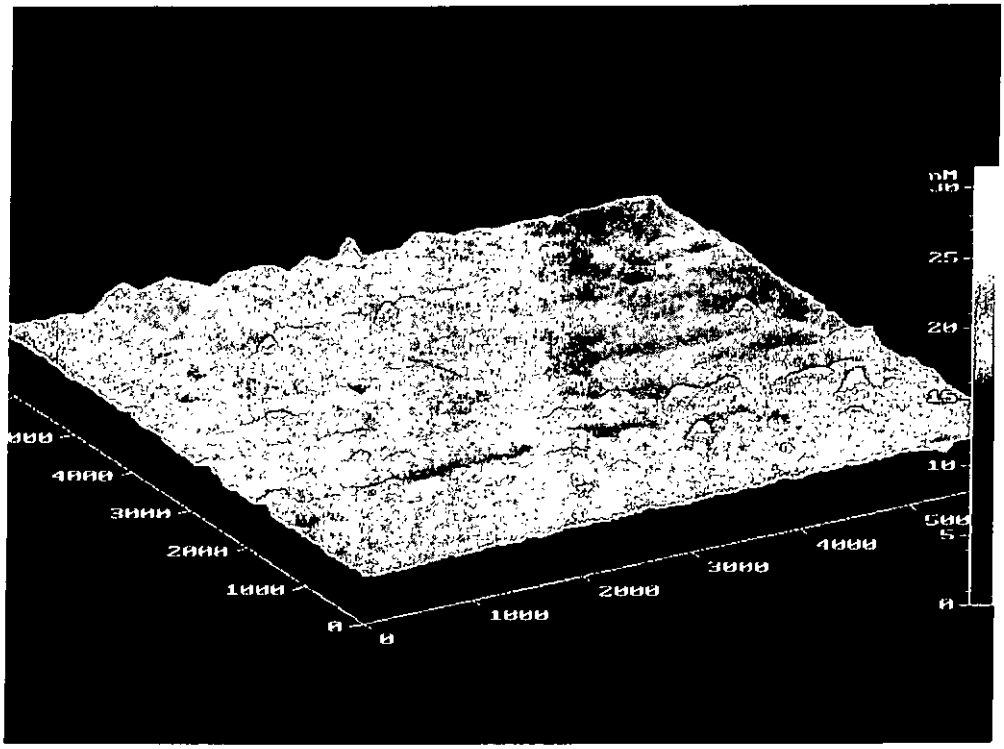

Fig. 5.4.2b AFM image showing the roughness of TaN thin films.

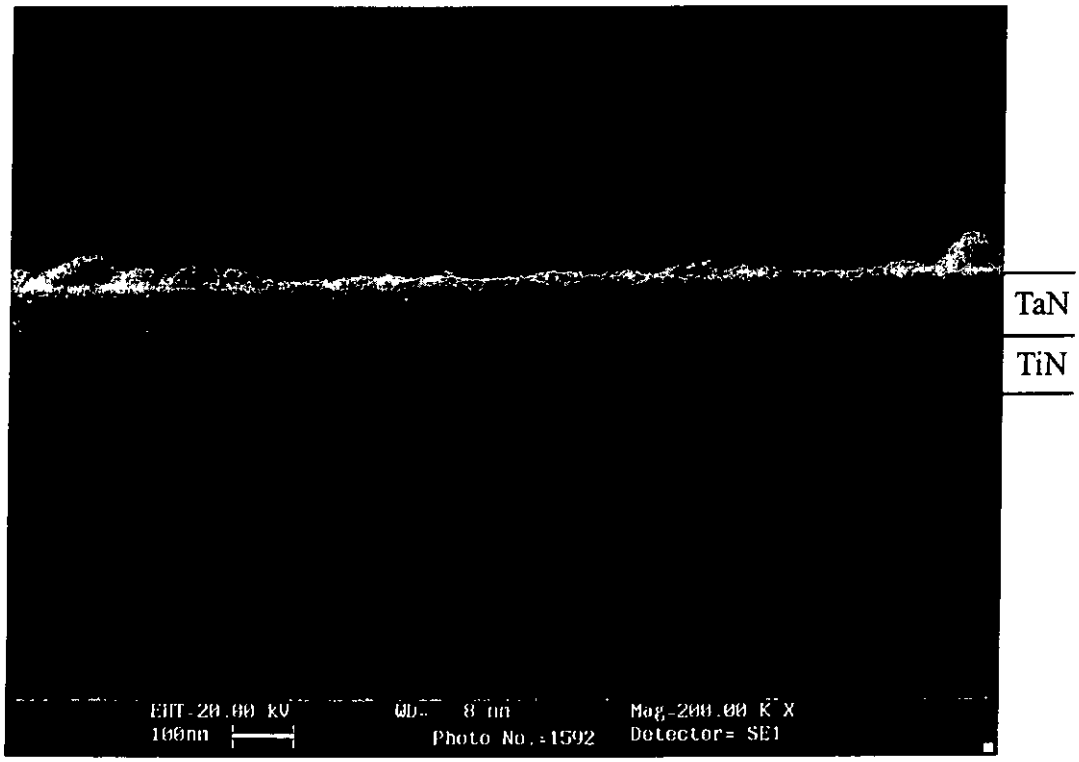

Fig. 5.4.2c SEM cross-sectional micrograph showing 100 nm TaN deposited on TiN buffered Si substrates.

5.5 Electrical properties of TaN and TaN/TiN films

The electrical properties of the TaN films grown on MgO single crystal substrates were investigated. Crystalline TaN layer of about 200nm thick were deposited at 550°C under a base pressure of 5 x 10^{-6} Torr. The resistivity versus temperature curve is plotted in Fig. 5.5a. Temperature range covered was from 78 K to 300 K. It can be seen that the room temperature resistivity of the TaN grown on MgO(001) is about 600 μΩcm. From this curve, we can clearly see that pure cubic TaN is nonmetallic with negative $\frac{d\rho}{dT}$. It is noted that the resistivity of TaN films decreases as the temperature increases and the films exhibited reasonably good electrical conductivity over the full temperature range of interest. This result is consistent with reported by J. E. Greene [Greene et al., 1999].

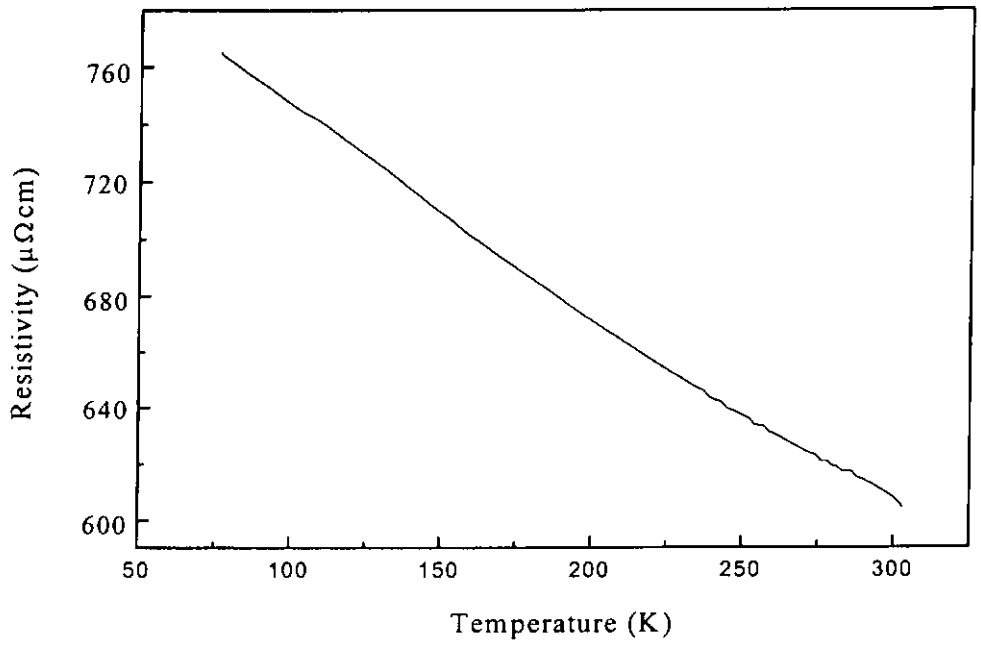

Fig. 5.5a The temperature dependence of ρ in TaN film deposited on MgO substrate at 550°C.

For the TaN films grown on TiN buffered Si substrates. Both TiN and TaN have good conductance at room temperature. As mentioned before, TiN is metallic with a positive $\frac{d\rho}{dT}$ and resistivity of about 44 μΩ cm at room temperature. And TaN is nonmetallic with negative $\frac{d\rho}{dT}$. Fig. 5.5b shows the R-T profile of the epitaxial TaN/TiN heterostructures. Both TaN and TiN layers were deposited at low deposition temperature of 550°C and in high vacuum at 5 x 10^{-6} Torr. The corresponding thickness was estimated to be 200 nm and 100 nm, respectively. The as-grown films were post-annealed for 20 minutes during the deposition process. An interesting finding was that a properly tuned TaN/TiN bi-layer structure could produce a nearly flat R-T curve. That means $\frac{d\rho}{dT}$ is close to zero over a reasonable wide range of temperature.

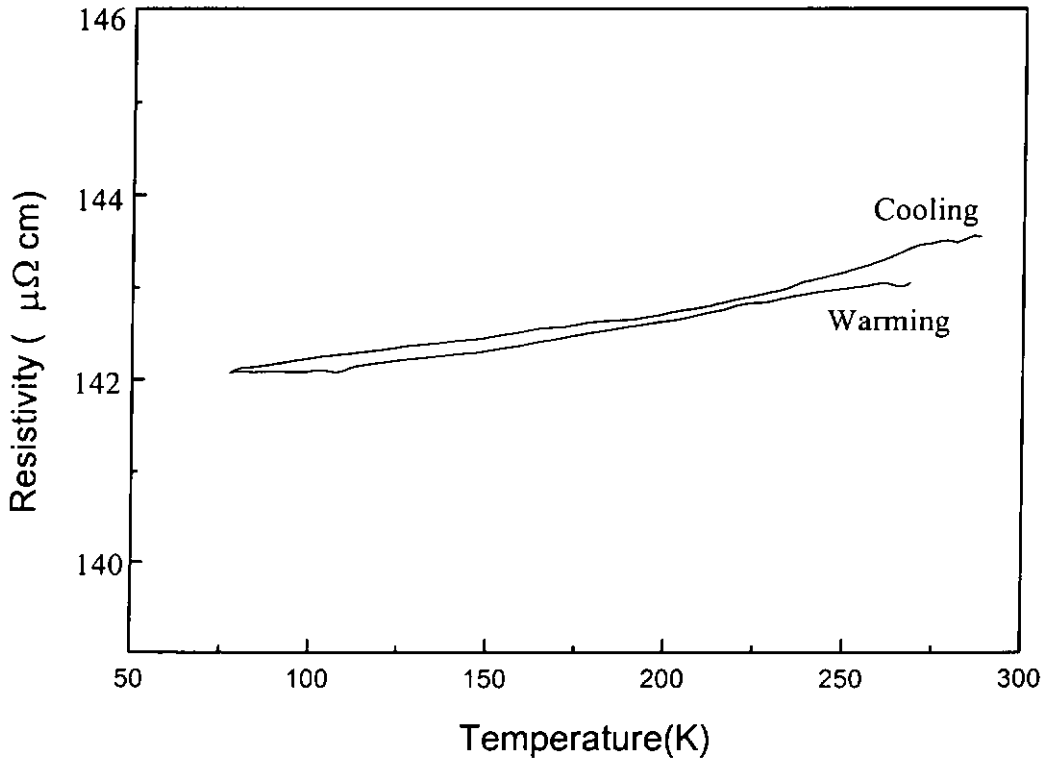

Fig. 5.5b The R-T profile of the epitaxial TaN/TiN heterostructures.

Chapter 6

Characterization of $SrTiO_3$/TiN/Si

6.1 Introduction

With the increase of device number density in dynamic random access memories (DRAMs), the charge-storage limit of Si-based dielectrics in capacitor cells is being rapidly approached for the new generation of microelectronics and superconducting devices. One class of very attractive materials is the family of crystalline perovskites. $SrTiO_3$ (STO) films directly deposited on silicon are polycrystalline. High quality epitaxial growth is not possible because STO reacts with silicon to form amorphous layer before epitaxy occurs. Since the grain boundaries induce high leakage current and amorphous layers have a low dielectric constant, heteroepitaxial growth of perovskites on semiconductors such as Si is immensely important because they have outstanding properties that can be exploited for the future development of microelectronics and optoelectronics.

STO is among some perovskite oxides that can be grown successfully under high vacuum by PLD technique [Koinuma, H., Lee, M. B., 1997; Wenbin Wu et al., 2000]. In order to achieve epitaxial perovskite on Si, a suitable buffer layer is inserted between them. Previous attempts using oxide buffer layers of MgO, SiO_2 and RuO_2, have led to some successes. These oxide buffer layers, however, must be grown at substrate temperature > 600°C and at ambient oxygen. This inevitably causes oxidation of the Si surface as well as a severe atomic diffusion into the Si substrate. The method of PLD has an attractive feature of ease to preserve the

stoichiometry and the good structural quality of the target in the grown films.

In the present study, epitaxially grown cubic-TiN buffered Si promotes high degree of epitaxy for STO. The advantages of the epitaxial TiN include (i) an electrical contact for devices (conducting layer with low electrical resistivity of the order of $\mu\Omega$ cm at room temperature for contact metallization) and (ii) the domain matching epitaxial growth eliminates grain boundaries and fast dopant diffusion along grain boundaries. Besides, TiN has excellent structural, chemical and thermal compatibility with STO and Si compared to Pt [Rao, G. M., and Krupanidhi, S. B., 1994], $SrVO_3$ [Moon, B. K., and Ishiwara, H., 1995] buffer layers.

Excellent quality ceramics based on heteroepitaxial structures of oxide-nitride-semiconductors, i.e., $SrTiO_3$/TiN/Si(001) have been fabricated by *in-situ* PLD method. The crystallinity and surface morphology of the epitaxial STO films with underlying TiN layer are presented. Moreover, the significant dependence of substrate temperature on the crystalline quality of the STO films on Si with epitaxial TiN template has been examined systematically in this chapter.

6.2 Analysis of $SrTiO_3$ (STO) target

Commercial hot-pressed STO target of 99.9% purity was used to fabricate the films. Again, the crystal phases and structures of this target were determined by XRD. The θ-2θ scan is shown below in Fig. 6.2.

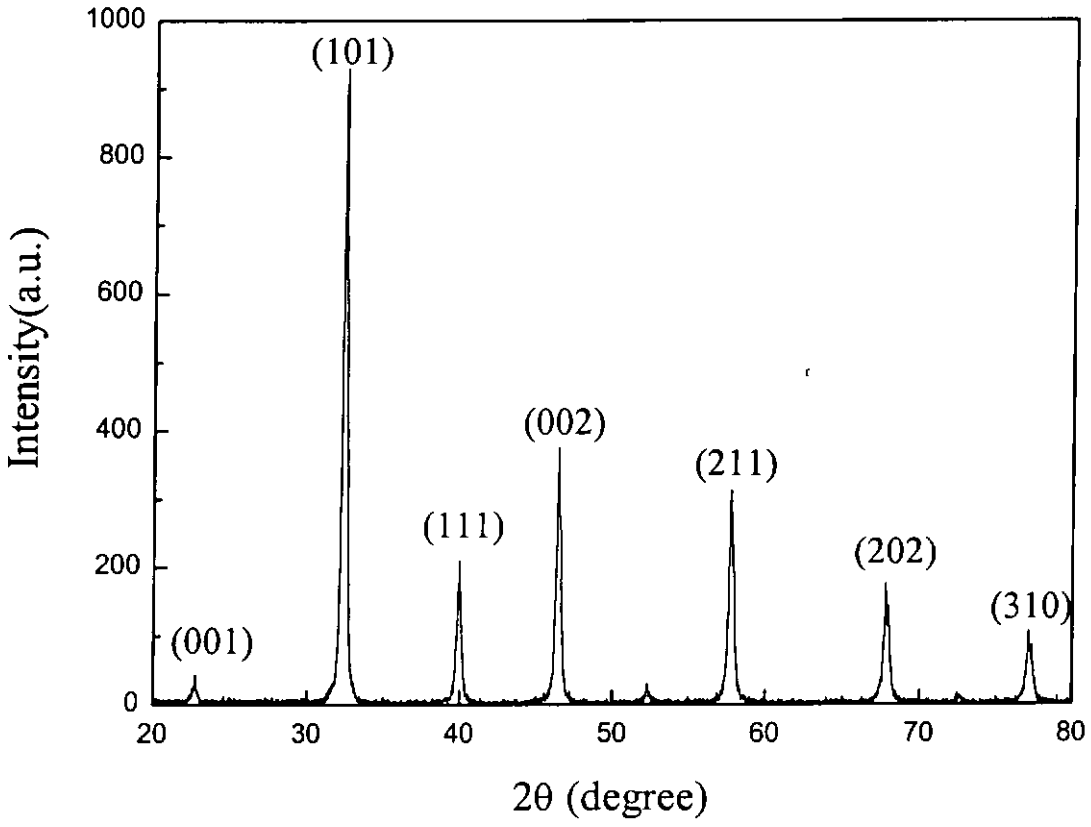

Fig. 6.2 The XRD pattern of the hot-pressed STO target.

6.3 Cubic perovskite

Perovskite, was first described in the 1830's by the geologist Gustav Rose. It is the most abundant mineral on earth and have been receiving a great deal of attention and interest recently. It is well known and recognized as a common mineral in aluminum and silica rock types. Fig. 6.3 shows the perovskite structure of ABO_3. The principle perovskite structure found in ferroelectric materials is a pseudo cubic structure containing three different ions of the form ABO_3. The A and B atoms represent +2 and +4 ions, respectively, while the O atom is the oxygen –2 ion. This ABO_3 structure can be thought of as a face centered cubic (fcc) lattice with A atom at the corners and the O atoms on the faces. The B atom is located at the center of the lattice. This A atom is the largest of the atoms and consequently increases the size of the AO_3 (fcc) structure. As a result, there is minimum energy positions off centered from the original octahedron that can be occupied by the B atom. Shifting of this atom due to applied electric fields causes the structure to be altered, creating electric dipoles.

The atomic structure of ferroelectric thin films is very sensitive to temperature of the crystal. As the temperature is changed, the crystallographic dimensions change due to distortion of the octahedral. The distorted octahedral are coupled together, and a very large spontaneous polarization can be achieved. This large spontaneous polarization will lead to a large dielectric constant. Therefore, most perovskites have high electrical resistivities, which makes them useful as dielectric.

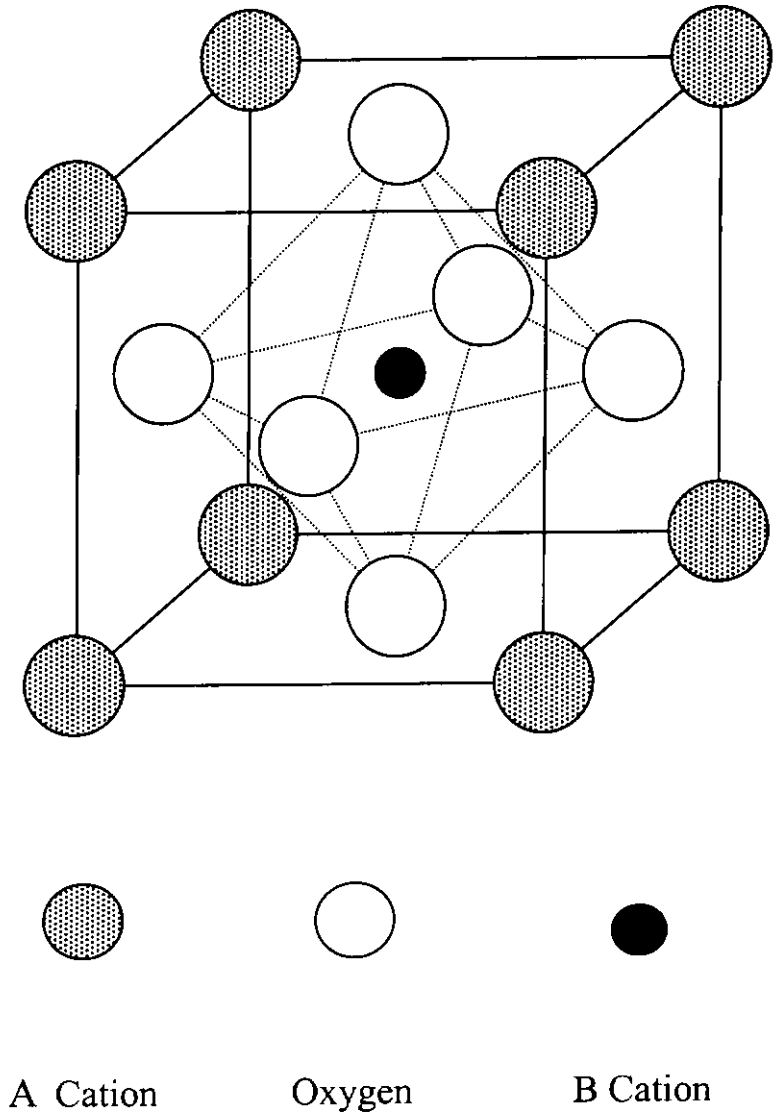

Fig. 6.3 The perovskite structure of ABO_3.

6.4 Structural analysis of $SrTiO_3$ films

STO is an insulating oxide with high dielectric constant of 300 at room temperature. It should be mentioned that STO films deposited on Si substrates were found to be either polycrystalline or poorly aligned with extensive interdiffusion at the interface, which severely limited the usefulness of this structures. STO has a cubic perovskite structure and its lattice constant of 3.905 Å, which is closely matched with TiN (4.24 Å). The relative parameter mismatch is about 8%.

A KrF excimer laser was used to ablate stoichiometric, hot-pressed TiN target at an energy density of 4 J/cm^2, and a single-crystal STO target at 3 J/cm^2. In the case of TiN deposition, films were grown at different temperature ranging from 550 to 750°C under high vacuum condition in order to avoid undesirable oxidation. The typical thickness of prepared TiN films was 200 nm. All STO films were prepared at a laser pulse repetition rate of 10 Hz. The deposition lasted for 10 minutes resulting a 200 nm thick film. The deposition was carried out in vacuum (4 x 10^{-6} Torr) without filling any reactive nitrogen gas. The substrate temperature was fixed at 650°C.

X-ray diffraction was used to determine the crystallinity and the preferred orientation of all deposited films. Fig. 6.4a displays the linear XRD profile where the STO film grown on TiN/Si at substrate temperature of 650°C under high vacuum of 4 x 10^{-6} Torr. This pattern shows only strong (00*l*) diffraction peaks of STO and those from the substrate and TiN underlayer, indicating that the films have neither randomly oriented grains along the surface normal direction nor impurity phases. Fig. 6.4b depicts the rocking curves for STO(002) and TiN(002) reflections. Their

FWHM are 1.51° and 1.74° respectively. This indicates the films are highly oriented. The characteristics of in-plane epitaxy were obtained using Φ-scans and the results are shown in Fig. 6.4c. No mis-oriented in-plane was observed. Four sharp peaks are obtained at every 90° interval, showing a clear 4-fold symmetry of a cubic. Structural characterization reveals the epitaxial relationship is $<001>_{STO}||<001>_{TiN}||<001>_{Si}$. This suggests the applicability of TiN films to the formation of epitaxial contact with perovskite-type oxides as well as Si. The relatively sharp peaks indicate that the films grown under the above deposition conditions have good crystallinity. It has also been demonstrated (not shown) that all the STO films are cube-on-cube grown on the TiN/Si substrates even at high processing temperature up to 750°C.

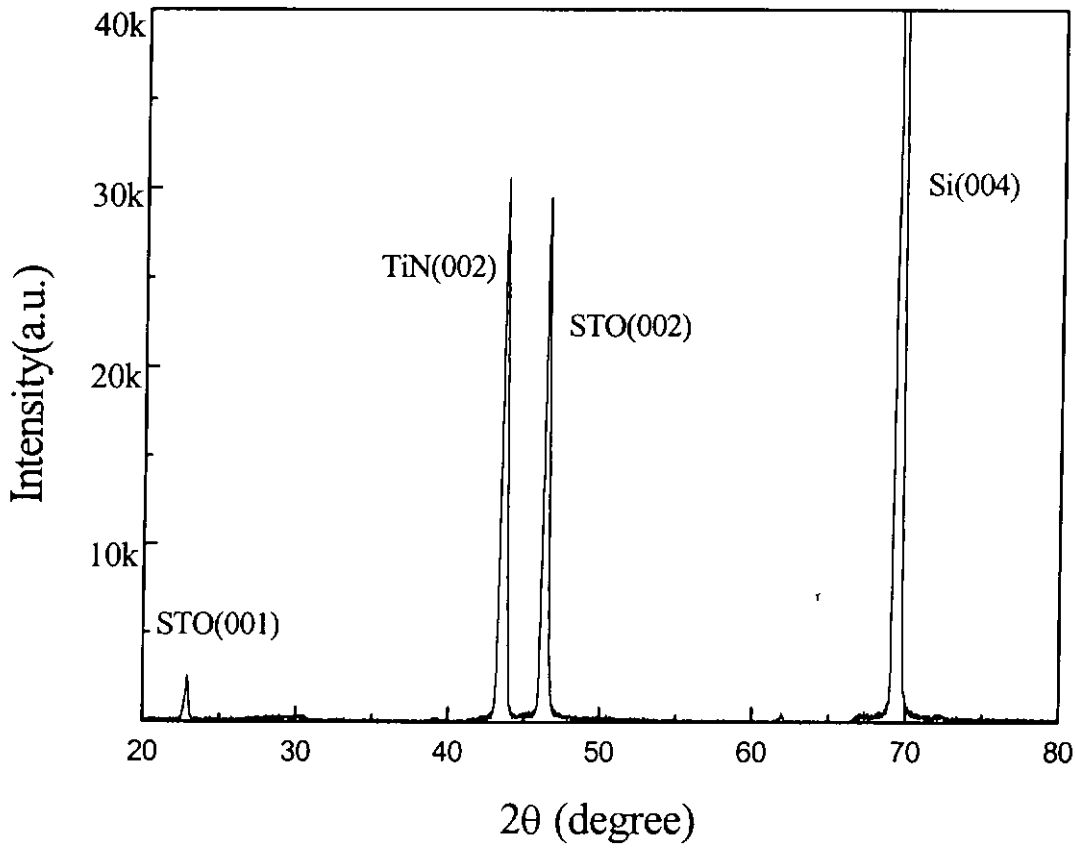

Fig. 6.4a The θ-2θ XRD pattern of STO film grown on TiN/Si at substrate temperature of 650°C under high vacuum of 4 x 10^{-6} Torr.

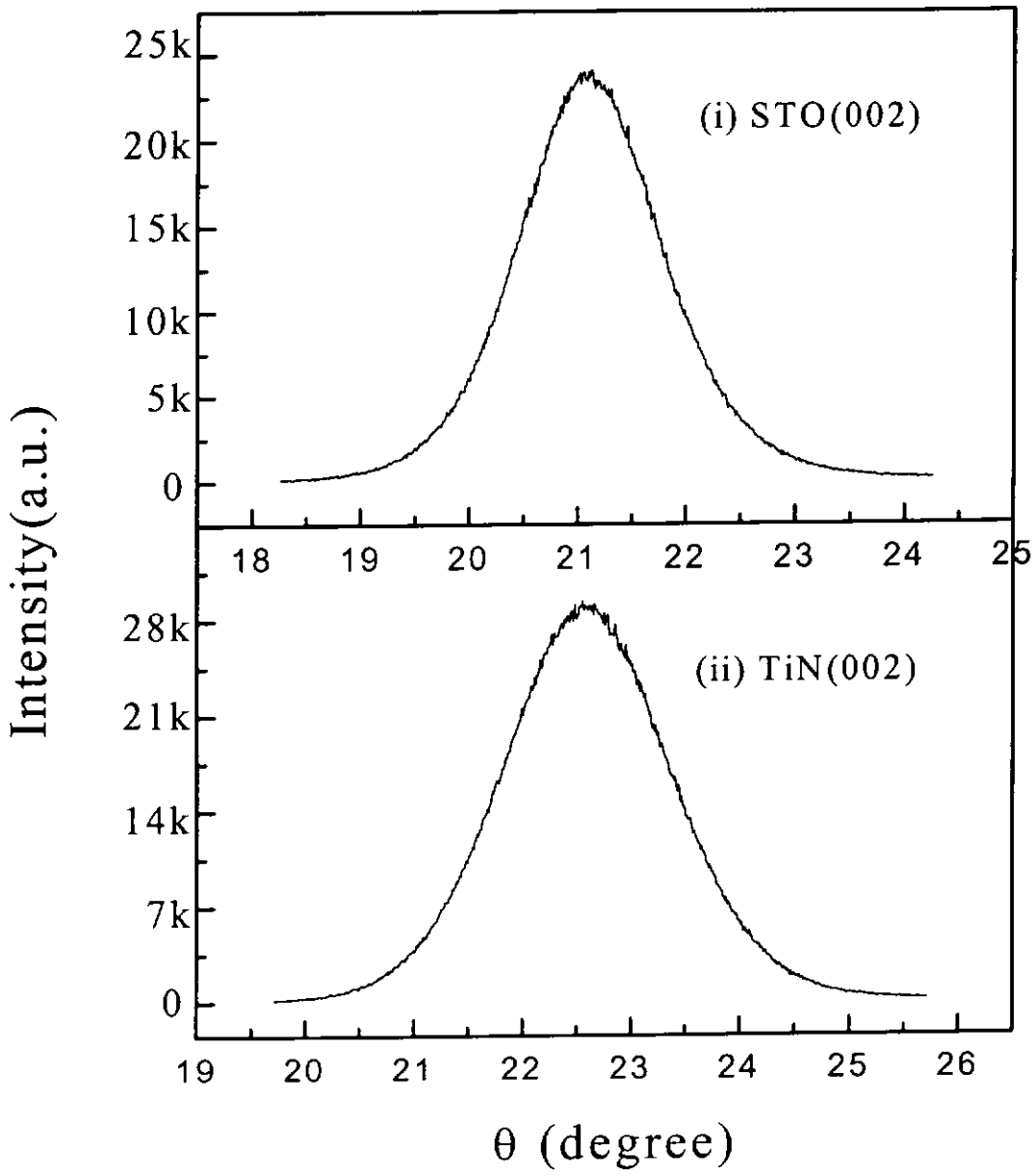

Fig.6.4b Rocking curves of (i) STO(002) and (ii) TiN(002) diffraction peaks which exhibit 1.51° and 1.74°, respectively.

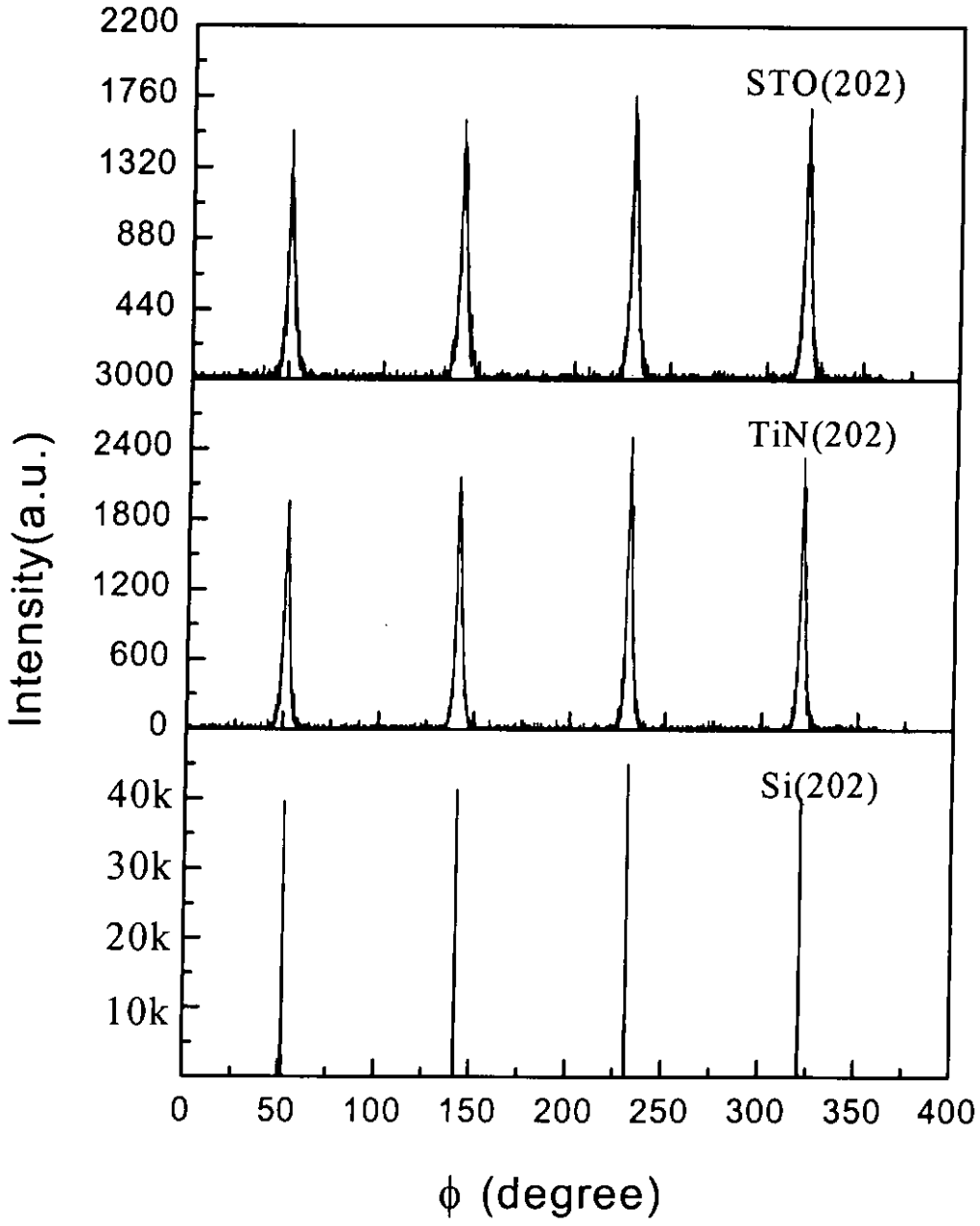

Fig. 6.4c The 360°-Φ scan diffraction pattern of the STO/TiN/Si heterostructures.

6.5 Substrate temperature dependence

We have shown that epitaxial STO films can be grown on TiN buffered Si(001) substrates. However, the growth temperature of TiN has distinct effect on the epitaxial relationship of STO/TiN heterostructures. As we have discuss before that TiN can be epitaxially grown on Si via a Volmer-Weber type 4-on-3 mode or a Stranski-Krastinov 5-on-4 mode. In this section, we would like to compare the substrate temperature dependence growth modes of the underlying TiN buffer layer on the subsequently deposited STO layer.

Fig.6.5a shows a series of X-ray θ-2θ diffraction patterns for STO/TiN/Si with the TiN grown *in-situ* at (i) 550°C, (ii) 650°C, and (iii) 750°C, respectively whereas the STO film was grown at a fixed temperature of 650°C. For comparison, it is found that for TiN grown at 550°C or 650°C the epitaxial relationship is $<001>_{STO}||<001>_{TiN}$. A STO film with TiN layer grown at 750°C is also single crystalline phase but with the following orientation relationship: $<101>_{STO}||<001>_{TiN}$. This change of relationship is accompanied by reduction in the out-of-plane lattice constant of the TiN layer. A small peak due to residue CuK_β radiation is labeled at 62°. In Fig 6.5a(i),(ii) the diffraction patterns are almost identical. According to Fig 6.5a(iii), it shows the prominent presence of the STO(101) reflection where no trace of the STO(00*l*) reflections was detected. The rocking curve on the STO(101) reflection yielded a FWHM of 1.9° (not shown). Moreover, the TiN(002) peak slightly shifts to a higher 2θ position relative to the peaks shown in Fig.6.5a(i),(ii), as expected [Wenbin Wu et al., 2000]. Besides, the FWHM of TiN(002) reflection was about 1.5°, indicating a very good orientation film can be obtained even at such high

processing temperature (~ 750°C) during the PLD growth.

The change of out-of-plane orientation of STO on TiN grown at different temperature can be explained as follow. The STO (a = 3.905 Å)/TiN(a = 4.24 Å) has a lattice mismatch of only –3.3% and cube-on-cube growth mode is favored. When the in-plane lattice constant of TiN is increased at higher deposition temperature, the STO/TiN lattice mismatch becomes bigger and the epitaxial relationship between the STO film and the TiN layer changes [Wenbin Wu et al., 2000].

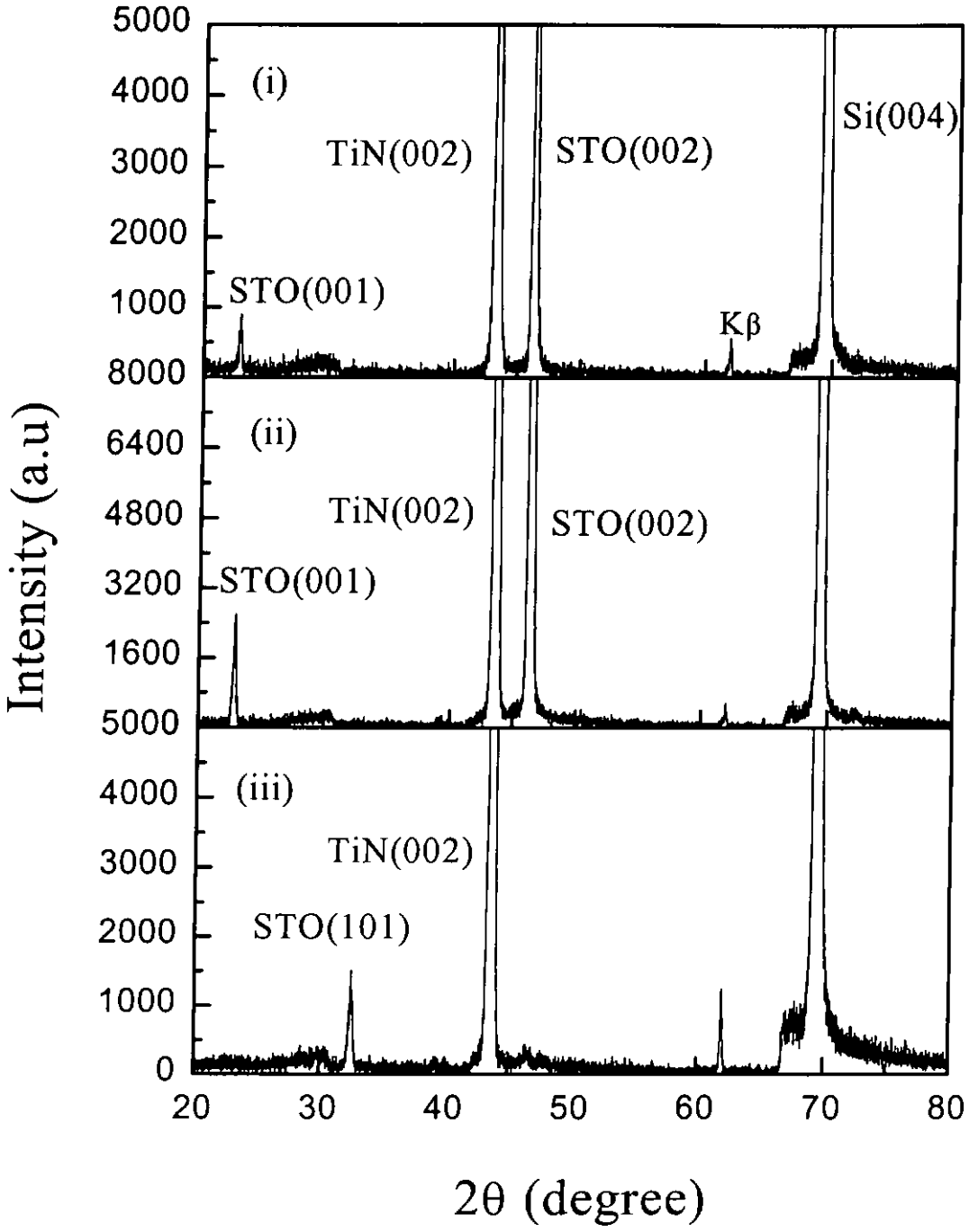

Fig. 6.5a The X-ray θ-2θ diffraction pattern for STO/TiN/Si with the TiN grown at (i) 550°C, (ii) 650°C, and (iii) 750°C, respectively.

6.6 Cross-section and surface morphology

In the previous section, we have shown the θ-2θ XRD pattern of single phase STO films grown on TiN/Si. Structural characterization reveals excellent quality for both the STO and TiN layers. The surface morphology of the films was also investigated. The SEM micrograph of 200 nm thick epitaxial STO film grown on TiN/Si heterostructure is shown in Fig. 6.6a. The STO and the underlying TiN layer were deposited at substrate temperature of 650°C and 550°C, respectively under high vacuum of 4 x 10^{-6} Torr. The surface morphology was found to be very smooth without microcracks. This may be due to the very small difference in thermal expansion coefficients (α_{STO} = 8 x 10^{-6}/K and α_{TiN} = 9.35 x 10^{-6}/K) between STO and TiN. The SEM image of fractured cross-section of the STO/TiN/Si heterostructure was depicted in Fig. 6.6b showing a thickness of 750 nm for TiN and 350 nm for STO layer. Apart from seeing two distinct layers, this image also reveals that the structure of the as-deposited films comprised of columnar grains propagating through the entire film. In addition, Fig. 6.6c displays the AFM image of this heterostructure. Uniform fine grains are clearly observed. As shown in Fig. 6.6d, the corresponding surface roughness is estimated to be about 0.62 nm over the area of 5 μm x 5 μm. This reveals that it is possible to obtain a good crystalline film with very smooth surface even in a few hundred nanometers thick film.

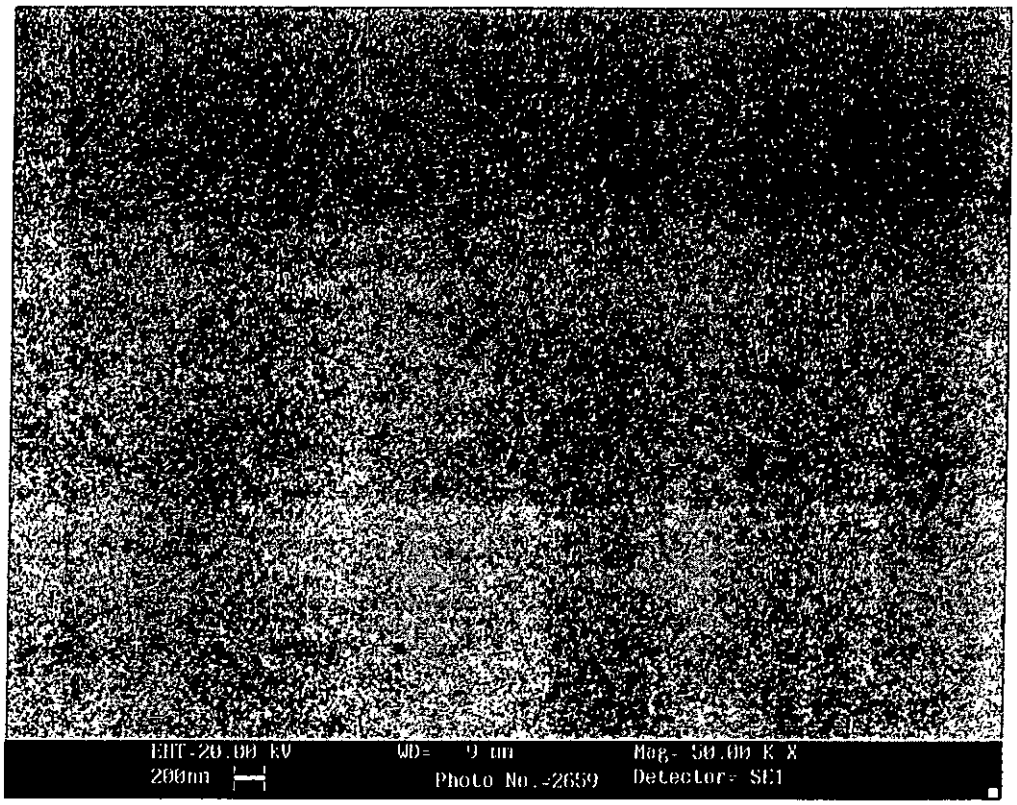

Fig. 6.6a SEM micrograph of epitaxial STO film grown on TiN/Si(001) showing a very smooth surface.

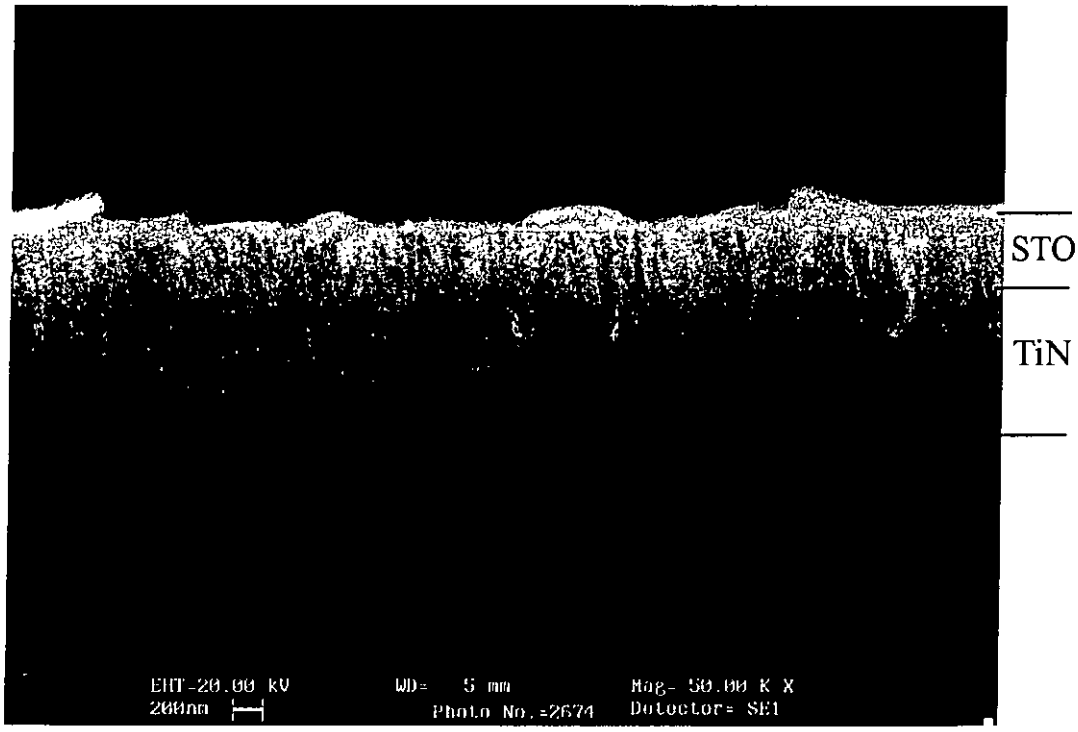

Fig. 6.6b The SEM cross-section of the STO/TiN/Si heterostructure, with STO deposited at 650°C whereas TiN at 550°C under high vacuum of 4×10^{-6} Torr.

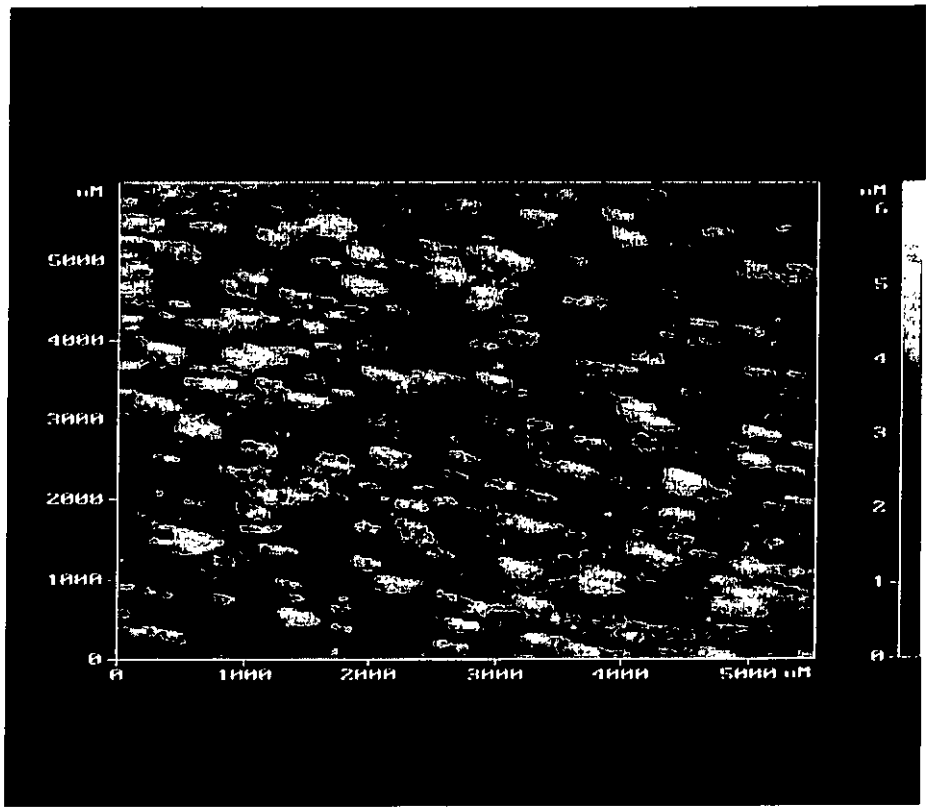

Fig. 6.6c AFM image of the STO surface deposited on TiN buffered Si substrates under 4 x 10^{-6} Torr.

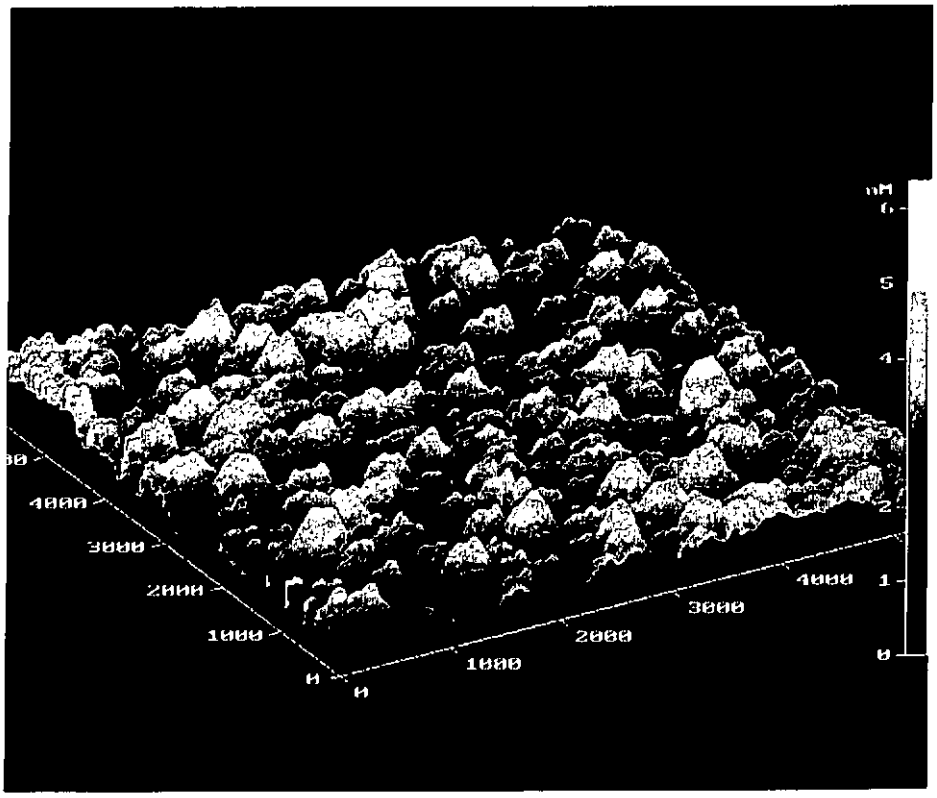

Fig. 6.6d The AFM image showing the relative roughness of the film.

For the STO/TiN/Si heterostructure, their microstructures and grain size vary significantly with the deposition temperature and show a strong dependence on the growth condition of the TiN buffer layers. When TiN grown at low temperature whereas STO was fixed at 650°C, the grains are so small and not completely formed. However, large grains can be obtained when TiN grown at high temperature. All the grains develop into a bigger size. Fig. 6.6e shows the AFM images of the TiN films grown at 550°C, 650°C and 720°C respectively whereas STO was fixed at 650°C. From the surface morphology of the STO films shown, we can observe the grain size increase as the deposition temperature of underlying TiN increases. This phenomenon verified that the films grown at high temperature are thus of good orientation and crystalline quality. On the other hand, these films showed more roughness as evidenced by the AFM images. The surface roughness over the area (5 μm x 5 μm) increases accordingly from 1.82 nm to 7.8 nm. Our results indicate that the grain size of the films is greatly affected by the substrate temperature. Although the films are rough, they are still highly oriented. In general, films grown at relatively low temperature are quite smooth. Notably, it is suggested that better crystallinity of STO films can be achieved by improving the quality of the template TiN layer.

(i)

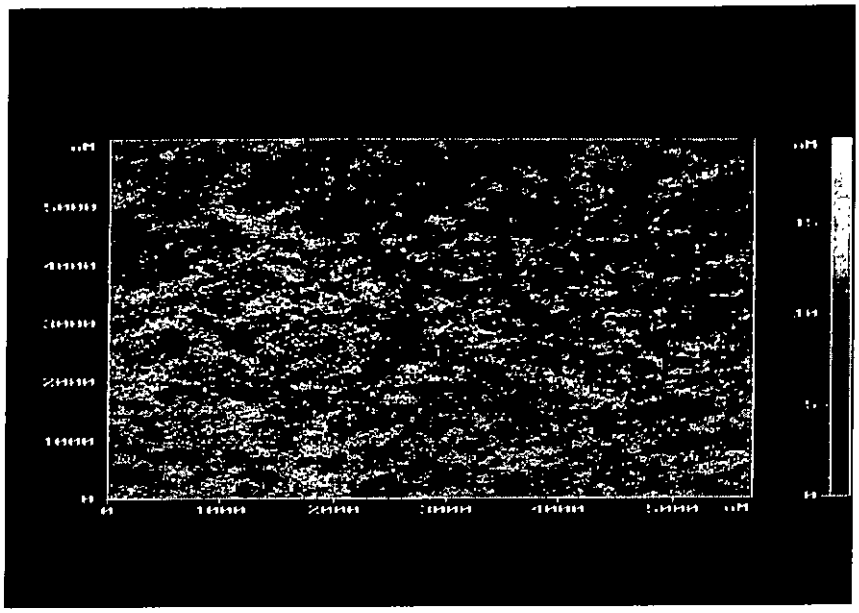

(ii)

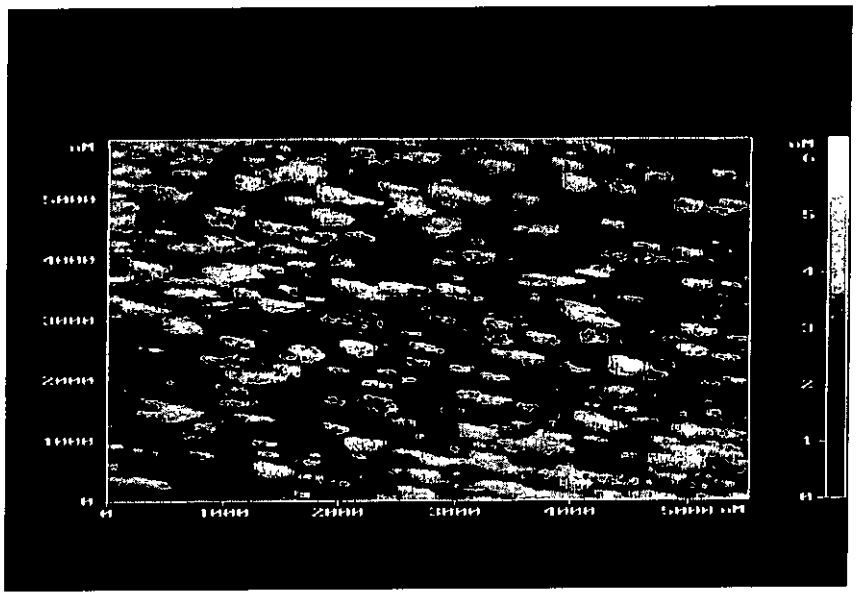

(iii)

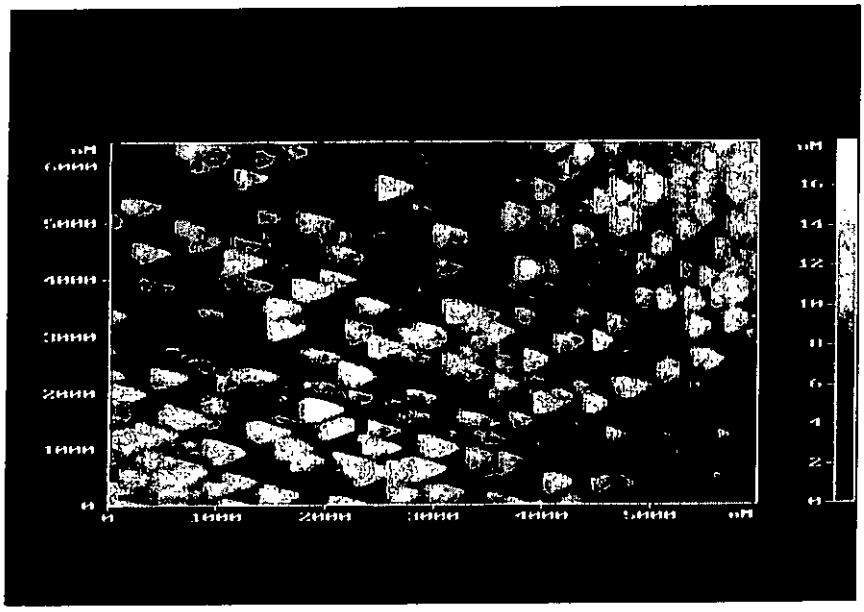

Fig. 6.6e The variation of the grain size for underlying TiN at (i) 550°C (ii) 650°C (iii) 720°C.

Chapter 7

Microhardness measurement

7.1 Introduction

Nanoindentation techniques have been developed and provide a mean to analyze the mechanical properties of thin films such as hardness, elasticity and friction coefficients. It often yields important quantitative information for research, development and production.

The hardness of materials is not only characterized by the interatomic bond strength, but also by the operative deformation mechanism. The deformation mechanism is related to the dislocation and its interaction with other micro-structural features. The hardness H and Young's modulus E of our samples in the present study were determined from a series of indentations on each film. A Nanoindenter (Nano Instruments, Inc. model IIs) was employed throughout. The minimum load of this intrument is as low as 500 μN, and the resolution of the penetration depth is claimed to be as good as 0.04 nm. With such a low load range, the influence of substrate deformation in a hardness test is practically negligible. Calibrations of the load frame stiffness and the area function of the diamond tip were importance for attaining reliable results. Indentation loads and the corresponding displacements were recorded continuously throughout each test. Each set of H and E was obtained by averaging the results of 40 identical indents at different positions on the film surface. The hold period of 10 s was used for all loads in order to minimize the effects of time-dependent plasticity on the measured hardness. All tests were conducted at

maximum contact displacement ranging from 0 to 250 nm using a Berkovich indentation head.

Hardness values obtained from most of the existing nanoindentation data in the literature show an indentation size dependence of the measured hardness [Oliver et al., 1992], i.e., a decrease in hardness is observed with increasing load. A number of reasons for this behaviour has been proposed: uncertainty in accurately determining the contact area; surface artifacts such as abrasive or contamination, etc. One of the most important problems is that films are constrained by substrates, hence the properties of the films depend on a penetration depth even in a depth shallower than film thickness. Therefore, the ratio of h_{cr}/t must be clarified, where t is the thickness of film, and h_{cr} is a critical penetration depth at which the substrate begins to affect the properties of films. The plastic deformation zone beneath an indenter expands with increasing penetration depth of the indenter. The indenter reaches the film/substrate interface as depicted in Fig. 7.1a.

An effective elastic modulus E^* can be written as:

$$\frac{1}{E^*} = \frac{1-\gamma_s^2}{E_s} + \frac{1-\gamma_i^2}{E_i}$$

where E and γ are Young's modulus and Poisson's ratio, subscripts s and i represent the specimen and the indenter. The Young's modulus and Poisson's ratio of diamond used are $E_i = 1141$ GPa, $\gamma_i = 0.07$. An estimated Poisson's ratio for TiN and TaN film is 0.33 and 0.25, respectively.

Each indentation cycle consists of a loading curve and an unloading curve, showing the displacement of the tip when the normal load is increased and reduced, respectively. The typical load-displacement data is shown schematically in Fig. 7.1b. Oliver et al found that the final depth gives a better estimate of the contact area. With the contact area determined, the film hardness H is then calculated as:

$$H = \frac{P_{max}}{A}$$

In the present work, the fundamental mechanical properties of epitaxial nitride films have been studied. The undersirable effects due to grain boundary, orientation, and defect at the interface have been minimized. Enhancement caused by TaN/TiN bi-layer structure has also been investigated. For our samples, 40 indentations were made on each film at different points separated from each other by 50μm. There are totally 4 experiments and each of them was repeated 10 times to get the average values of H and E.

In this chapter, we report the mechanical results on epitaxial single layer film corresponding to TiN, TaN and bi-layer TaN/TiN/Si heterostructures. It has been shown that the films with good crystalline quality have higher hardness and modulus values.

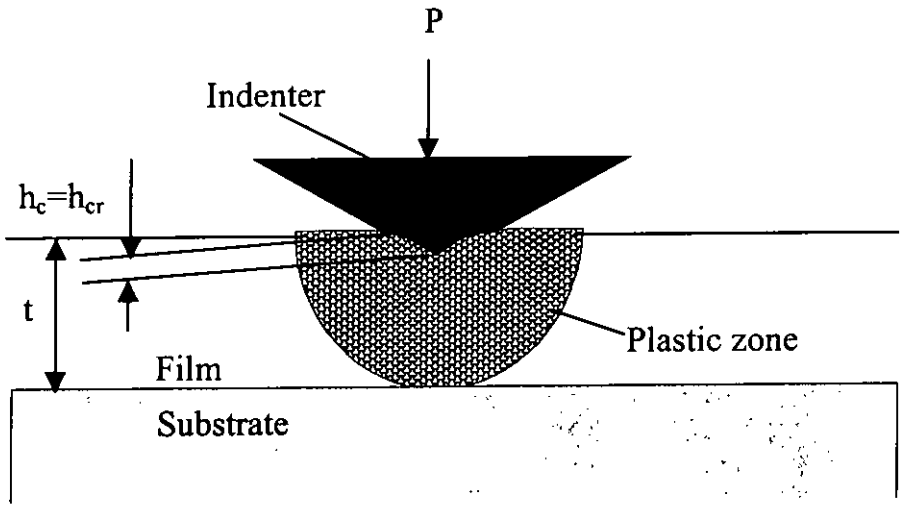

Fig. 7.1a Schematic diagram of the indenting process illustrating the expansion of plastic zone beneath the indenter. The notations t is the film thickness, P is the load and h_c is the penetration contact depth.

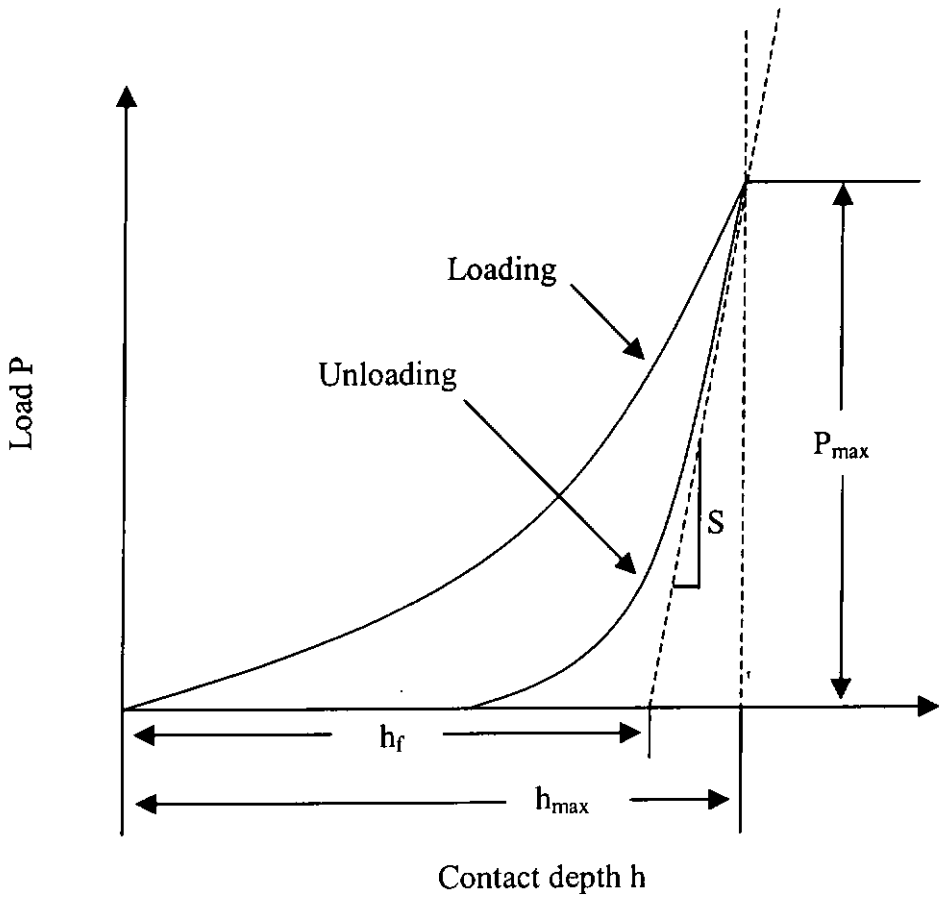

Fig. 7.1b A schematic representation of load versus indenter displacement data for an indentation experiment. The quantities shown are P_{max}: the peak indentation load; h_{max}: the indenter displacement at peak load; h_f: the final depth of the contact impression after unloading; and S: the intial unloading stiffness.

7.2 TiN/Si

Interest in Titanium Nitrides (TiN) thin film is based on its unique combination of good chemical inertness, high thermal and electrical conductivity, excellent wear resistance and beautiful lustrous colour. These characteristics make TiN films a wide range of application such as diffusion barriers, wear-protecting coatings on mechanical components, etc. Theoretically, the relative hardness of TiN films can be up to 40 GPa [Nakamura et al., 1977]. Reported mechanical properties of TiN layers depend strongly on deposition parameters including stoichiometry, microstructure and texture [Petrov et al., 1992].

Fig. 7.2a displays a typical load-penetration depth curve for our TiN film with thickness of 200 nm. By applying different maximum loads --- 3, 7.5 and 15 mN as shown systematically, indentation on TiN film grown at optimum temperature of 650°C under 4 x 10^{-6} Torr, yields a hardness (H) value of about 25 GPa and a Young's modulus (E) of 375 GPa. The relative H for Si(001) is only 10 GPa. The surface of the film was very smooth as shown previously by SEM and AFM observations. This allows reliable nanoindentation measurements. Indeed, this is the best data obtained from the deposited epitaxial TiN film under the optimum growth conditions. It exhibits higher hardness and modulus values compared to the films deposited at temperatures above 700°C. On the other hand, the lack of crystallinity and decrease in hardness (20 GPa) for TiN films grown at 550°C appear to be related to the low processing temperature.

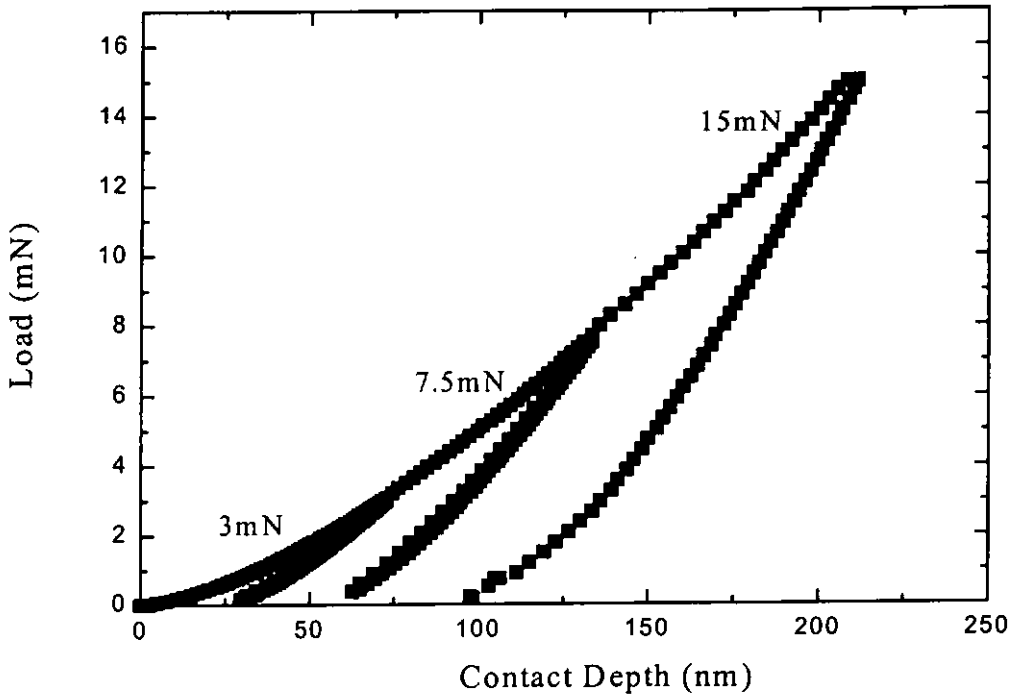

Fig. 7.2a Load vs. penetration depth curve for TiN film of 200 nm thick, with 3, 7.5 and 15 mN maximum loads.

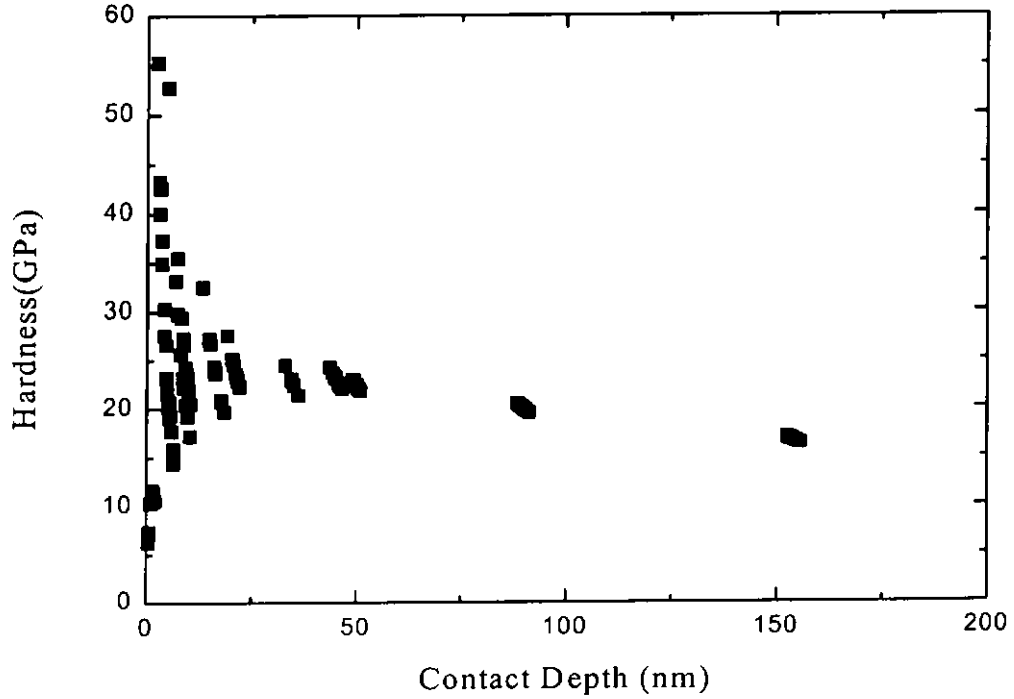

Fig. 7.2b The hardness values obtained from the TiN film.

7.3 TaN/MgO

In previous sections, the X-ray diffraction patterns have been shown that the cubic TaN films can be deposited on MgO(001) at 550°C under high vacuum of 5 x 10^{-6} Torr. It was also observed that these good quality films with excellent structural and epitaxial relationship. The FWHM of TaN(002) was only 0.3°, indicating a highly oriented and good crystalline film. The thickness of the TaN film was about 250 nm. The load (P) and hardness (H) of the film as functions of contact depth are shown in Fig. 7.3a and Fig. 7.3b. In the present case, the MgO single crystal substrate has the H value about 9 GPa. The measurable substrate contributions were also observed in Fig. 7.3b. In this curve, we can clearly see that the measured TaN hardness values consist of larger contributions from the MgO substrate. Similarly, the obtained H for single-layered TaN is 22 GPa at the maximum displacements up to 220nm. The decrease in hardness of deposited TaN films was observed with increasing load. This may be attributed to the substrate effect becoming significant. In general, high load hardness measurements in thin films can be influenced by substrate contribution. The average of the Young's modulus data obtained from this sample is about 313 GPa.

Also, the Ta/N ratio can influence the mechanical properties of the films significantly. At present the relationship between the mechanical properties and the degree of nitrogen difficient in TaN film is not known. It will be, nevertheless, a subject for further investigation.

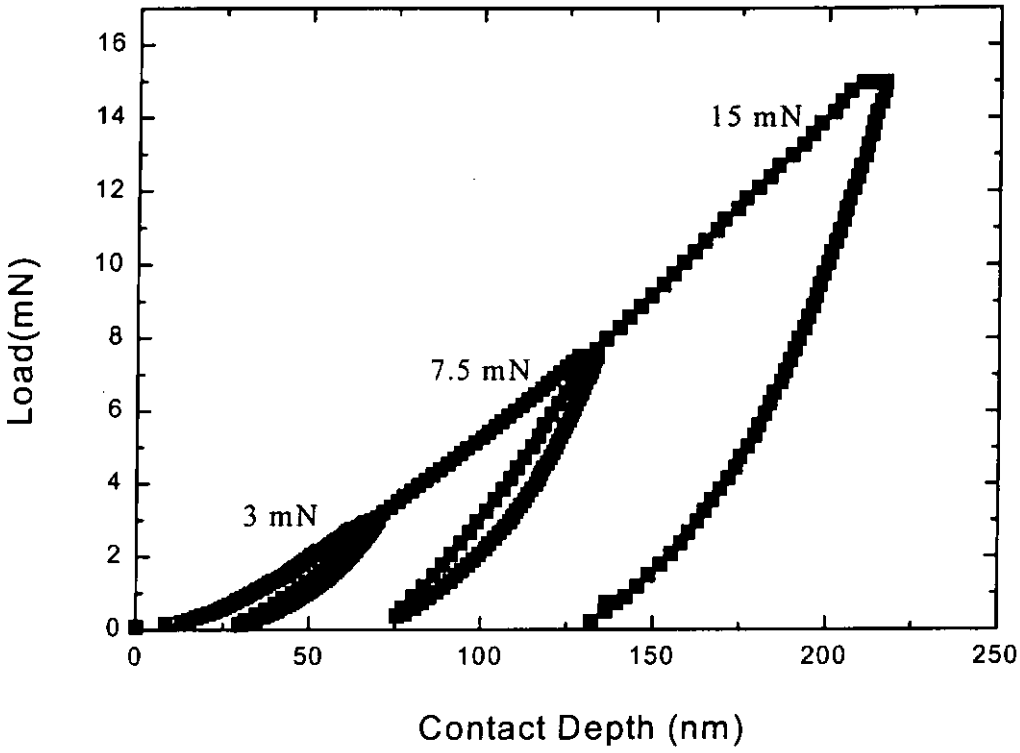

Fig. 7.3a The load-displacement curve, with 3, 7.5 and 15 mN load respectively for TaN film deposited on MgO substrate.

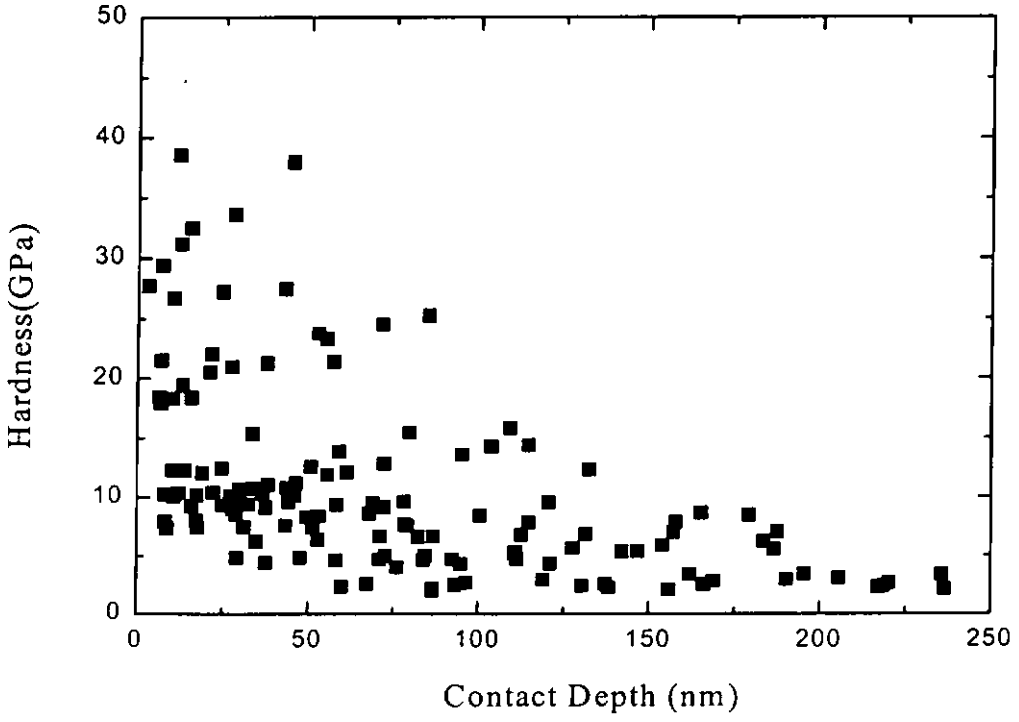

Fig. 7.3b The hardness values obtained from the TaN film.

7.4 TaN/TiN/Si

A mean to obtain a hard coating with improved toughness is to deposit a layered structure of different hard coating materials. In one of the early attempts, multi-layer coatings have been found to possess superior mechanical and tribological properties as compared with single-layered coatings [Duckworth, R. G., 1980]. In the present work, multi-layered TaN/TiN films were also investigated. By depositing bi-layer films and single layered films, we made comparative studies on their mechanical properties. A remarkably increase in hardness for those multi-layered films was obtained. The results indicate that for TiN grown at 600°C and TaN at 650°C, the mean hardness of TaN/TiN bi-layer film is about 28 GPa. Fig. 7.4a shows the load-penetration depth curve with three different maximum loads for the epitaxial TaN/TiN/Si heterostructure. The thickness for both films was 200 nm. Nanoindentation hardness values of the same sample are plotted in Fig. 7.4b as a function of contact depth. It is found that the multi-layered TaN/TiN films exhibit the highest hardness value of 28 GPa. The measured E is about 451 GPa. As a comparison, the load (15 mN) on the above three different samples as a function of typical nanoindentation contact depths are shown in Fig. 7.4c. The load and unloaded curve for multi-layer structure is quite close to each other, indicating the film has a high elastic coefficient. This high elasticity is desirable for tools coating such as cutting applications. Therefore, we can conclude that stoichiometric multi-layer TaN/TiN/Si films have higher hardness and Young's modulus value compared to those of single layer film. As a result, these kind of multi-layers are expected to serve efficiently as a barrier layer and an enhanced hard coatings.

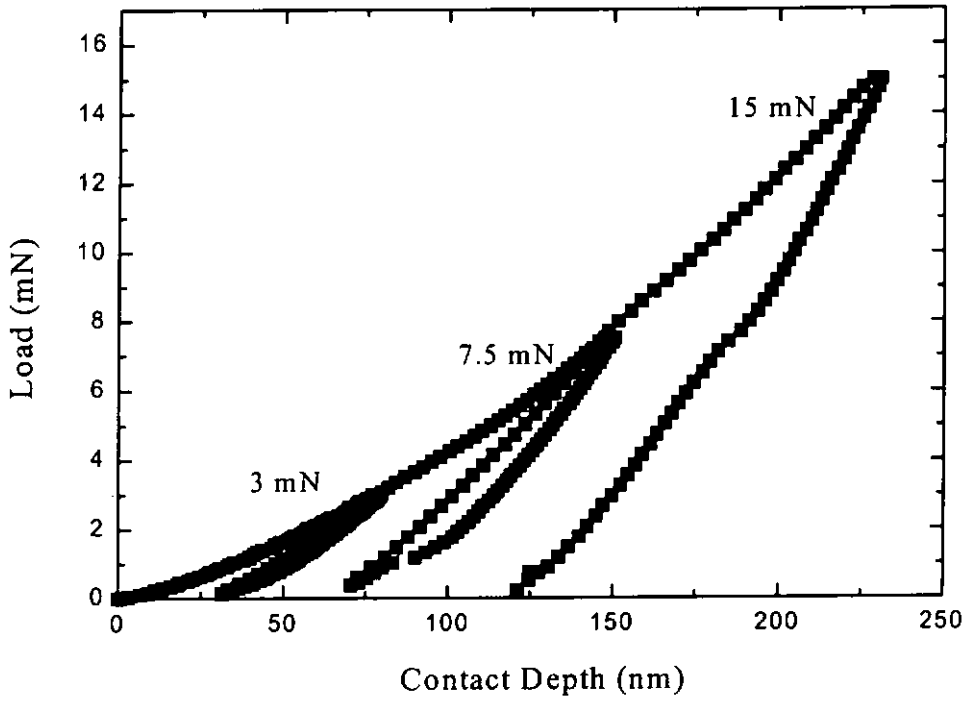

Fig. 7.4a The load-penetration depth curve, with 3, 7.5 and 15 mN maximum loads for the epitaxial TaN/TiN/Si heterostructure.

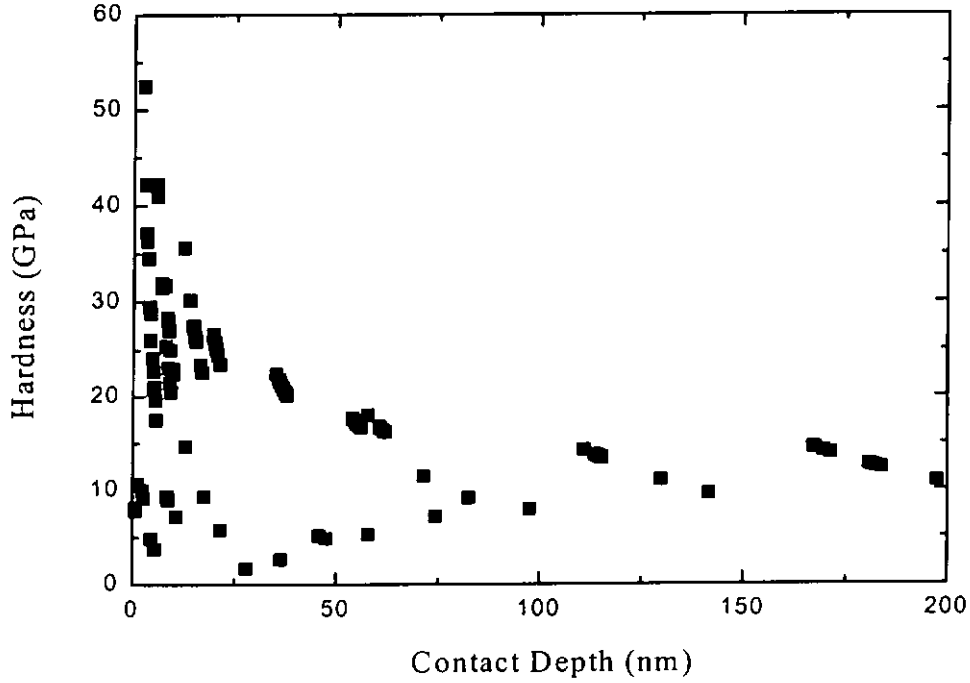

Fig. 7.4b The hardness values as a function of contact depth during nanoindentation measurements on TaN films.

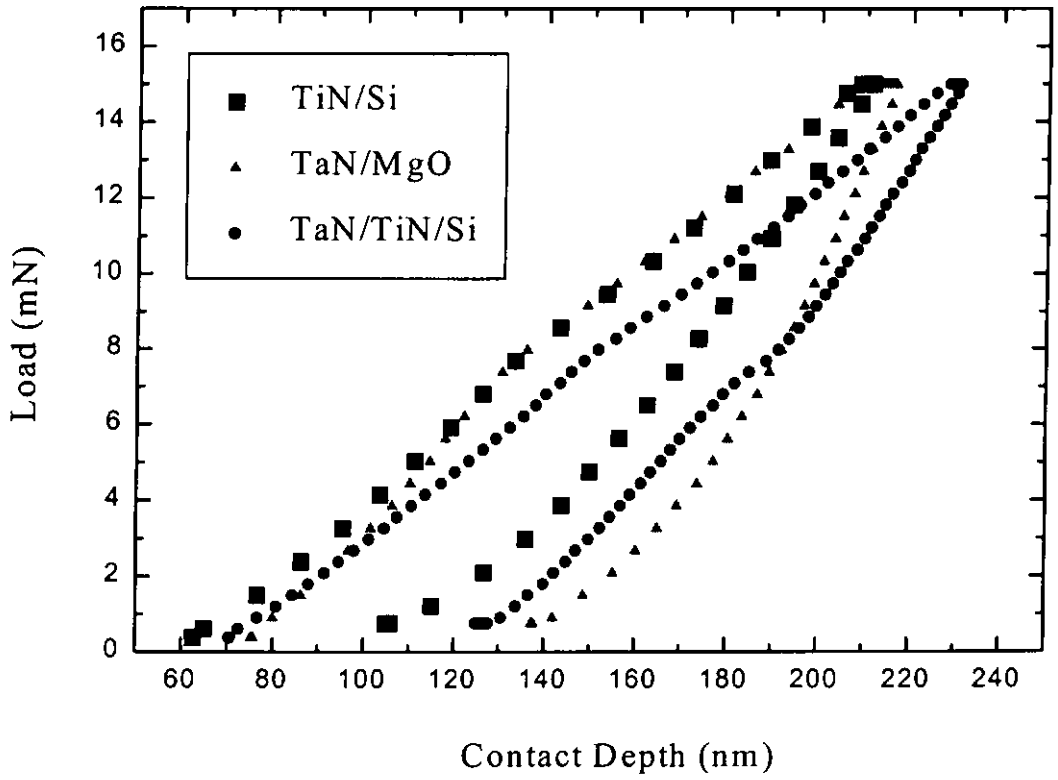

Fig. 7.4c The load (15 mN) on the three different samples as a function of typical nanoindentation contact depth.

Chapter 8

Conclusions and suggestions for future work

In the present work, epitaxial TiN(001) and TaN(001) thin films were successfully grown on Si(001) and MgO(001) single crystal substrates by PLD method. They were structurally characterized by X-ray diffractometer using CuK_α radiation. Apart from the (002) reflections from the films and the substrates, no trace of other reflections was observed. Resistivity-temperature measurements of the epitaxial TiN, TaN and heteroepitaxial TaN/TiN layers were performed by a standard four-point-probe technique over the temperature range from 78 K to 300 K. The interface boundary and the surface roughness were studied by SEM and AFM in details. The mechanical properties of the deposited films, as determined by nanoindentation measurements were also obtained and described.

It was found that crystalline TiN films could be obtained at oxygen free environment (4×10^{-5} Torr) over a wide temperature ranged from 500°C to 720°C. The corresponding FWHM of rocking curve of TiN(002) varied from 2.2° to 1.17°. All the TiN films fabricated under these deposition conditions had a characteristic golden colour. In addition, TiN layers grown on Si showed high degree of in-plane epitaxy. Relationships between the substrate temperature and lattice parameter d for the TiN films were obtained. From the film thickness studies, it was noted that the out-of-plane lattice constant of TiN layer deposited at a fixed temperature of 550°C decreased gradually with increased thickness. This suggests that thicker films relax from the strained interface layer. On the other hand, when increase the growth

temperature to 650°C, the out-of-plane lattice constant of TiN increases from 4.13 Å to 4.19 Å. The R-T characteristics exhibit a typically linear metallic behavior and a resistivity of about 44 μΩ cm is obtained at room temperature. All TiN films are thus of good electrical properties. SEM analysis revealed smooth and crack-free surface in most TiN films. However, AFM images have indicated that the microstructures and roughness of the films changed dramatically at elevated deposition temperature.

Considerable effort has been devoted to the fabrication and characterization of TaN films. Crystalline TaN layers of about 100 nm thick were fabricated on MgO(001) single crystal substrates. Excellent quality TaN films were obtained at growth temperature ranging from 500°C to 700°C under a base pressure of 5×10^{-6} Torr. According to the ω-scan rocking curve, the FWHM of TaN(002) reflection peak can be as narrow as 0.3°. This strongly suggests a very good orientation of the TaN film. XRD peaks indicate that all the TaN films grown under the above said deposition conditions have good crystallinity and parallel epitaxial properties with the orientation relationship $<001>_{TaN}||<001>_{MgO}$. Plan-view and cross-sectional electron microscopy analysis reveal excellent structural quality. For the films grown at higher energy density, they show significantly more rough surface but remain highly oriented with respect to the substrates. In spite of the ball-shaped particles, a very sharp interface boundary of TaN layer is observed. From the R-T curve, we can clearly see that pure cubic TaN is nonmetallic with negative $\frac{d\rho}{dT}$.

On the other hand, TaN films grown on TiN(001) buffered Si(001), showed a mixture of TaN_x (with $x \leq 1$) components. Although the (001)-orientated TaN is always present prominently, the nitrogen deficient TaN_x components are often

co-existed in the films and show up as a broad peak in the X-ray diffraction profile. Indeed, earlier reports have identified that TaN films often show non-stoichiometric composition due to their defective structure. The present investigations show that films under some optimum condition, apart from the (00*l*) reflections from the TaN and the underlying TiN layers, no trace of other reflections is observed. Stoichiometric and single phase TaN(001) films can only be obtained in a narrow temperature window at around 550°C. This low processing temperature is highly desirable and compatible to silicon industry technology. The epitaxial relationship obtained is $<001>_{TaN}||<001>_{TiN}||<001>_{Si}$. We have found that the formation of ball-shaped particulates in TaN thin films is prominently present in most samples. It is mainly induced either directly by the target ablation process or by super-saturation condensation at near the substrate surface during the deposition process. This can be eliminated, if need be, by placing a shadow mask between the target and substrate. Both TiN (positive $\frac{d\rho}{dT}$) and TaN (negative $\frac{d\rho}{dT}$) have good conductance at room temperature. An interesting finding is that a properly tuned TaN/TiN/Si film can produce a nearly flat profile in the R-T curve, i.e. $\frac{d\rho}{dT} \approx 0$.

Nanoindentation measurements on TiN, TaN and TaN/TiN films have been carried out. Results show that the TiN films grown under optimized deposition conditions at 650°C (4 x 10^{-5} Torr), give a high hardness (H) value of about 25 GPa and a large Young's modulus (E) of 375 GPa. Similarly, cubic TaN films deposited on MgO(001) substrates at 550°C (5 x 10^{-6} Torr) exhibit high H of about 22 GPa at maximum displacements of up to 220 nm. The corresponding E is about 313 GPa. The bi-layered TaN/TiN films have also been investigated. The results indicate that

for TiN grown at 600°C and TaN at 650°C, the mean H and E are as high as 28.3 GPa and 451 GPa, respectively. All these data suggest that it is possible to obtain enhanced H and E values for the multi-layer structures compared with those produced by single layer films. Therefore, these kind of multi-layers nitride films are expected to serve as efficient diffusion barrier and super-hard protective coatings. They deserve more intensive research in the coming years.

The detailed mechanisms for preventing the undesirable particulates in the TaN thin films, the mechanical properties of TaN phase mixtures with different Ta/N ratio, however, need further studies and clarification. Moreover, the interest in sub-0.25 μm ULSI circuits has been developed [Oku et al., 1996; Chen et al., 2000]. Copper (Cu) has drawn much attention as a new interconnecting material due to its low resistivity (1.7 μm). Its high electromigration, however, can easily deteriorate the device operation if Cu diffuses into the Si regions. TaN is presently one of the most widely used buffer materials. It shows not only a relatively high melting point, but is also known for its thermodynamic stability. Previous studies have also revealed that stoichiometric TaN films to be excellent diffusion barriers. A more detailed study of the effect involving diffusion and intermixing of Cu through TaN, on the barrier properties needs to be carried out.

References

Abdin, S., and Val, C.
"The production of Tantalum nitride film resistors using a continuous sputtering machine"
Thin Solid Films., Vol. 57, pp.327 (1979)

Adams, P. M., Speckman, D. M., and Radhakrishnan, G.
"Low temperature pulsed laser deposition of titanium carbide on bearing steels"
Thin Solid Films., Vol. 358 (1-2), pp.131 (2000)

Au, C. L., Anderson, W. A., Schmitz, D. A., Flassayer, J. C., and Collins, J.
"Stability of tantalum nitride thin film resistors"
J. Mater. Res.5., pp.1224 (1990)

Bunshah, R. F.
"Deposition technologies for films and coatings"
Noyes Publisher-Park Ridge (1982)

Chang, L. D., Tseng, M. Z., Hu, E. L., and Fork D. K.
"Epitaxial MgO buffer layers for $YBa_2Cu_3O_{7-x}$ thin films on GaAs"
Appl. Phys. Lett., Vol. 60(14), pp.1753 (1992)

Chen, G. S., Chen, S. T.
"Diffusion barrier properties of single and multilayered quasi-amorphous tantalum nitride thin films against copper penetration"
J. Appl. Phys., Vol. 87, pp.8473 (2000)

Chen, G. S., Huang, S. C., Chen, S. T., and Yang, T. J.
"An optimal quasisuperlattice design to further improve thermal stability of tantalum nitride diffusion barriers"
Appl. Phys. Lett., Vol. 76(20), pp.2895 (2000)

Choi, C. H., Hultman, L., Chion, W. A., and Barnett, S. A.
"Growth of epitaxial TiN thin films on Si(100) by reactive magnetron sputtering"
J. Vac. Sci. Tech., B9, pp.221 (1991)

Chowdhury, R., Vispute, R. D., Jagannadham, K., and Narayan, J.
"Characteristics of titanium nitride films grown by pulsed laser deposition"
J. Mater. Res.6., Vol. 11, pp.1458 (1996)

Chrisey, D. B., and Hubler, C. K.
"Pulsed laser deposition of thin films"
Wiley, New York (1994)

Ensinger, W.
"Low-temperature formation of metastable cubic tantalum nitride by metal condensation under ion irradiation"
J. Appl. Phys., Vol. 77, pp.6630 (1995)

Ezugwu, E. O.
"Manufacture and properties of ceramic cutting tools"
Mater. Sci. Technol., Vol. 3, pp.881 (1987)

Fork, D. K., Fenner, D. B., Connell, G. A. N., Phillips, J. M., and Geballe, T. H.
"Epitaxial yttria-stabilized zirconia on hydrogen-terminated Si by pulsed laser deposition"
Appl. Phys. Lett., Vol. 57, pp.1137 (1990)

Fork, D. K., Nashmoto, K., and Geballe, T. H.
"Epitaxial $YBa_2Cu_3O_{7-x}$ on GaAs(001) using buffer layers"
Appl. Phys. Lett., Vol. 60, pp.1621 (1992)

Greene, J. E., Shin, C. S., Gall, D., Desjardins, P., Vailionis, A., Kim, H., Petrov, I.
"Growth and physical properties of epitaxial metastable cubic TaN(001)"
Appl. Phys. Lett, Vol. 75, pp.3808 (1999).

Holloway, K., Fryer, P. M., Cabral, C., and Harper, J. M. E.
"Tantalum as a diffusion barrier between copper and silicon: failure mechanism and effect of nitrogen additions"
J. Appl. Phys., Vol. 71, pp.5433 (1992)

Horwitz, J. S., Grabowski, K. S., Chrisey, D. B., and Leuchtner, R. E.
"In situ deposition of epitaxial $PbZr_xTi_{(1-x)}O_3$ thin films by pulsed laser deposition"
Appl. Phys. Lett., Vol. 59, pp.1565 (1991)

Hugh O. Pierson.
"Handbook of refractory carbides and nitrides: Properties, characteristics, processing and applications"
Academic, USA, 1996

Iwabuchi, M., Kinoshita, K., Ishibashi, H., and Kobayashi, T.
"Reduction of pinhole leakage current of $SrTiO_3$ films by ArF excimer laser deposition with shadow mask ("Eclipse method")
Jpn. J. Appl. Phys., Vol. 33, pp.L610 (1994)

Kanamori. S.
"Investigating of reactively sputtered TiN films for diffusion barriers"
Thin Solid Films., Vol 136, pp.195 (1986)

Kirby, P. L.
"Applications of resistive thin films in electronics "
Thin Solid Films., Vol. 50, pp.211 (1978)

Koinuma, H., Lee, M. B.
"Structural and dielectric properties of epitaxial $SrTiO_3$ films grown on Si(100) substrate with TiN buffer layer"
J. Appl. Phys., Vol. 81, pp.2358 (1997)

Lewis, B., and Anderson, H.
"Nucleation and growth of thin films"
Academic Press, New York (1978)

Mehrotra, B., and Stimmell, J.
"Properties of direct current magnetron reactively sputtered TaN"
J. Vac. Sci. Technol. B., Vol. 5, pp.1736 (1987)

Moon, B. K., and Ishiwara, H.
"Formation and electrical properties of heteroepitaxial $SrTiO_3/SrVO_{3-x}/Si$ structures"
Appl. Phys. Lett., Vol. 67, pp.1996 (1995)

Lee Myung Bok., Masashi Kawasaki., Mamoru Yoshimoto., and Masao Kumagai.
"Epitaxially growth of highly crystalline and conductive nitride films by pulsed laser deposition"
Jpn. J. Appl. Phys., Vol. 33, pp.6308 (1994)

Nakamura, K., Inagawa, K., Tsurvoka, K., Komiya, S.
"Application of wear resistant thick films formed by physical vapor deposition processes"
Thin Solid Films., Vol. 40, pp.155 (1977)

Narayan, J., Tiwari, P., Chen, X., Singh, J., Chowdhury, R., and Zheleva, T.
"Epitaxial growth of TiN films on (100) silicon substrates by laser physical vapor deposition"
Appl. Phys. Lett., Vol. 61 (11), pp.1290 (1992)

Nicolet, M. A.
"Diffusion barriers in thin films"
Thin Solid Films., Vol. 52, pp.415 (1978)

Noya, A., Sasaki, K., and Takeyama, M.
"Auger electron spectroscopy study on the stability and the interfacial reaction of Ta, Ta-N and TaN films as a diffusion barrier between Cu_9Al_4 film and Si"
Jpn. J. Appl. Phys., Vol. 32, pp.911 (1993)

Oku, T., Kawakami, E., Uekubo, M., Takahiro, K., Yamaguchi, S.,
and Murakami, M.
"Diffusion barrier property of TaN between Si and Cu"
Appl. Sur. Sci., Vol. 99, pp.265 (1996)

Oliver, W. C., Pharr, G. M.
"An improved technique for determining hardness and elastic modulus using load and displacement sensing indentation experiments"
J. Mater. Res.6., Vol. 7, pp.1564 (1992)

Olowolafe, J. O., Mogab, C. J., Gregory, R. B., and Kottke, M.
"Interdiffusions in Cu/reactive-ion-sputtered TiN, Cu/chemical vapor deposited TiN, TaN/Cu/TaN thin film structures: Low temperature diffusion analysis"
J. Appl. Phys., Vol. 72, pp.4099 (1992)

Parker, E. H. C.
"The technology and physics of molecular beam epitaxy"
Plenum-New York (1986)

Petrov, I., Hultman, L., Sundgren, J. E., and Greene, J. E.
"Polycrystalline TiN films deposited by reactive bias magnetron sputtering: Effects of ion bombardment on resputtering rates, film composition, and microstructure"
J. Vac. Sci. Technol. A10., pp.265 (1992)

Prusseit, W., et al.
"Epitaxial growth of $YBa_2Cu_3O_{7-x}$ films on GaAs with MgO buffer layers"
Appl. Phys. Lett., Vol. 61, pp.1841 (1992)

Ramesh, R., et al.
"Epitaxial growth of ferroelectric bismuth titanate thin films by pulsed laser deposition"
Appl. Phys. Lett., Vol. 57, pp.1505 (1990)

Rao, G. M., and Krupanidhi, S. B.
"Study of electrical properties of pulsed excimer laser deposited strontium titanate films"
J. Appl. Phys., Vol. 75, pp.2604 (1994)

Saenger, K. L.
"Time-resolved optical emission during laser ablation of Cu, CuO and high-T_c superconductors: $Bi_{1.7}Sr_{1.3}Ca_2Cu_3O_x$ and $Y_1Ba_{1.7}Cu_{2.7}O_y$"
J. Appl. Phys., Vol. 66, pp.4435 (1989)

Shengwen Yu, Guanghou Wang, Shuangye Yin, Yunxiang Zhang and Zhiguo Liu
"Nanostructured films of Boron suboride by pulsed laser deposition"
Physics Letters A., Vol. 268 (4-6), pp.442 (2000)

Smith, H. M., and Turner, A. F.
"Vacuum deposited thin films using a Ruby laser"
Applied Optics., Vol. 4, pp.147 (1965)

So, F. C. T., Kolawa, E., Zhao, X. A., Pan, E. T. S., and Nicolet, M. A.
"Reactively sputtered TiN as a diffusion barrier between Cu and Si"
J. Appl. Phys., Vol. 64, pp.2787 (1988)

Takeo Oku., Eiji Karva., Masaki Uekubo., Katsumi Takahiro., Sadae Yamaguchi., Masanori Murakami.
"Diffusion barrier property of TaN between Si and Cu"
Appl. Surf. Sci., Vol. 99, pp.265 (1996)

Timm, R., Willmott, P. R., and Huber, J. R.
"Parallel epitaxy of TiN(100) thin films on Si(100) produced by pulsed reactive crossed-beam laser ablation"
Appl. Phys. Lett., Vol. 71, pp.1966 (1997)

Toth, L. E.
"Transition Metal Carbides and Nitride"
Academic, New York, (1971)

Tsvetanka Zheleva, Jagannadham K., and J. Narayan.
"Epitaxial growth in large-lattice-mismatch systems"
J. Appl. Phys., Vol. 75 (2), pp.860 (1994)

Venables, J. A., Spiller, G. D. T., and Hanbucken, M.
Rep. Prog. Phys., Vol. 47, pp.399 (1984)

Venkatesan, T., Trajanovic, Z., Choopun, S., Sharma, R. P.
"Stoichiometry and thickness variation of Yba2Cu3O7-x in pulsed laser deposition with a shadow mask"
Appl. Phys. Lett., Vol. 70, pp.3461 (1997)

Willmott, P. R., Timm, R., Huber, J. R.
"RHEED analysis of interface growth modes of TiN films on Si(001) produced by crossed beam laser ablation"
Appl. Surf. Sci., Vol. 105-110, pp.127 (1998)

Wittmer Marc
"Barrier layer: Principles and applications in microelectronics"
J. Vac. Sci. Technol. A2., pp.273 (1984)

Wittmer Marc
"TiN and TaN as diffusion barriers in metallizations to silicon semiconductor devices"
Appl. Phys. Lett., Vol. 36, pp.456 (1980)

Wittmer Marc
"Interfacial reactions between aluminium and transition-metal nitride and carbide films"
J. Appl. Phys., Vol. 53, pp.1007 (1982)

Wenbin Wu, K. H. Wong and C. L. Choy.
"Epitaxial growth of $SrTiO_3$ films with different orientations on TiN buffered Si(001) by pulsed laser deposition"
Thin Solid Films., Vol. 360, pp.103 (2000)

Xin Sun, Elzbieta Kolawa, Jen-Sue Chen, Jason S. Ried and Marc-A. Nicolet.
"Properties of reactively sputter-deposited Ta-N thin films"
Thin Solid Films., 236, pp.347 (1993).

X. Y. Chen, B. Yang, T. Zhu, K. H. Wong, J. M. Liu, Z. G. Liu.
"Growth of completely (110)-oriented Pt film on Si(100) by using MgO as a buffer by pulsed laser deposition"
Applied Physics A (in press)

Zhang, Q. Y., Chen, B., Li, G. B., Jin, S., Chen, F. X., Yang, D. Z., and Zhu, Y. C.
"Investigation of TaN films implanted with nitrogen and argon ions"
Surf. Coat. Technol., Vol. 66, pp.468 (1994)